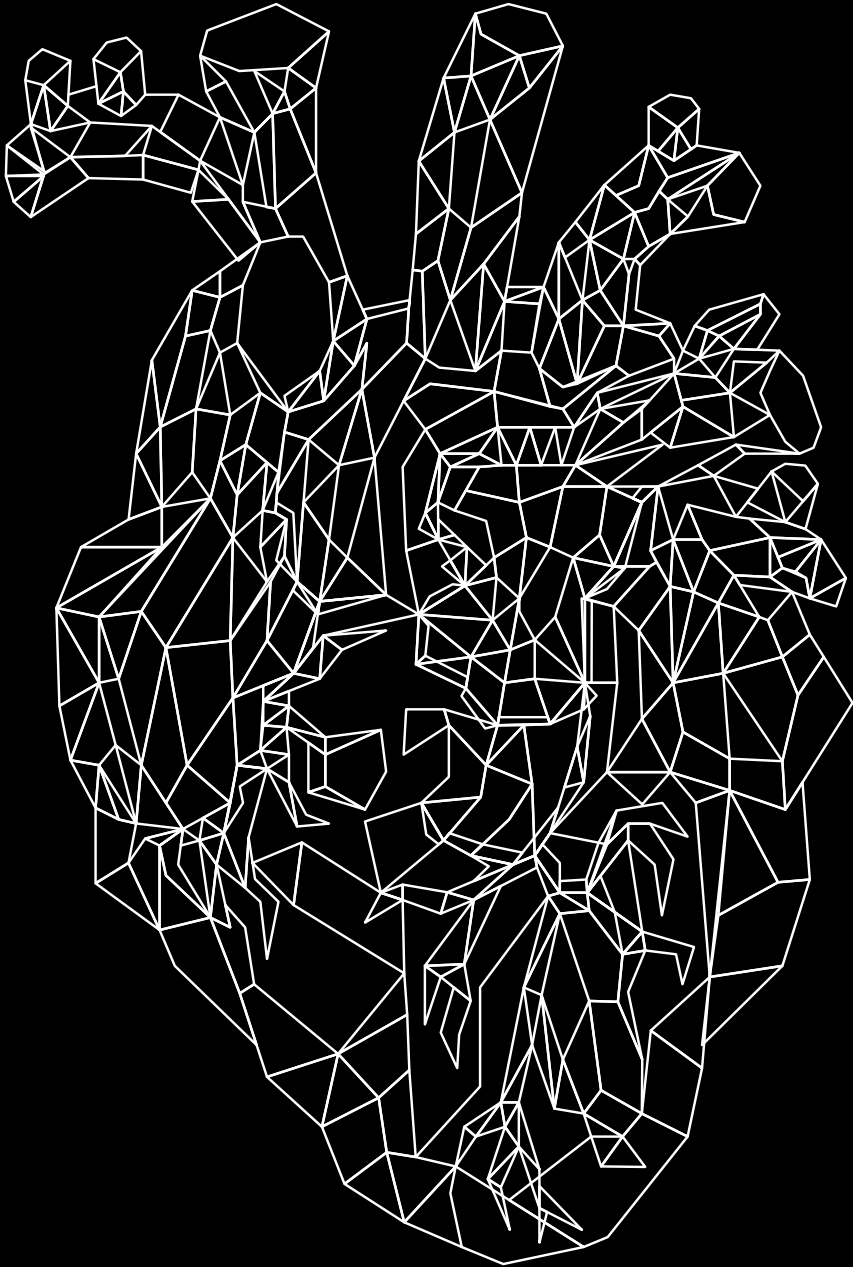


# RNA Targets in Cardiac Disease

Joep Eding



# RNA Targets in Cardiac Disease

RNA-therapieën voor hartziekten

(met een samenvatting in het Nederlands)

## RNA Targets in Cardiac Disease

Joep Eding

ISBN: 978-90-393-7264-7

NUR: 881 - Medische biologie

Printed by: Proefschrift All in One

The research described in this thesis was performed at the Hubrecht Institute of The Royal Netherlands Academy of Arts and Sciences (KNAW), Utrecht, the Netherlands.

The research described in this thesis was supported by grants of the Dutch Heart Foundation (CVON2014-27 REMAIN, CVON2017-18 ARENA-PRIME, CVON2014-40 DOSIS)

Financial support by the Dutch Heart Foundation for publication of this thesis is gratefully acknowledged.

Publication of this thesis was additionally supported by ChipSoft.

## Proefschrift

ter verkrijging van de graad van doctor aan de Universiteit Utrecht op gezag van de rector magnificus, prof.dr. H.R.B.M. Kummeling, ingevolge het besluit van het college voor promoties in het openbaar te verdedigen op dinsdag 2 april 2020 des ochtends te 10.30 uur

door

**Joep Egbert Coenraad Eding**

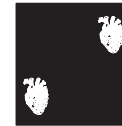
geboren op 28 december 1989

te Wageningen



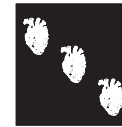
General Introduction

6



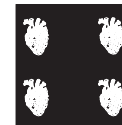
The Efficacy of Cardiac anti miR-208a Therapy is Stress Dependent

14



Hydrogel-Based Delivery of anti miR-195 Improves Cardiac Efficacy After Ischemic Injury

38



Single-Cell Transcriptomic Profiling Provides Insights Into Disease-Related Processes in Human Hypertrophic Cardiomyopathy

58



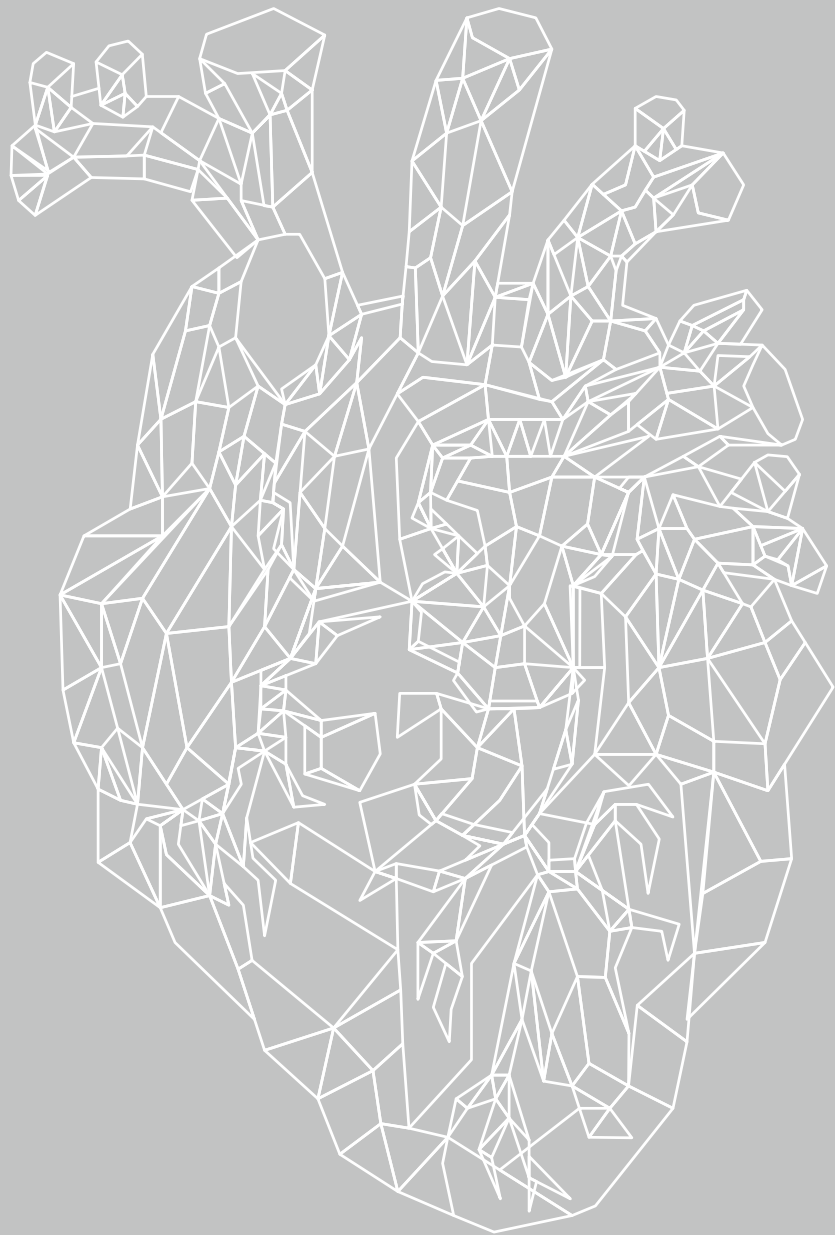
Discussion

78



Appendices

88



# Chapter 1

## General Introduction

J.E.C. Eding

## Cardiac disease

Cardiovascular disease (CVD) is the leading cause of death worldwide<sup>1</sup>. Of the CVD-related deaths, approximately 50% is due to ischemic heart disease (IHD), 35% to cerebrovascular disease, 5% to hypertensive heart disease and 2% to cardiomyopathies and myocarditis. The remainder is due to several other rarer diseases<sup>1</sup>.

### Ischemic heart disease

IHD is the form of CVD that causes most deaths worldwide. IHD is a consequence of atherosclerosis, the process in which lipid particles accumulate in the tunica intima, the inner layer of the arterial wall, forming an atheroma. Atherosclerosis progresses with age and is worsened by an unhealthy lifestyle (smoking, Western diet), male sex and several gene polymorphisms. During the progression of atherosclerosis, which is associated with ongoing inflammation, the atheroma grows. The inflammation leads to gradual thinning of the fibrous cap covering the atheroma. Eventually, the fibrous cap ruptures and a thrombus forms that (partially) occludes the artery. After formation of a thrombus, a fibrous cap overgrows the thrombus and the growth of the atheroma progresses until the next rupture. Partial occlusion of an artery may cause relative ischemia, where the narrowed vessel can supply enough oxygen to the tissue at rest but not during exercise. In the case of coronary atherosclerosis this results in chest pains during exercise. The occlusion of the artery progresses until flow through the artery is fully blocked, causing infarction of the tissue downstream of the blockage. Atherosclerosis can occur in all arteries and can lead to peripheral artery disease, aortic aneurysms, ischemic stroke and myocardial infarction<sup>2</sup>.

An average myocardial infarction results in the loss of a billion cardiomyocytes<sup>3</sup>. The size of the infarcted regions depends, among others, on the affected coronary artery, how proximal or distal the occlusion was, whether there were any collateral coronary arteries and the time until revascularization. The cells lost in a myocardial infarction are not replenished. Post-natal cardiomyocytes have long been considered to be post-mitotic cells incapable of dividing and regenerating lost cells. However, in recent years, it was shown that regeneration of lost myocardium is possible in the neonatal mouse<sup>4</sup> and even in the neonatal human heart<sup>5</sup>. In adult human hearts, carbon-dating studies have shown a very limited turnover of adult cardiomyocytes<sup>6,7</sup>. This is clearly not enough to regenerate the heart after myocardial infarction. Thus, cardiomyocytes that are lost in an infarction in an adult heart are not replaced by new cardiomyocytes, but rather a fibrotic scar is formed.

When someone has suffered from a myocardial infarction both lifestyle interventions, such as smoking cessation, and drug therapy, such as antiplatelet therapy and statins, are important to prevent recurrent myocardial infarction<sup>8</sup>. Moreover, as the damage from the infarction puts the patient at risk for adverse remodeling, heart failure, and dangerous arrhythmias, patients are also treated with beta-blockers and angiotensin-converting enzyme inhibitors. In principle, these drugs are lifelong prescriptions as they serve a role in secondary prevention and symptom management, but do not repair the damage. Regeneration of cardiomyocytes would allow for restoration of cardiac function and therefore has the potential to truly cure patients. Therefore, new therapies that are able to repair the heart after myocardial infarction are being sought.<sup>8</sup>

## Cardiomyopathies

Cardiomyopathies are classified based on their structural or functional consequences: (1) dilated cardiomyopathy (DCM) for dilation of the left ventricle (LV); (2) hypertrophic cardiomyopathy (HCM) for hypertrophy of the left ventricular wall; (3) restrictive cardiomyopathy (RCM) for a stiffened left ventricular wall that restricts filling of the heart; (4) arrhythmogenic cardiomyopathy for a cardiomyopathy characterized by ventricular arrhythmias, dilation and replacement of myocardium by fibrofatty tissue; and finally, (5) 'unclassified' cardiomyopathy for several remaining cardiomyopathies that do not fit the previously described categories<sup>9</sup>. Each of these classes can be subdivided into a familial (genetic) and non-familial (non-genetic) subgroup. A cardiomyopathy is considered familial when it is caused by a known pathogenic mutation or when other family members suffer from the same disease, even if no known mutation can be identified. Typically, familial cardiomyopathies are caused by mutations in a distinct set of genes<sup>9,10</sup>.

The most common genetic cardiomyopathy is hypertrophic cardiomyopathy, HCM, which is characterized by (1) hypertrophy that is not explained by another cause, such as aortic valve stenosis, (2) hypercontractility, (3) reduced relaxation of the heart muscle, and (4) increased energy consumption. HCM is often caused by mutations in the genes encoding proteins in the sarcomere. The sarcomere is the complex of proteins in the cardiomyocyte that generates the force of contraction. Mutations in the sarcomeric proteins alter the way that force is generated<sup>11</sup>. The two most commonly mutated sarcomeric genes are the  $\beta$ -myosin heavy chain (*MYH7*) and myosin-binding protein C (*MYBPC3*)<sup>11</sup>. While the pathological mechanism of HCM has not been fully elucidated, several theories exist to explain the molecular mechanism by which a mutation in a sarcomere protein leads to the HCM phenotype<sup>12,13</sup>.

The process of contraction in a cardiomyocyte is started by depolarization of the cardiomyocyte cell membrane. This opens a channel that allows  $\text{Ca}^{2+}$  to enter the cell and bind the ryanodine receptor (RyR2) to release more  $\text{Ca}^{2+}$  from the sarcoplasmic reticulum into the cytoplasm. The released calcium binds cardiac troponin T (TNNT2), which subsequently changes conformation and allows for crossbridge cycling between actin and myosin. This crossbridge cycling generates force, leading to shortening of the cell and contraction of the muscle. Sarcoplasmic reticulum  $\text{Ca}^{2+}$  ATPase2 (SERCA2) transports the  $\text{Ca}^{2+}$  back into the sarcoplasmic reticulum, allowing for relaxation<sup>14</sup>.

HCM-causing mutations might influence the relaxation of myosin heads. Myosin heads are located in pairs along the thick filament and have two relaxation states. There's a disordered relaxation state (DRX), in which only one of two myosin heads is folded back and unavailable for contraction. In this state, the other head can still metabolize ATP and participate in contraction. Additionally, there's a super relaxed state (SRX) in which both myosin heads are folded back and can neither metabolize ATP nor bind actin for contraction. In SRX, the myosin heads are in an energy-saving configuration, functioning as a reserve set of myosin heads in case of a need for an extra boost of contractile strength. Mutations in the myosin proteins, or in proteins regulating the relaxation state of myosin, may shift the balance between the DRX and SRX states towards more DRX, resulting in hypercontractility and increased energy consumption<sup>13</sup>. Alternatively, mutations in phosphorylation sites in the sarcomeric components might alter the way these proteins are phosphorylated by, for example, protein kinase A, protein kinase C,  $\text{Ca}^{2+}$ -calmodulin-dependent protein kinase<sup>13</sup>. This may then alter their calcium sensitivity and

thus influence contractility, relaxation, energy consumption and activation of hypertrophic signaling through altered cellular calcium handling. Finally, in addition to increasing ATP consumption, mutations may cause reduced ATP production. The increased calcium sensitivity of the sarcomere components may reduce calcium availability for the Krebs' cycle and thereby influence energy production<sup>12, 13</sup>. The energy deficiency by itself can cause altered calcium dynamics in the cell because pumping  $\text{Ca}^{2+}$  back into the sarcoplasmic reticulum requires large amounts of ATP, and this may lead to arrhythmias<sup>12</sup>.

Current pharmacological treatment cannot cure HCM. Instead, it is mostly symptom management. Heart failure symptoms in HCM mostly arise from impaired filling of the LV. Filling is improved by lengthening the diastolic phase using beta-blockers, verapamil or diltiazem<sup>15</sup>. In HCM patients experiencing angina, beta-blockers and calcium antagonists reduce myocardial oxygen demand and improve diastolic perfusion of the myocardium by lengthening the diastolic phase<sup>15</sup>. In patients that have additionally developed significant left ventricular outflow tract obstruction due to hypertrophic growth, interventional treatment may be required. The thickness of the basal septum can be reduced by either a surgical septal myectomy or by ethanol injection into one of the branches of the left anterior descending coronary artery that supplies the basal septum<sup>15</sup>.

### Experimental therapies for cardiac regeneration

Treatment options after a myocardial infarction are focused on damage control, with emergency revascularization meant to save as much myocardium as possible and subsequent pharmaceutical therapy to manage symptoms and prevent recurrence and further deterioration. None of those therapies actually regenerate the heart. However, cardiac regeneration would significantly improve patients' quality of life. Research focusing on cardiac regeneration has typically focused on two avenues to replace lost cardiomyocytes. Firstly, methods are being sought to inject stem cells that subsequently engraft and differentiate into new myocytes. Secondly, researchers attempt to induce remaining cardiomyocytes to start proliferating again to replenishing the cardiomyocyte population.

#### Cell-based therapies

Replacing the lost cardiomyocytes by injecting new cells seems a logical course of action for the restoration of cardiac function. Indeed, this idea has led to hundreds of clinical trials<sup>16</sup>. In the initial trials with patients suffering from advanced ischemic cardiomyopathy, skeletal myoblasts were injected into the myocardial scar in order to promote contractility. However, these cells were unable to improve cardiac function and increased the risk of arrhythmias because they lacked the capacity to form gap junctions to electrically integrate with the host myocardium<sup>16</sup>. Then, bone marrow derived mononuclear cells (BMMNCs) were used both with intracoronary and intramyocardial (transendothelial) delivery methods. While these yielded somewhat positive results there was a large variation in efficacy between trials, which was attributed to (1) differences in the composition of the bone marrow cells between patients and (2) reduced efficacy of stem cells obtained from older patients. This led to trials with selected bone marrow cell populations (either mesenchymal stem cells or CD34+/CD133+ cells) and trials where the stem cells were not obtained from the patient him- or herself but rather from healthy donors<sup>16</sup>. More recently, trials have been conducted using cardiac stem

cells (CSCs), cardiosphere-derived cells (CDCs) and even cardiomyocyte progenitors derived from embryonic stem cells<sup>16, 17</sup>. Interestingly, animal studies showed no evidence of significant engraftment of transplanted cells, even though a persistent positive effect on cardiac function was observed. This suggests that these cells exert their beneficial effect in a paracrine fashion rather than through differentiation into cardiomyocytes<sup>16, 18</sup>.

#### Stimulating cardiomyocyte proliferation

With the proof that there is a very low percentage of endogenous cardiomyocyte renewal in the adult human heart and that this renewal most likely originates from adult cardiomyocyte proliferation, came a renewed hope of regenerating the damaged heart by boosting this system of cardiomyocyte proliferation<sup>6, 7, 19</sup>. It was initially thought that a resident cardiac stem cell population (such as the c-Kit+ cells) transdifferentiates into cardiomyocytes. However, extensive lineage tracing research revealed that none of the cardiac non-myocyte cells make a meaningful contribution to the generation of new cardiomyocytes, neither upon aging nor upon injury<sup>20</sup>. As it is known that neonatal cardiomyocytes largely lose their proliferative capacity quickly after birth<sup>4</sup>, a method is sought to enable them to proliferate again. Therefore, many studies have tried to reactivate cell cycle activity of adult cardiomyocytes. Modulating the expression of genes that govern the cell cycle (*Ccnd1*, *Cdk2*, *E2f1*, *E2f2*), and modulating endogenous signaling pathways that control cardiomyocyte proliferation (YAP/TAZ, NRG1/ERBB) have both been shown to induce reactivation of the cell cycle in vitro<sup>20</sup>. If these signaling pathways can be influenced by extracellular signaling peptides, modulation of these pathways by treatment with a specific signaling peptide might be a means to induce regeneration of heart tissue after an infarction<sup>20</sup>. If the pathways are completely intracellular, direct modulation of gene expression might be required.

#### RNA therapeutics

Modulation of gene expression is possible with RNA therapeutics. RNA therapeutics aim to modulate RNA levels in the cells, for example those of microRNAs (miRs). miRs are short RNA molecules of ~20 nucleotides that are integrated into the RNA-Induced Silencing Complexes (RISC) and direct these protein complexes to specific, complementary mRNAs. When a RISC binds an mRNA, it blocks the mRNA's translation or causes its degradation. Both cases lead to a reduction in the amount of protein formed from the specific mRNA<sup>21</sup>. Therefore, miRs give the cell an extra layer of control over protein synthesis after transcription. Interestingly, miRs seem to gain a more important function under pathological conditions<sup>21</sup>.

#### Increasing gene expression

Inhibition of miRs will result in increased mRNA translation and thus contribute to increased protein production. For example, after myocardial infarction the inhibition of miRs that target pro-proliferative genes might activate the cell cycle in cardiomyocytes and cause them to proliferate. There are also other options to increase protein production. A straightforward method is using a virus to deliver a constitutively active transgene encoding the mRNA. However, this method comes with several drawbacks. First of all, targeting the virus to a specific organ or cell type is challenging. Second, as the goal is the delivery of pro-proliferative genes, there is a risk of tumorigenesis with these overexpression strategies. The risk of tumorigenesis is enhanced further as some of these viral delivery factors lead to incorporation of the transgene

into the host genome at a random site, which risks disrupting tumor suppressor genes<sup>22</sup>. Finally, these transgenes stay active for a very long time. This makes finetuning of the amount of gene expression difficult.

These drawbacks are not associated with the inhibition of miRs by synthetic antisense molecules, so-called anti-miRs. These anti-miRs block the binding of a miR to its target mRNAs. This relieves the miR-induced degradation or repression of mRNA translation and results in increased protein synthesis<sup>21</sup>.

### Decreasing gene expression

In addition to increasing the expression of proliferative genes, inhibiting the expression of cell cycle inhibiting genes can also result in increased cardiac regeneration. Additionally, inhibition of gene expression may be used to decrease the fibrosis that occurs after myocardial infarction<sup>23</sup>. Inhibition of gene expression is the main function of miRs. It is possible to make this inhibition stronger by artificially boosting miR levels by treatment with synthetic microRNAs, so-called miR mimics. Generally, a miR tends to target multiple genes in a certain pathway, finetuning the activity of that pathway<sup>21</sup>. Therefore, artificially increasing the level of a miR in a cell is expected to reduce the translation of several mRNA targets. When this is undesirable, it is also possible to synthesize miR-like RNA molecules that are specific to a single mRNA target. These silencing RNAs (siRNA) are synthesized to be fully complementary to a region that is specific to the target mRNA, unlike the partial complementarity that is generally seen in miRs<sup>22</sup>. Both miRNAs and siRNAs target RISC to the target mRNA, but siRNAs result in degradation of the mRNA more often than miRs.

### Challenges in finding RNA targets

As described above, oligonucleotide therapies are available to specifically inhibit or derepress certain genes in a therapeutic manner. An important remaining challenge is finding the right targets. For regenerating the infarcted heart, it makes sense to look at genes involved in the cell cycle and to try to reactivate or inhibit those as is appropriate. For hypertrophic cardiomyopathy, where the pathogenesis has not been fully elucidated, target identification is much harder.

Finding a miR to modulate can be done in two ways. First, miR levels in healthy and diseased tissue can be compared to identify miRs that are differentially regulated between the two conditions. The identified miRs can then be experimentally inhibited or boosted in order to elucidate their effect on the disease phenotype<sup>23</sup>. The other option is starting from a known pathway and identifying one or a couple of genes to modulate. Then, several online databases (miRBase, TargetScan, microRNA.org) can predict which miRs will target the 3' UTRs of each of those genes. When inhibition of just a single gene is indicated, siRNAs can be designed to specifically inhibit this one gene.

To identify new mRNAs to target in the treatment of HCM, it makes sense to look for genes that are differentially expressed between healthy tissues and diseased tissues. Alternatively, when healthy tissue is hard to obtain, it might be possible to look for genes that change in expression with the severity of the disease. Finally, recent advances in transcriptomics allow quantification of genome-wide gene expression at the single-cell level. This single-cell resolution allows for a new angle from which to investigate the pathological mechanism in HCM. While all single-cell transcriptomes obtained from myocytes show similarities because they are myocytes, the

differences between them can be used to distill patterns in gene regulation that may be specific for HCM. These patterns may provide new insight into HCM pathogenesis and thus help identify new targets for RNA therapeutics.

### In this thesis

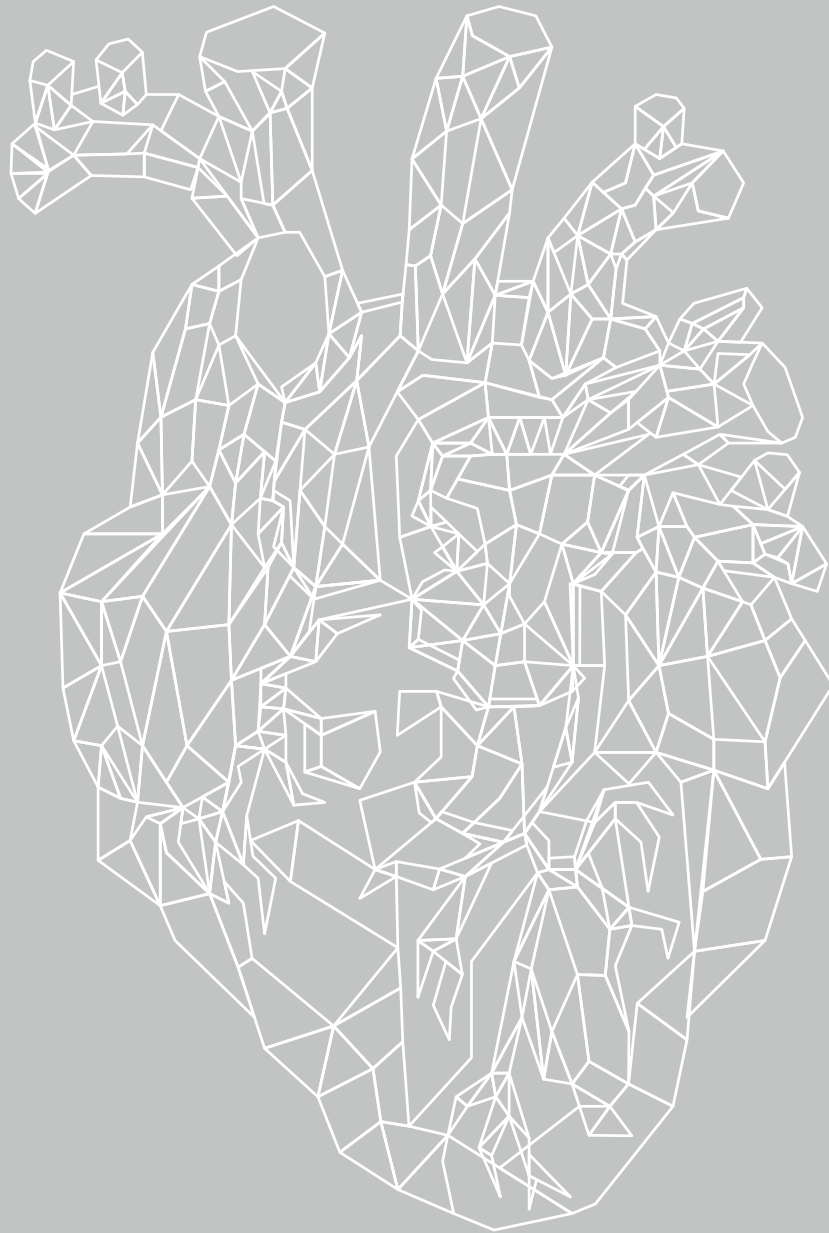
As discussed above, RNA therapeutics are promising as novel treatment strategies for cardiac disease. Research to identify new targets for RNA therapeutics and new delivery strategies is presented in the following chapters.

**Chapter 2.** Cardiac disease is associated with a disease-related shift in gene expression. Therefore, we expect that the pool of available miR targets is different in diseased versus healthy tissue. Consequently, the effect of a miR is probably different in diseased versus healthy tissue. This idea is reinforced by the observation that mouse models lacking a certain miR tend to not have a phenotype under baseline conditions but will respond differently to a disease-inducing intervention than wild-type control mice. In this chapter we compare the effects of anti-miR-208a on the transcriptome of different rat cardiac disease models. We show that different genes are regulated by anti-miR-208a treatment in healthy versus diseased conditions and between different disease conditions. These findings are important for the design of future (pre)clinical trials of miR-therapeutics.

**Chapter 3.** Some miRs, like *miR-208a*, are specific to a certain cell type. Other miRs, such as the *miR-15* family, are expressed in multiple cell types. The *miR-15* family is implicated in the regulation of the cell cycle and inhibition of this miR family has been shown to help trigger regeneration after myocardial infarction<sup>24</sup>. Because the *miR-15* family is expressed in multiple cell types, systemic treatment with an inhibitor for this miR family may trigger unwanted proliferation in other organs. Therefore, targeted delivery of the inhibitor is important. In this chapter we investigate the use of a pH-sensitive, catheter-injectable hydrogel as a sustained release drug depot for intramyocardial delivery of an anti-miR. We show that using this hydrogel as a delivery vehicle for anti-miR-195 improves the efficacy over using PBS as a delivery vehicle, but not enough to improve cardiac function after myocardial infarction.

**Chapter 4.** With the advent of single cell RNA-sequencing techniques it has become possible to investigate gene expression in disease conditions at the single-cell level. This technique can be used to gain a better understanding of pathophysiological mechanisms in disease, and in the context of RNA therapeutics it can be a useful tool with which to identify new targets for therapy. In this chapter we perform single cell RNA-sequencing of cardiac tissue of patients with hypertrophic cardiomyopathy. We identify several groups of coregulated genes and we identify genes that are correlated to cardiomyocyte cell size. These genes are potential targets for RNA therapeutics.

**Chapter 5.** Finally, in chapter 5 our findings are placed in context with current literature and the implications for future research are discussed.



# Chapter 2

## The Efficacy of Cardiac antimiR-208a Therapy is Stress Dependent

Joep E.C. Eding<sup>1†</sup>, Charlotte J. Demkes<sup>1,2†</sup>, Joshua M. Lynch<sup>3</sup>, Anita G. Seto<sup>3</sup>, Rusty L. Montgomery<sup>3</sup>, Hillary M. Semus<sup>2</sup>, Aimee L. Jackson<sup>3</sup>, Marc Isabelle<sup>4</sup>, Stefano Chimenti<sup>4</sup> and Eva van Rooij<sup>1,2</sup>

<sup>1</sup> Hubrecht Institute, KNAW and University Medical Center Utrecht, the Netherlands.

<sup>2</sup> Dept. of Cardiology, University Medical Center Utrecht, the Netherlands.

<sup>3</sup> MiRagen Therapeutics, Inc., Boulder CO, USA.

<sup>4</sup> Servier Research Institute, Suresnes, France.

† These authors contributed equally to this work.

Adapted from:

Eding JE, Demkes CJ, Lynch JM, et al. The Efficacy of Cardiac Anti-miR-208a Therapy Is Stress Dependent. *Mol Ther.* 2017;25(3):694–704. doi:10.1016/j.ymthe.2017.01.012

## Abstract

MicroRNAs (miRs) are important regulators of biology and disease. Recent animal efficacy studies validate the therapeutic benefit of miR modulation and underscored the therapeutic value of miR-targeting oligonucleotides. However, whether disease conditions (stress) influence the pharmacological effects of an anti-miR is currently unknown.

To study the effect of disease on target regulation after anti-miR treatment, we injected animals with anti-miR-208a, a synthetic oligonucleotide that inhibits the cardiomyocyte-specific *miR-208a*. Our data indicate that the presence of stress increases the number of regulated *miR-208a* targets and that higher stress levels correlate with stronger target derepression. Additionally, the type of stress also influences which targets are regulated upon *miR-208a* inhibition. Studies in a large animal model indicate a similar stress-dependent anti-miR effect. Subsequent in vitro studies suggest that the influence of stress on anti-miR efficacy depends at least in part on increased cellular anti-miR uptake.

These data indicate that the pharmacological effect of anti-miRs is stronger under disease conditions and that both the type and severity of disease determine the therapeutic outcome. These facts will be important for assessing the therapeutic dose and predicting the therapeutic outcome when applying anti-miRs in a clinical setting.

## Introduction

MicroRNAs (miRs) are short single-stranded RNAs that anneal with complementary sequences in target mRNAs, thereby suppressing protein formation. The function of a given miR is determined by its mRNA targets<sup>25</sup>. Since an individual miR can engage numerous mRNA targets, often encoding multiple components of complex intracellular networks, the regulation of a single miR can have a profound impact on cellular phenotypes<sup>26</sup>. It is well accepted that miRs are important regulators of biology and disease. Their obvious relevance in disease, as well as their known conserved sequence, catalyzed efforts to explore miRs as novel drug targets. Antisense chemistries, known as anti-miRs, can function to target disease related miRs *in vivo*. They can reduce the levels of pathogenic or aberrantly expressed miRs<sup>25, 27,28</sup> and are efficacious in both animals and humans<sup>26, 29</sup>. Because miRs typically act as inhibitors of gene expression, anti-miRs will derepress expression of the mRNAs that are normally targeted by the miR<sup>27</sup>. Previously, we reported that systemic delivery of an antisense oligonucleotide against *miR-208a* induced potent and sustained silencing of *miR-208a* in the heart<sup>30</sup>. Therapeutic inhibition of *miR-208a* by subcutaneous delivery of anti-miR-208a during hypertension-induced heart failure in Dahl hypertensive rats dose-dependently prevents pathological myosin switching and cardiac remodeling, while improving cardiac function, overall health and survival<sup>30</sup>. These data recapitulated the cardioprotective effects seen after genetic deletion of *miR-208a* in mice<sup>31</sup>.

An intriguing feature of miR biology has been the minimal effects of miR loss-of-function under homeostatic conditions<sup>32,33</sup>. Instead, the actions of miRs in general seem to become pronounced under conditions of injury or stress. Thus, elimination of some miRs sensitizes cells to stress; resulting in exacerbated pathology, while the absence of other miRs can confer resistance to stress<sup>26</sup>. While most anti-miR studies appear to indicate the absence of an effect under baseline, unstressed conditions, it is currently unknown whether disease (stress) influences the pharmacological effects of an anti-miR.

Using *miR-208a* as a model system, we show that stress changes the effect of anti-miR treatment on mRNA targets. In vitro analysis indicates that the influence of stress on anti-miR efficacy might depend on an increase in cellular anti-miR uptake under stress conditions. Together our data show that anti-miRs have stronger pharmacological effects during disease and that the origin of disease determines the therapeutic outcome. These considerations will be important for assessing the therapeutic dose and predicting the therapeutic effect in patients.

## Materials & Methods

### Animal studies

Animal experiments were performed in accordance with the Institutional Animal Care and Use Committee (IACUC) at miRagen Therapeutics, Inc. (anti-miR studies in sham- or MI-operated rats and high-salt diet Dahl rats), the institutional review committee of the Royal Netherlands Academy of Arts and Sciences (KNAW) (anti-miR studies in Angiotensin II-treated rats), or the Servier Research Institute ethical committee (porcine studies), and comply with the Federal and State guidelines concerning the use of animals and research as defined by the Guide For the Care and Use of Laboratory Animals (NIH Publication No. 80-23, revised 1985) or with national animal welfare laws under a project license of the Dutch or French government.



**Rat MI-studies**

Adult Wistar (Charles River) male rats were anesthetized with isoflurane at 5% for 2-3 minutes, intubated and ventilated using a rodent ventilator (Hallowell Microvent I). Isoflurane was maintained at 1.5-2.5%. Surgery was performed on a heated plate to maintain body temperature at 37°C, body temperature was monitored via rectal probe. The heart was reached through a left sided thoracotomy between ribs 4 and 5, the left anterior coronary artery was ligated using a 7-0 silk suture. Successful ligation was confirmed by loss of color of the myocardium distal to the ligation. The chest wall and skin were closed and rats were allowed to recover. Once awake, they were removed from ventilator and moved to a warm recovery cage. Once fully ambulatory, they were returned to normal housing and given 0.01mg/kg Buprenorphine subcutaneously. Sham-operated rats were subjected to the same procedure, with the exception that no ligation of the coronary artery was performed. After surgery the rats were kept for 8 weeks before sacrifice and tissue collection.

**Dahl salt-sensitive rat**

Male Dahl rats (Harlan) were maintained on a 6% NaCl diet for eight weeks starting at 7 weeks of age.

**Angiotensin II delivery**

Adult male Sprague Dawley rats received Angiotensin II (AngII, Sigma Aldrich, 0.25mg/kg/day) for 8 weeks by osmotic minipumps (ALZET model 2004, DURECT Corporation, Cupertino, CA). Rats were anesthetized with 4-5% isoflurane and maintained with 1-2% isoflurane supplemented with oxygen. Surgery was performed on a heated plate to maintain body temperature at 37°C. A subcutaneous pocket on the back of the rats (interscapular) was created using blunt-end scissors after which the AngII filled osmotic minipump was placed in this pocket and the wound was closed with wound clips (ALZET, DURECT Corporation, Cupertino, CA). After 4 weeks the pump was replaced with a new AngII filled pump. Control animals received the same procedure with pumps filled with vehicle (saline).

**Porcine IR studies**

Göttingen minipigs (Ellgaard, Dalmose, DK) were subjected to ischemia-reperfusion (IR) by a closed-chest approach and clinical cardiac catheterization techniques<sup>51, 52</sup>. Adult (12-15 months) male pigs were sedated with a mixture of tiletamine and zolepam (Zoletil®, 15 mg/kg). Following adequate sedation, the neck was shaved, properly scrubbed and disinfected with vetedine soap (Vetoquinol). An intravenous catheter was placed in a marginal vein of one ear for the administration of fluids and anesthetic agent, an endotracheal tube was inserted for mechanical ventilation and body temperature was maintained 36.5-39°C with a blanket during the procedure. Surface ECG used to monitor the onset of arrhythmias (ventricular tachycardia and fibrillation). Thiopental was used (~10mg/kg/h i.v.) for stable and prolonged anesthesia.

The carotid artery was exposed and access gained by the Seldinger technique. Under fluoroscopy guidance, a JR3.5 catheter was advanced over the wire to the level of the coronary sinus and placed at the coronary ostium without full engagement. Good placement was confirmed with a bolus of contrast agent (Telebrix®) to visualize the left main, circumflex and anterior descending coronary. Heparin (300 UI/kg i.v.) was given just before left anterior descending artery (LAD) occlusion to prevent clotting. A guide wire was advanced into the LAD followed by

a balloon catheter (3.5 x 15-20) that subsequently was inflated at 4-6 atm to ensure occlusion of the LAD for 150 minutes. After the 150 minute occlusion the balloon catheter was deflated and slowly removed. A bolus of lidocaine (2 mg/kg i.v.) and nitroglycerin (40 µg/kg intracoronary) was administered to avoid vasospasm and arrhythmia. During the recovery period, buprenorphine (50 µg/kg i.m.) was given for analgesia. After waking up under a warming lamp the pigs were extubated and butorphanol (Dolorex®, 0.2 mg/kg s.c.) and amoxicillin (Dufamox®, 0.015 mg/kg i.m.) was given for post-procedural care.

**AntimiR injections**

AntimiRs (designed and synthesized by miRagen) were dissolved in saline and delivered by subcutaneous injection. Used anti-miRs are LNA-DNA mixmers, these 16-mers are complementary to *miR-208a* specifically and have high nuclease resistance as well as high duplex melting temperature<sup>30</sup>. Animals were injected every other week with 25 mg/kg of anti-miR-208a or a comparable volume of vehicle starting 1 week after the intervention (Sham or MI, HS diet, PBS or AngII).

**RNA extraction**

Total RNA was extracted from LV tissue or cultured NRVM with TRIZOL® according to the manufacturer's protocol (Invitrogen, Monza Italy).

**Gene expression analysis**

Gene expression profiling was performed by a service provider (MOgene, St. Louis, MO) on Agilent SurePrint G3 Rat Gene Expression, 8x60 microarrays. Sample integrity was assessed with Agilent Bioanalyzer prior to microarray analysis. Data were analyzed using Array Studio software. Significantly regulated genes were defined using a Benjamini-Hochberg false discovery rate (BH-FDR) corrected p-value cutoff of  $\leq 0.05$  to control for multiple testing. Differential gene expression reflects statistically significant expression in the treatment group compared to the saline treated group. Hierarchical clustering was performed using the software program R using an agglomerative metric with Euclidean distance. For this study genes containing a 6-, 7- or 8-mer *miR-208a* binding site in their 3' untranslated were considered as potential *miR-208a* target. For these target genes, an average fold change in gene expression after anti-miR-208a treatment over control was calculated for each animal model (n=4 per group). The genes that show a significant derepression after anti-miR-208a were used to generate the heat maps shown in Figure 1a and 2a. A cutoff value of  $p < 0.05$  was used to determine differential expression.

**Real-time PCR**

cDNA was synthesized from 400-1000ng of total RNA extracted from tissue or cells using the iScript cDNA Synthesis Kit (Bio-Rad) for genes and miScript® II RT Kit (Qiagen) for miRs. Real-time PCR was performed to analyze the expression levels of individual mRNAs/miRs, using a specific set of primers (Table I in the online-only Data Supplement\*) and iQ SYBR Green Supermix (Bio-Rad) on a real-time PCR machine (CFX Connect™ Real-Time PCR Detection System, Bio-Rad). Expression levels were normalized to the levels of glyceraldehyde 3-phosphate dehydrogenase (*Gapdh*) mRNA levels for genes or RNU6b snRNA (*U6*) for miRs and fold changes in gene/miR expression were calculated according to the  $2^{-\Delta\Delta CT}$ -method and expressed as mean fold change  $\pm$  SEM.

### Cell culture and neonatal rat cardiomyocytes

Neonatal rat ventricular cardiomyocyte (NRVM) cultures were isolated by enzymatic dissociation of neonatal rat hearts, as described previously.<sup>26</sup> In short, hearts from 1-2 day old rat pups were collected, the atrias were removed and the ventricular cells were enzymatically dissociated with trypsin (Life Technologies) in a water (37°C) jacketed spinner flask. The single cell suspension was filtered and pre-plated to remove debris and non-myocytes respectively. Primary cardiomyocytes were initially maintained in Ham's F10 medium (Gibco) supplemented with 5% FBS (Sigma-Aldrich) and 1% penicillin/streptomycin (Life Technologies). The day after isolation, cardiomyocytes were switched to serum-free Ham's F10 medium, supplemented with 1% penicillin/streptomycin and 1µl/ml insulin-transferrin-sodium-selenite supplement (Sigma-Aldrich, catalog number 11074547001).

For stress experiments, isoproterenol (ISO, 10µM final concentration, Sigma-Aldrich, catalog number I6504) or phenylephrine (PE, 10µM final concentration, Sigma-Aldrich, catalog number P6126) was added to the (serum-free) culturing medium. For subsequent anti-miR treatment, the Cy3-labeled anti-miR-208a (1µM final concentration, unless otherwise indicated) was added to the medium after 8 hours of culture (without transfectant), without removing the stressor. Cells were then cultured for a further 16 hours before fixing and imaging.

### Confocal microscopy

NRVM cultured on coverslips were fixed with 4% paraformaldehyde, permeabilized with 1% Triton X-100 (Sigma-Aldrich), blocked with 1% fish gelatin (Sigma-Aldrich) and stained with an anti-α-actinin primary antibody (ACTN2; 1:500; Sigma-Aldrich, A7811) and an Alexa-488 conjugated secondary antibody (1:200; Sigma-Aldrich, A11001). Coverslips were then mounted with ProLong Gold antifade reagent with DAPI (Life Technologies, P36935). Cells were imaged using a Leica TCS SPE. Cross-sectional area (CSA) and uptake of Cy3-labeled anti-miR (as indicated by Cy3 fluorescence intensity) were measured using ImageJ. For all experiments where fluorescence intensity was quantified, laser and detector settings were kept consistent across the experiment. Quantifications were based on 17-43 cells per biological replicate, collected from 10 fields per replicate, for 8-12 replicates per condition.

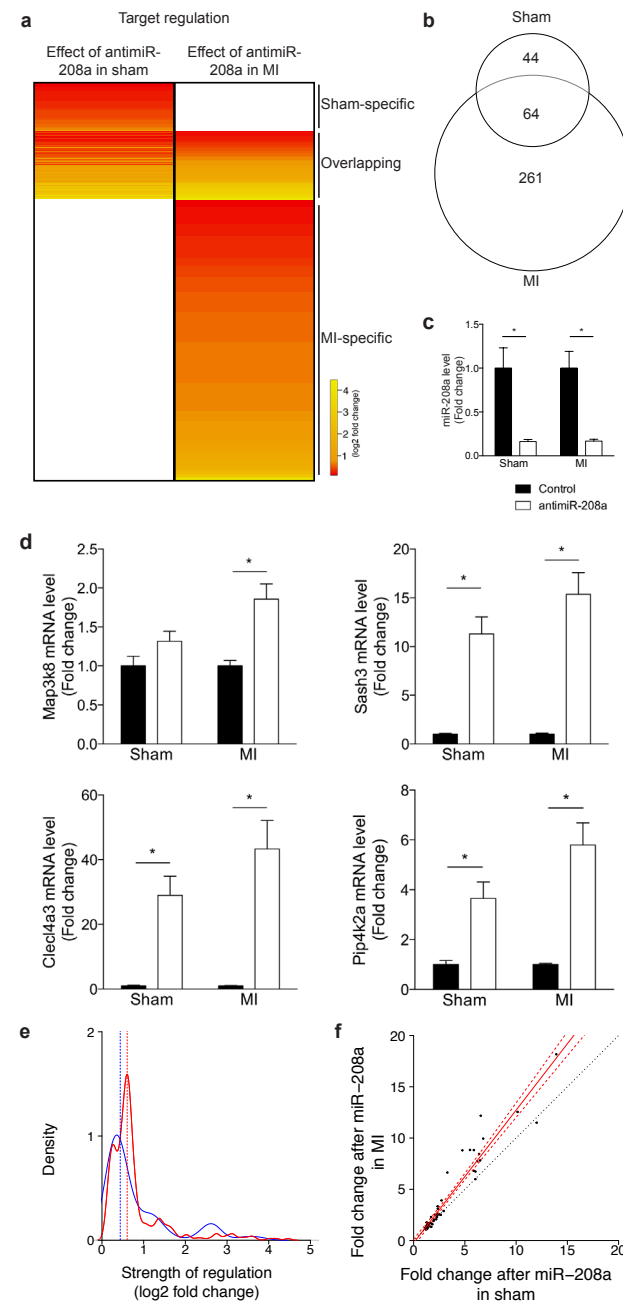
### Statistical analysis

Values are presented as mean ± SEM. Outliers were identified and excluded using a Grubbs test (GraphPad, using α=0.05). Statistical significance was evaluated using an unpaired t-test for comparisons between two groups, using GraphPad Prism software. The kernel density plot was generated using R, as were the regression line and matching confidence interval in Figure 1f. A p-value < 0.05 was considered significant.

## Results

### In vivo effect of anti-miR-208a is more pronounced under stress conditions

Anti-miRs function through the inhibition of a specific miR and thereby have a derepressive effect on the direct targets of this miR. In an effort to explore whether the effect of anti-miR-208a changes under disease conditions, we performed microarray analysis on cardiac tissue from rats treated with either anti-miR-208a or control and searched for mRNAs with a binding site for *miR-208a* that were significantly upregulated in the anti-miR-208a treated group.



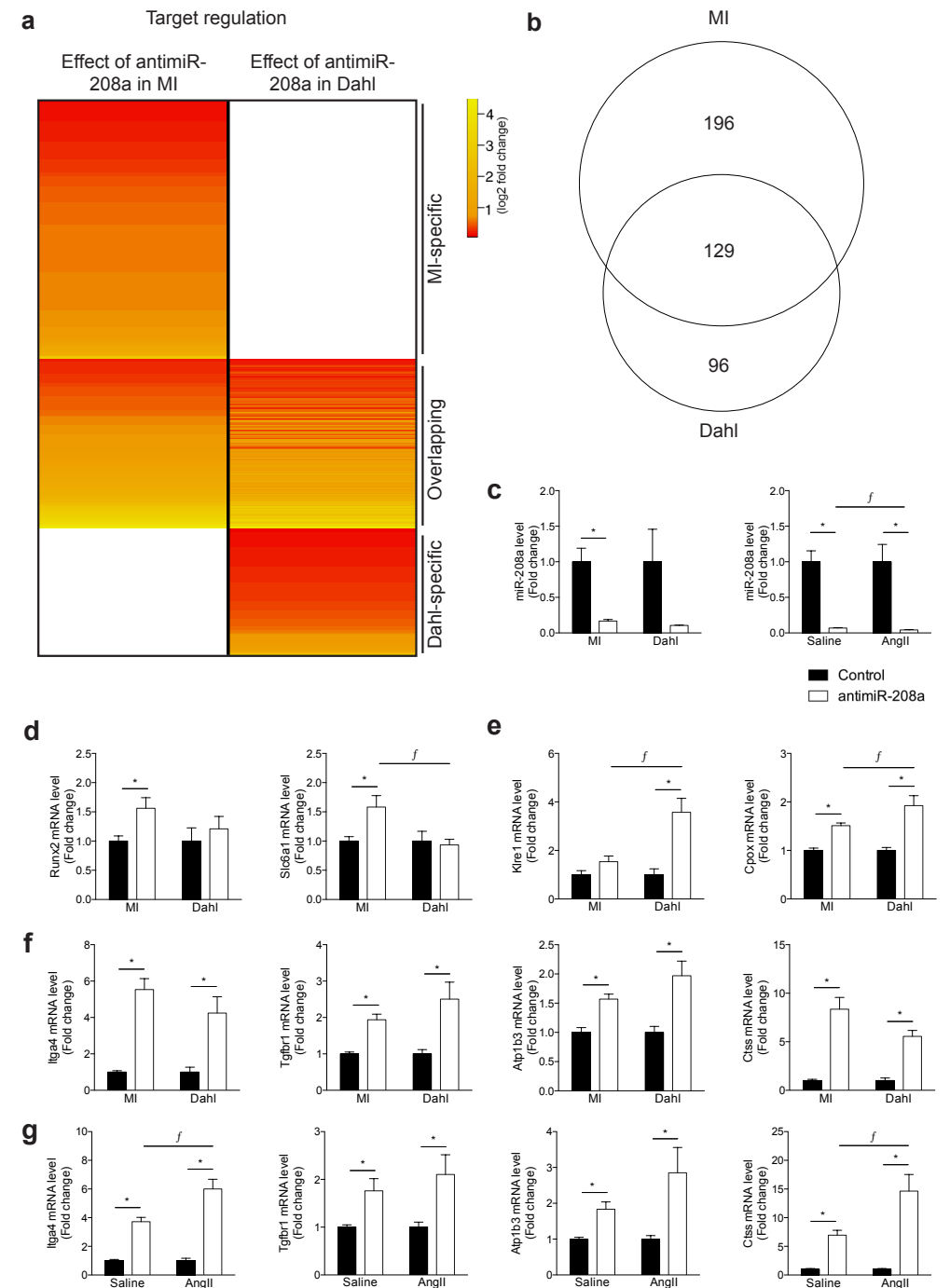
This was done on left ventricular tissue in rats 8 weeks after they were subjected to sham surgery (sham) or myocardial infarction (MI) (n=4 per group). Microarray analysis in the sham rats indicated that anti-miR-208a treatment resulted in the derepression of 108 genes that contained a potential *miR-208a* binding site in their 3' untranslated region compared to control. However, while using the same treatment regime, in the MI group inhibition of *miR-208a* resulted in the

derepression of 325 genes that contain a potential *miR-208a* binding site in their 3' untranslated region. Although 64 of these anti*miR-208a* regulated targets were overlapping in both the sham- and MI-operated rats, a large portion also appeared to be either sham or MI specific (Figure 1a-b, Table II in the online-only Data Supplement\*).

To explore these data in more detail we set out to determine the cardiac level of *miR-208a* in response to both stress and after anti*miR-208a* treatment. The levels of *miR-208a* did not change significantly in response to stress (Supplemental Figure 1). Compared to control, *miR-208a* was significantly inhibited after anti*miR-208a* treatment, with no detectable difference in the level of inhibition between sham or MI (Figure 1c). Real-time PCR analysis for a subset of randomly selected overlapping targets could largely confirm the upregulation of the genes after anti*miR-208a* treatment compared to control in both sham and MI (Figure 1d, Supplemental Figure 2a). This effect was not due to an effect of stress on the expression level of the mRNA targets, since these remained unchanged (Supplemental Figure 2b). Based on our microarray and the real-time PCR data there appeared to be a trend towards a stronger derepression after MI compared to sham (Figure 1a and d). The level of derepression after anti*miR-208a* treatment varied between 1,1 - 13,9 fold change for target genes regulated in the sham group, while this regulation was between 1,1 - 22,1 for the target genes regulated in the MI group. From the array data, we generated kernel density plots for the strength of derepression of the potential targets for both groups (n = 108 and n = 325) and observed a shift to the right for the strength of regulation in the MI group compared to sham, indicating that target derepression was generally stronger in MI than in sham (Figure 1e). We could confirm this observation when comparing the fold change in regulation in the subset of targets regulated in both the sham and MI groups (n = 64) (Figure 1f).

Together, these data indicate that treatment with anti*miR-208a* leads to derepression of more *miR-208a* targets after MI than after sham surgery and that the level of derepression is increased during disease.

**Figure 2. Target derepression is dependent on the type of stress.** (a) Gene array analysis of LV tissue of rats that were subjected to myocardial infarction (MI) or Dahl rats on a high-salt diet, after which both groups were treated with either control or anti*miR-208a*. The heat map expresses the log<sub>2</sub> fold change in expression for the significantly upregulated *miR-208a* targets in anti*miR-208a* treated rats compared to control rats in either MI or Dahl. (b) Venn diagram showing the number of *miR-208a* targets that are significantly upregulated by anti*miR-208a* in either the MI or Dahl rats. (c) Real-time PCR analysis of *miR-208a* showing inhibition after anti*miR-208a* treatment (d) Real-time PCR analysis of *miR-208a* targets shown to be upregulated by gene array after anti*miR-208a* treatment in MI but not in Dahl rats. (e) Real-time PCR analysis of *miR-208a* targets shown to be upregulated by gene array after anti*miR-208a* treatment in Dahl but not in MI rats. (f) Real-time PCR analysis of *miR-208a* targets shown to be upregulated by gene array after anti*miR-208a* treatment in both MI and Dahl rats. (g) Real-time PCR analysis of *miR-208a* targets in rats infused with angiotensin II (AngII) or vehicle (Saline) and treated with anti*miR-208a* or control. In d, e, f and g the data are shown as mean fold change ± SEM and expressed as fold change for MI anti*miR-208a* (n=16-17) over MI control (n=18-19); Dahl anti*miR-208a* (n=6-7) over Dahl control (n=5-6); Saline-infused anti*miR-208a* (n=5-6) over Saline-infused control (n=5-6) or AngII-infused anti*miR-208a* (n=5-6) over AngII-infused control (n=6). \* indicates p<0.05 for anti*miR-208a* treatment versus control treatment; f indicates p<0.05 for anti*miR-208a* treatment between models.



### Target regulation can be dependent on the type of stress

To determine whether the type of stress also influences the targets that are regulated by a miR, we compared the effect of anti*miR-208a* during cardiac remodeling in response to MI to the effect of anti*miR-208a* in Dahl salt-sensitive rats on a high salt diet<sup>34</sup>. Dahl rats develop hypertension and subsequent cardiac remodeling in response to a high-salt diet<sup>34</sup>. Compared to the 325 targets regulated in response to anti*miR-208a* after MI, we found 225 targets to be derepressed in the Dahl rats with a derepression level that varied between 1,1 - 18,3 fold change compared to control (Figure 2a-b, Table III in the online-only Data Supplement<sup>\*</sup>).

Real-time PCR analysis on cardiac tissue after anti*miR-208a* treatment showed a profound inhibition of *miR-208a* for both MI and Dahl hearts (Figure 2c). Of all the 325 regulated targets, 196 targets were specific for rats exposed to MI. Real-time PCR analysis for randomly selected MI-specific target genes confirmed the MI-specific derepression by anti*miR-208a* (Figure 2d, Supplemental Figure 3). Also for the Dahl-specific targets we could validate the derepression by real-time PCR, showing derepression after anti*miR-208a* compared to control (Figure 2e, Supplemental Figure 4). Although microarray analysis indicated these targets to be either MI- or Dahl-specific, real-time PCR analysis actually showed that some targets were also regulated after anti*miR-208a* treatment the other stress group (Figure 2d-e, Supplemental Figure 3a-4a). This observation might be due to the greater sensitivity and the amplification steps of the real-time PCR assay compared to the microarray analysis or the larger number of animals used in the real-time analyses. The random selection of overlapping targets also by real-time PCR showed a strong derepression after anti*miR-208a* compared to control (Figure 2f, Supplemental Figure 5a-b), indicating that these targets are regulated by *miR-208a*, independent of the cause of disease. Indeed, also in Angiotensin II (AngII)-infused rats<sup>35</sup>, another rat model to induce cardiac remodeling, these targets were confirmed to be derepressed after anti*miR-208a* treatment compared to control (Figure 2g, Supplemental Figure 6). Although to a lower extent, the derepression of these selected targets also reached significance in the unstressed (saline) groups treated with anti*miR-208a* (Figure 2g, Supplemental Figure 6), while *miR-208a* inhibition appeared comparable (Figure 2c). Stress by itself appears to influence some of the targets (Supplemental Figure 3b, 4b, 5b and 6b).

These data show that a large portion of targets is consistently regulated across different disease models upon anti*miR-208a* treatment. However, the fact that we can observe derepression for different genes depending on the cause of disease, implies that *miR-208a* also regulates a divergent set of gene targets dependent on the disease etiology.

### AntimiR efficacy is dependent on the level of stress

Next, we aimed to investigate whether the severity of stress also influences the level of target derepression in response to anti*miR* treatment. To this end, we collected tissue from sham hearts and both the remote and infarct region after MI. Since an infarct induces a local injury to cardiac tissue, the area surrounding the damaged area presumably experiences more stress than more remote tissue. Indeed, both *Nppa* and *Myh7*, well-known markers for cardiac stress<sup>36, 37</sup>, were more highly expressed moving from the remote towards the infarcted region, indicating a gradient of stress exposure in these different regions (Figure 3a). Real-time PCR analysis of the level of *miR-208a* shows a profound *miR-208a* repression in cardiac tissue of Sham rats and the remote and infarct regions of MI rats in response to anti*miR-208a* treatment.

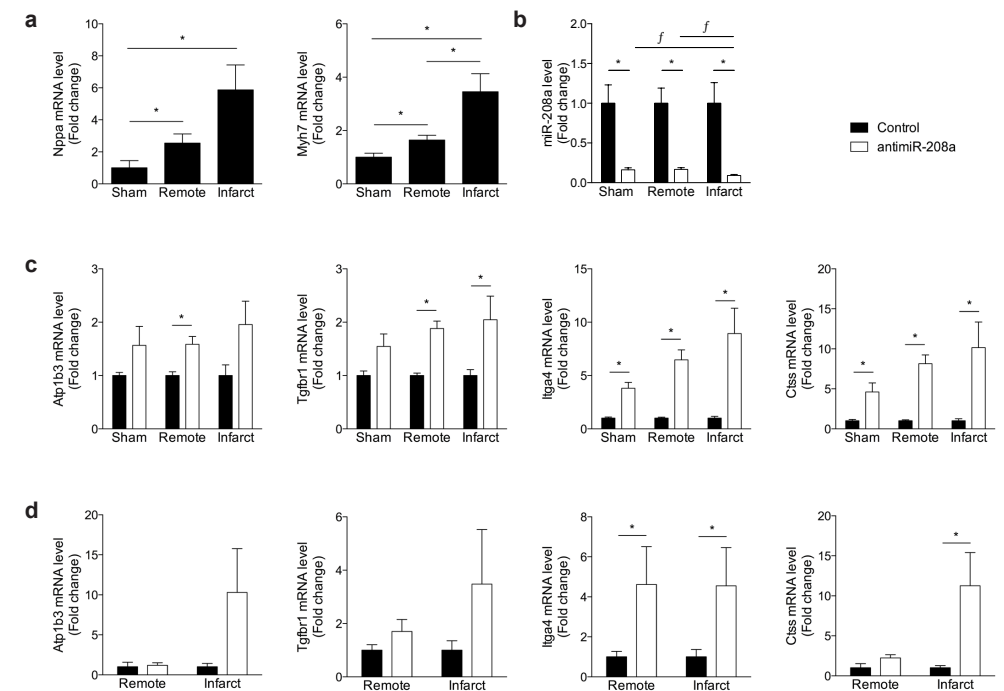
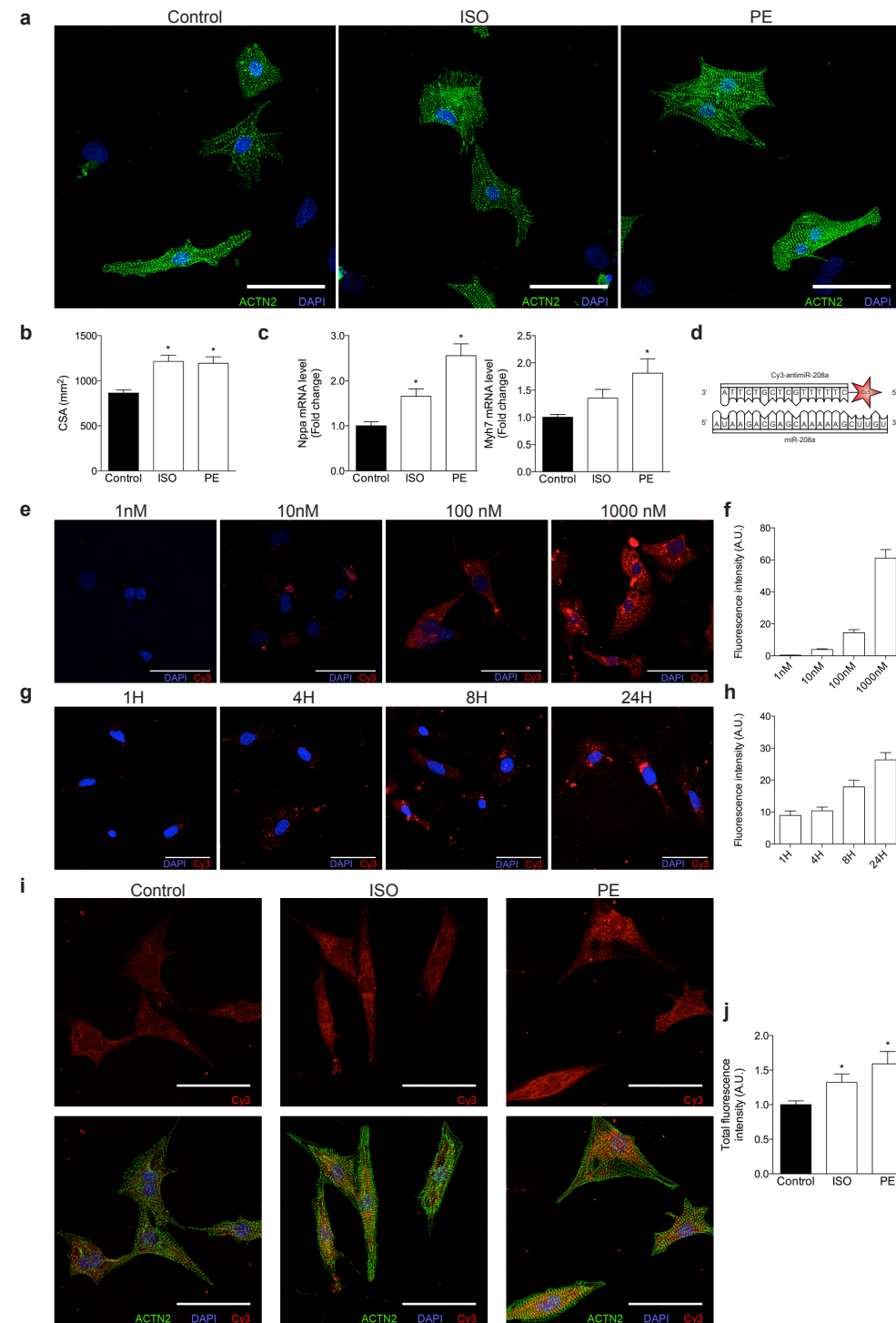


**Figure 3. AntimiR efficacy depends on the level of stress.** (a, b) Real-time PCR analysis of cardiac stress markers (a), *miR-208a* levels (b) or *miR-208a* target genes (c) on LV tissue from sham-operated rats (Sham) or different regions of MI-operated rats (Remote, Infarct) after control or anti*miR-208a* treatment. (d) Real-time PCR analysis of *miR-208a* target genes on LV tissue from different regions of infarcted pig hearts (Remote, Infarct) after control or anti*miR-208a* treatment. Data are shown as mean fold change  $\pm$  SEM and expressed as fold change for Sham anti*miR-208a* (n=6-7) over Sham control (n=5-6); MI remote anti*miR-208a* (n=15-17) over MI remote control (n=17-19); MI infarct anti*miR-208a* (n=15-17) over MI infarct control (n=17-19) or pig IR remote anti*miR-208a* (n=3-4) over pig IR remote control (n=6-7), and pig IR infarct anti*miR-208a* (n=3-4) over pig IR infarct control (n=5-6). \* indicates  $p < 0.05$  for anti*miR-208a* treatment versus control treatment.

Additionally, the *miR-208a* reduction in the infarct region was significantly bigger compared to the remote region or sham hearts (Figure 3b). While it did not reach statistical significance, the strength of regulation of the analyzed targets appeared to be trending to increase with an increasing level of stress (Figure 3c, Supplemental Figure 7). A comparable analysis in cardiac tissue from pig hearts exposed to ischemia reperfusion (IR) indicated that the *miR-208a* targets were conserved across species and the trend in larger derepression in the infarcted compared to the remote region was also observed in larger animals (Figure 3d, Supplemental Figure 8). Together, these data suggest that the level of stress influences the level of target derepression after anti*miR-208a* treatment and that target derepression for this subset of these genes is conserved in a large animal model of MI.

### Cellular uptake of anti*miR* changes under stress conditions

In an effort to explore the mechanism behind the increased target derepression under stress conditions, we used neonatal rat ventricular myocytes (NRVM) exposed to isoproterenol or phenylephrine, both known inducers of cardiomyocyte hypertrophy (stress)<sup>38</sup>. Cell size quantification confirmed the presence of cardiomyocyte hypertrophy in response to both ISO and



PE (Figure 4a-b). The increase in cell size corresponded to an increase in the expression of the cardiac stress markers *Nppa* and *Myh7*, indicating cardiomyocyte stress (Figure 4c). To be able to track anti-miR-208a *in vitro*, we treated NRVM with a Cy3-labeled anti-miR-208a (Figure 4d). To replicate *in vivo* therapy as best we could, no transfectants were used to aid uptake of the anti-miR.

Fluorescence intensity of individual cells was used as a measure of uptake of the labeled anti-miR. Fluorescence intensity increased upon treatment with increasing doses (Figure 4e-f) or increased incubation time (Figure 4g-h). While uptake was detected in unstressed cardiomyocytes, the cells appeared to take up more anti-miR under conditions of stress (Figure 4i). Quantification of uptake by measuring total cellular fluorescence revealed a significantly increased uptake in response to both stresses (Figure 4j). These data imply that an increase in cellular uptake with stress might be partially responsible for an increase in target derepression under disease conditions.

## Discussion

Anti-miRs have shown to be efficacious in establishing therapeutic benefit under multiple disease conditions. Mouse genetics has shown us that miR functions are often more pronounced during disease, and that the regulated mRNA targets can depend on the disease condition<sup>39</sup>. Also oligo-based miR inhibition has shown comparable effects. Independent of the anti-miR chemistry used (either antagomirs or LNA-modified anti-miRs) or tissue studied, several cases have been reported where there was a larger effect on specific target depression under conditions of stress<sup>40-42</sup>. However, so far, these observations have remained unstudied and it is unknown whether the effect of stress on anti-miR efficacy is a common phenomenon and/or whether the level and type of stress influences anti-miR function. To answer this research question *in vivo* we used an anti-miR, specifically targeting *miR-208a*. The cardiomyocyte-restricted expression of *miR-208a* prevents any interfering effects of cellular differences in target regulation, providing a clean experimental model to study the effect on target regulation by anti-miR-208a.

**Figure 4. Stress influences cellular uptake of anti-miRs in neonatal rat ventricular myocytes (NRVMs).** (a) NRVMs stained for ACTN2 after treatment with or without iso-proterenol or phenyl-ephrine for 24 hours. (b) Quantification of cross-sectional area (CSA) of NRVMs in the presence or absence of ISO or PE (Per condition 5-6 biological samples were generated, and per samples  $\pm 22-41$  cells were quantified). (c) Real-time PCR analysis of stress marker expression in NRVMs in the presence or absence of ISO or PE (n=6 per condition). (d) Schematic representation of *miR-208a* and the Cy3-labeled anti-miR-208a. (e) Fluorescent images of NRVMs treated with increasing doses of Cy3-anti-miR-208a for 24 hours (f) Quantification of Cy3 signal at different concentrations of anti-miR-208a. (g) Fluorescent images of NRVMs treated with 1 μM Cy3-anti-miR-208a for different time periods. (h) Quantification of Cy3 signal at different time points after 1 μM Cy3-anti-miR-208a (i) Fluorescent images of NRVMs that were either left untreated or stimulated with ISO or PE for 8 hrs after which they received 1 μM Cy3-anti-miR-208a (j) Quantification of total fluorescence (fluorescence intensity corrected for cell size, n=8-12). Data is represented as mean fold change  $\pm$  SEM. \* indicates p<0.05 for anti-miR-208a treatment versus control treatment. Scale bars in all images are 50 μm.

Our data indicate that anti-miR treatment under diseased conditions results in derepression of a larger number of target genes than anti-miR treatment under baseline conditions. Additionally, we show that the strength of target regulation is increased during stress in rats, which we can confirm in a porcine model of ischemic injury.

There are many potential explanations for our observations. The impact of stress on anti-miR efficacy might be due to a change in anti-miR activity or a direct effect of stress on target regulation. Stress might increase *miR-208a* inhibition by an increase in cellular uptake of anti-miR-208a, endosomal escape of anti-miR-208a, a change in cellular localization of either the anti-miR or miRNA that changes their interaction or even an expressional change in lncRNAs during stress that might influence the effect of the anti-miR by changing the cellular level of *miR-208a*.

The effect of a miR on its target depends on the ratio of miR to target<sup>43</sup> and is cell and context dependent<sup>44</sup>. Both a change in mRNA transcripts available to target by the miR as well as a change in miR activity could be responsible for the increased number of genes that are regulated during disease<sup>45</sup>. Disease might trigger an increase in expression of miR target genes, which thereby become susceptible to and available for miR regulation. In parallel it might also be caused by a change in miR function (abundance or activity) that is directing the increased number of gene targets that are being regulated during disease. Other possible explanations are that the efficiency of target regulation improves due to a change in secondary structure of the target region, a change in efficiency of RISC loading, or an effect of stress on the cellular localization of both the miR or the mRNA. Obviously, it could also very well be a combination of these proposed mechanisms which might additionally be miR or target dependent. While these aspects deserve further investigation, we know that *miR-208a* levels, because it is co-expressed with *Myh6*, remain unchanged or even decrease under conditions of disease, so *miR-208a* abundance is not the explanation in this particular study.

Although the anti-miRs are highly specific in targeting a miR, we can currently not exclude that the difference in target regulation is also partly due to a change in abundance of additional miRs that can also regulate the measured transcripts.

While the level of target regulation is likely also under the influence of mRNA abundance and activity of the miR itself, our *in vitro* data show that the stronger effect of anti-miR treatment under diseased conditions could potentially also be due to an enhanced uptake of the compounds when the cells become stressed. Several attempts to confirm this *in vivo* by injecting labeled anti-miR-208a failed, likely due to inefficient targeting of the heart.

Our study also showed that the genes that are derepressed by an anti-miR partially depend on the disease-driver. This effect is probably due to the fact that the target miR is regulating a different gene set when divergent signaling pathways and genes are activated in response to different stressors. Hypertension-induced cardiac remodeling will activate a different gene program than cardiac remodeling in response to MI. Therefore, it seems fair to assume that the divergence in gene regulation due to the presence of stress or under different disease conditions is largely due to the availability of the mRNA targets present in the cells.

In order to demonstrate efficacy of target engagement by anti-miRs *in vivo*, it is necessary to measure target derepression. While miR-induced changes in gene expression can both occur at the mRNA and protein level, the majority of changes occur due to mRNA destabilization<sup>46</sup>. The average level of target regulation is normally modest and ranges between 20-50% change in

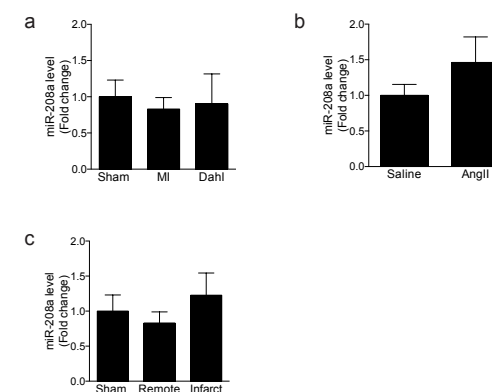
mRNA, making it difficult to determine significant changes above naturally occurring variation in gene expression<sup>47, 48</sup>. Additionally, proteomic studies in response to miR modulation have reported that the average changes in protein levels of miR targets are less than two-fold following miR inhibition<sup>49, 50</sup>. While our microarray data confirmed this level of regulation for the majority of the targets, our real-time PCR data indicated a greater fold change after anti-miR-208a treatment. It is currently unknown whether this increase in fold regulation is introduced by our experimental set-up. Nonetheless, real-time PCR analysis did confirm the derepression of most targets identified by microarray.

While the exact mechanisms of enhanced target regulation under diseased conditions remains to be defined, our observations could have far reaching implications for the clinical use of anti-miRs as novel therapeutics. The stronger pharmacological effects of anti-miRs during disease and the fact that disease etiology determines the therapeutic outcome of an anti-miR, will be important for assessing the therapeutic dose and predicting the therapeutic effect in patients. While this is important information to take along in developing an optimal therapy, both the importance of miRs and the potency of anti-miRs supports enthusiasm for further pursuing these gene expression regulators as novel therapeutic candidates.

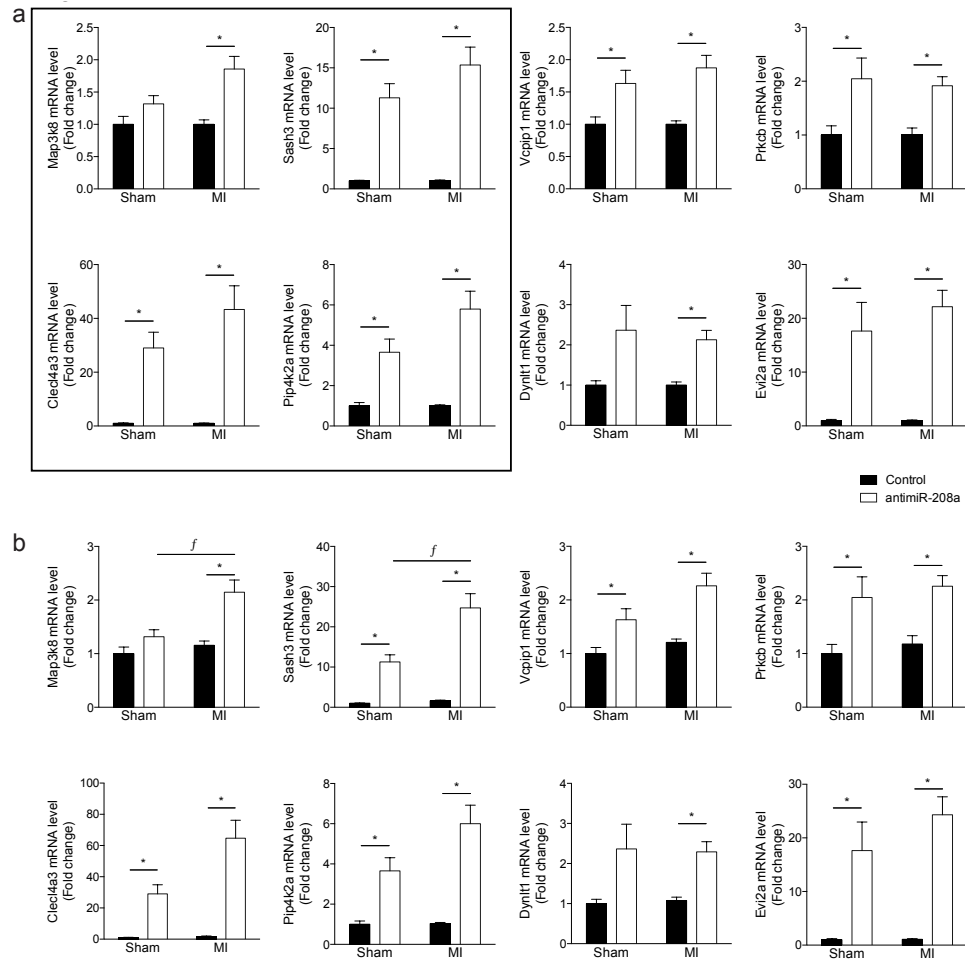
## Acknowledgements

We would like to thank Anko de Graaff and the Hubrecht Imaging Center for supporting the imaging. We gratefully acknowledge Catherine Rabouille for advice on confocal imaging and the cell culture experiments.

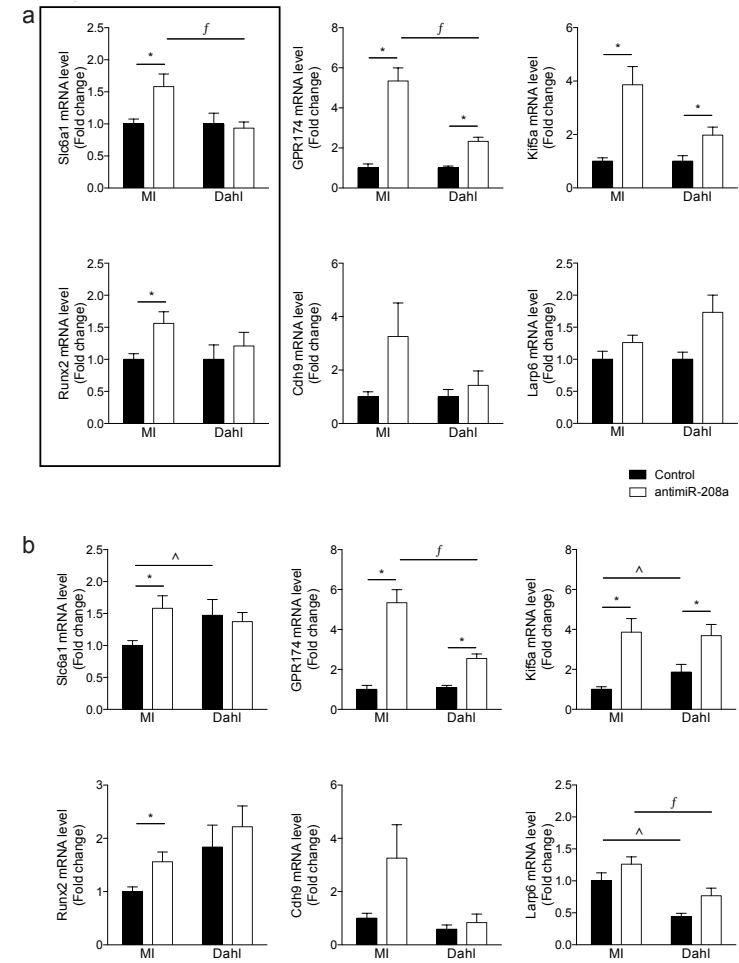
## Supplemental materials



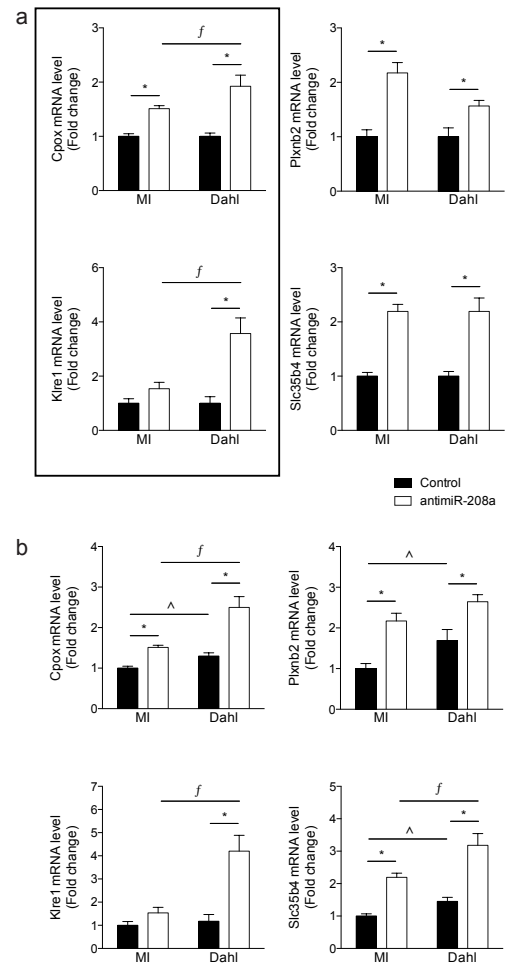
**Supplemental Figure 1. Real-time PCR analysis for *miR-208a* on LV tissue in (a) sham rats, MI rats and Dahl rats, (b) saline- and AngII-infused rats, (c) sham-operated rats (Sham) or different regions of MI-operated rats (Remote, Infarct). Data are expressed as mean fold change  $\pm$  SEM for Sham control (n=6), MI control (n=18), Dahl control (n=6), saline control (n=6), AngII control (n=6), MI remote control (n=18) and MI infarct control (n=19).**



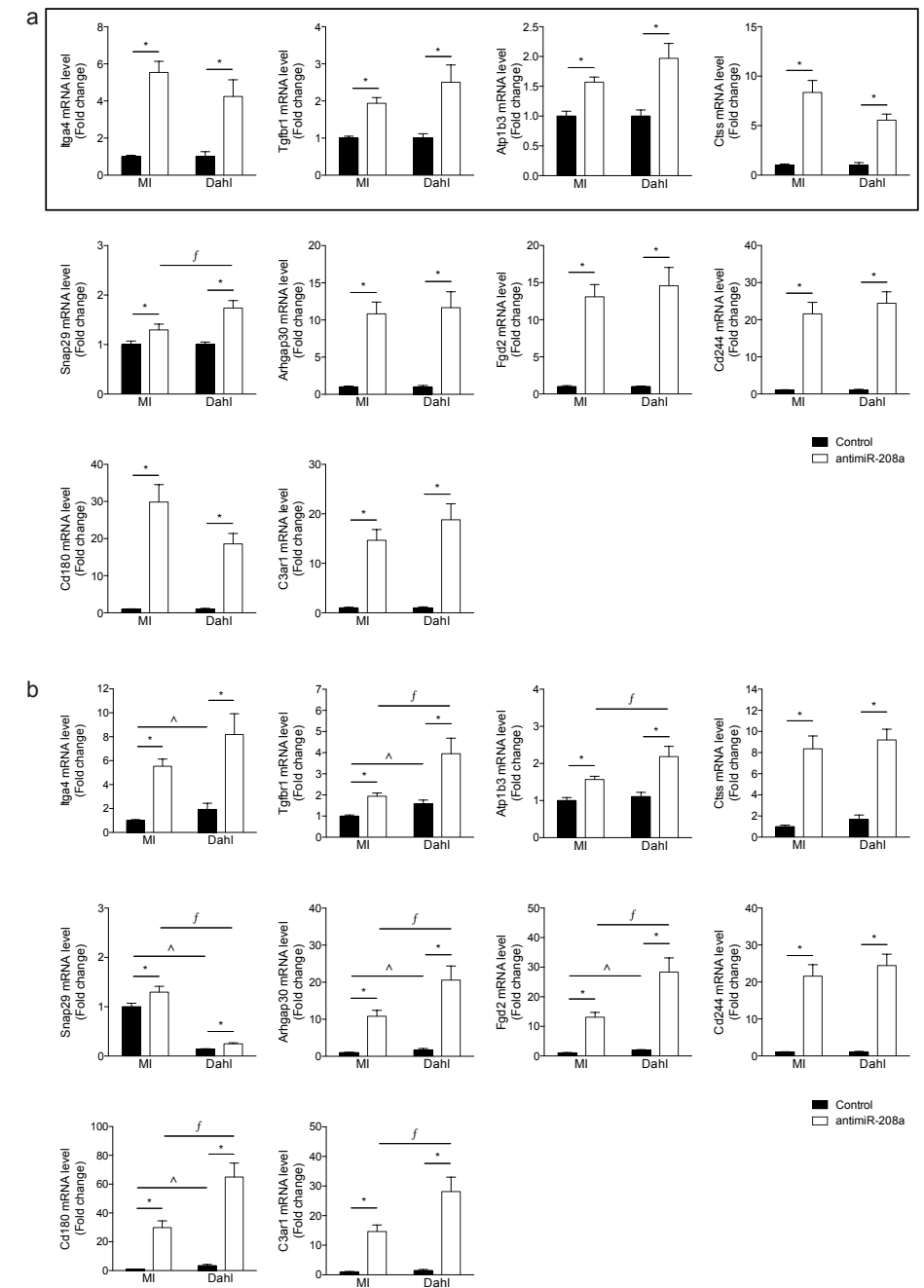
**Supplemental Figure 2. Real-time PCR analysis of derepressed *miR-208a* targets in both Sham and MI hearts.** Real-time PCR analysis of *miR-208a* targets shown to be upregulated by gene array after anti*miR-208a* treatment in both MI and sham surgery. **(a)** Data are expressed as mean fold change  $\pm$  SEM for Sham anti*miR-208a* (n=6) over Sham control (n=6) and MI anti*miR-208a* (n=16-17) over MI control (n=18-19). **(b)** Data are expressed as mean fold change  $\pm$  SEM for Sham anti*miR-208a* (n=6), MI control (n=18-19) and MI anti*miR-208a* (n=16-17) over Sham control (n=6). \* indicates  $p < 0.05$  for anti*miR-208a* treatment versus control treatment. Boxed graphs were shown in main figure 1d.



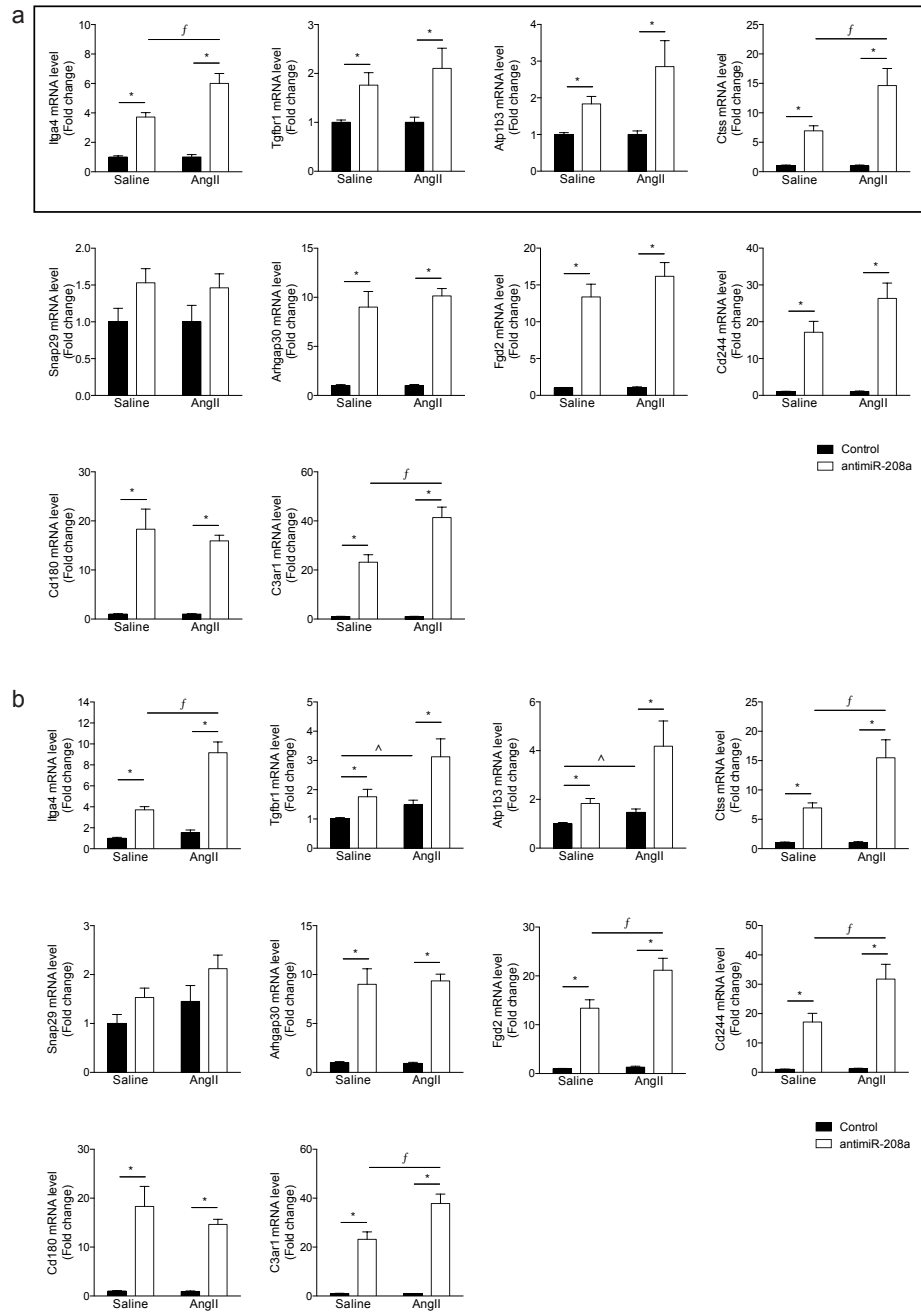
**Supplemental Figure 3. Real-time PCR analysis of *miR-208a* targets derepressed under MI stress, but not in Dahl stress.** Real-time PCR analysis of *miR-208a* targets shown to be upregulated by gene array after anti*miR-208a* treatment after MI surgery but not in Dahl rats. **(a)** Data are expressed as mean fold change  $\pm$  SEM for Dahl anti*miR-208a* (n=6-7) over Dahl control (n=5-6) and MI anti*miR-208a* (n=16-17) over MI control (n=18-19). **(b)** Data are expressed as mean fold change  $\pm$  SEM for MI anti*miR-208a* (n=16-17), Dahl control (n=5-6) and Dahl anti*miR-208a* (n=6-7) over MI control (n=18-19). \* indicates  $p < 0.05$  for anti*miR-208a* treatment versus control treatment; *f* indicates  $p < 0.05$  for anti*miR-208a* treatment between models. Boxed graphs were shown in main figure 2d.



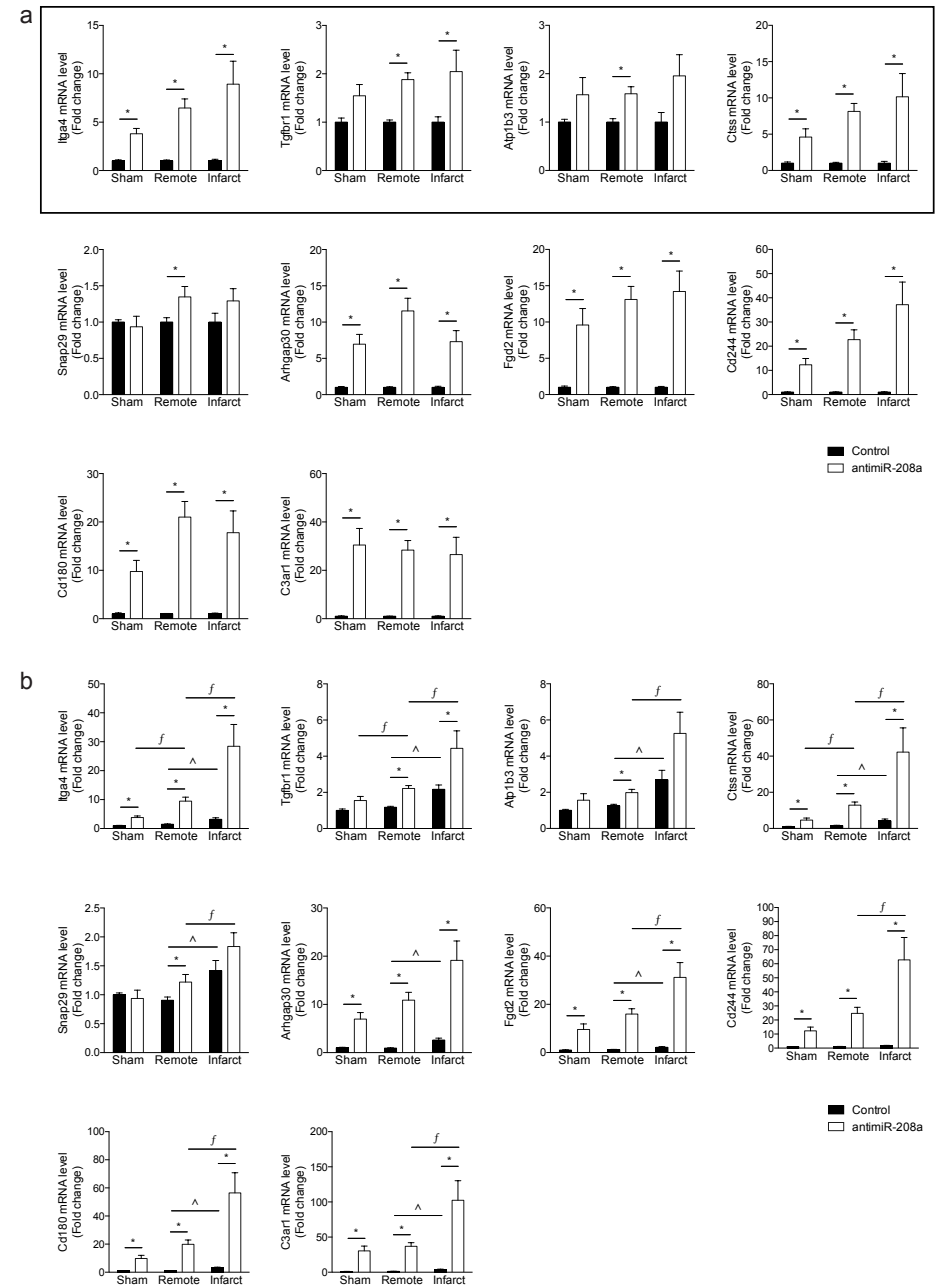
**Supplemental Figure 4. Real-time PCR analysis of *miR-208a* targets derepressed under Dahl stress, but not in MI stress.** Real-time PCR analysis of *miR-208a* targets shown to be upregulated by gene array after anti*miR-208a* treatment in Dahl rats, but not after MI surgery. **(a)** Data are expressed as mean fold change  $\pm$  SEM for Dahl anti*miR-208a* (n=6-7) over Dahl control (n=5-6) and MI anti*miR-208a* (n=15) over MI control (n=16-19). **(b)** Data are expressed as mean fold change  $\pm$  SEM for MI anti*miR-208a* (n=15), Dahl control (n=5-6) and Dahl anti*miR-208a* (n=6-7) over MI control (n=16-19). \* indicates  $p < 0.05$  for anti*miR-208a* treatment versus control treatment; *f* indicates  $p < 0.05$  for anti*miR-208a* treatment between models. Boxed graphs were shown in main figure 2e.



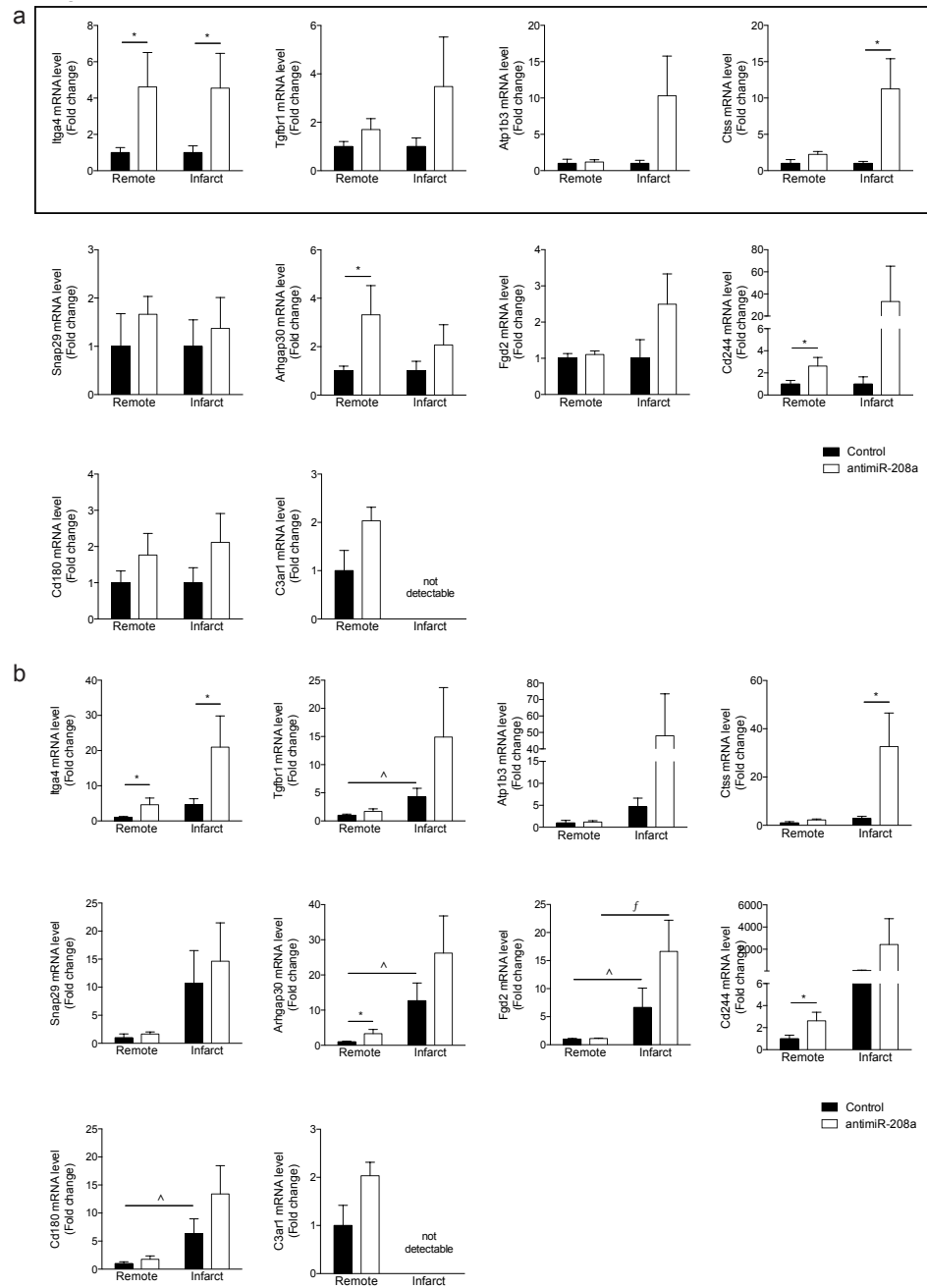
**Supplemental Figure 5. Real-time PCR analysis of *miR-208a* targets derepressed in both Dahl stress and MI stress.** Real-time PCR analysis of *miR-208a* targets shown to be upregulated by gene array after anti*miR-208a* treatment both after MI surgery and in Dahl rats. **(a)** Data are expressed as mean fold change  $\pm$  SEM for Dahl anti*miR-208a* (n=6-7) over Dahl control (n=5-6) and MI anti*miR-208a* (n=15-17) over MI control (n=17-19). **(b)** Data are expressed as mean fold change  $\pm$  SEM for MI anti*miR-208a* (n=15-17), Dahl control (n=5-6) and Dahl anti*miR-208a* (n=6-7) over MI control (n=17-19). \* indicates  $p < 0.05$  for anti*miR-208a* treatment versus control treatment; *f* indicates  $p < 0.05$  for anti*miR-208a* treatment between models. Boxed graphs were shown in main figure 2f.



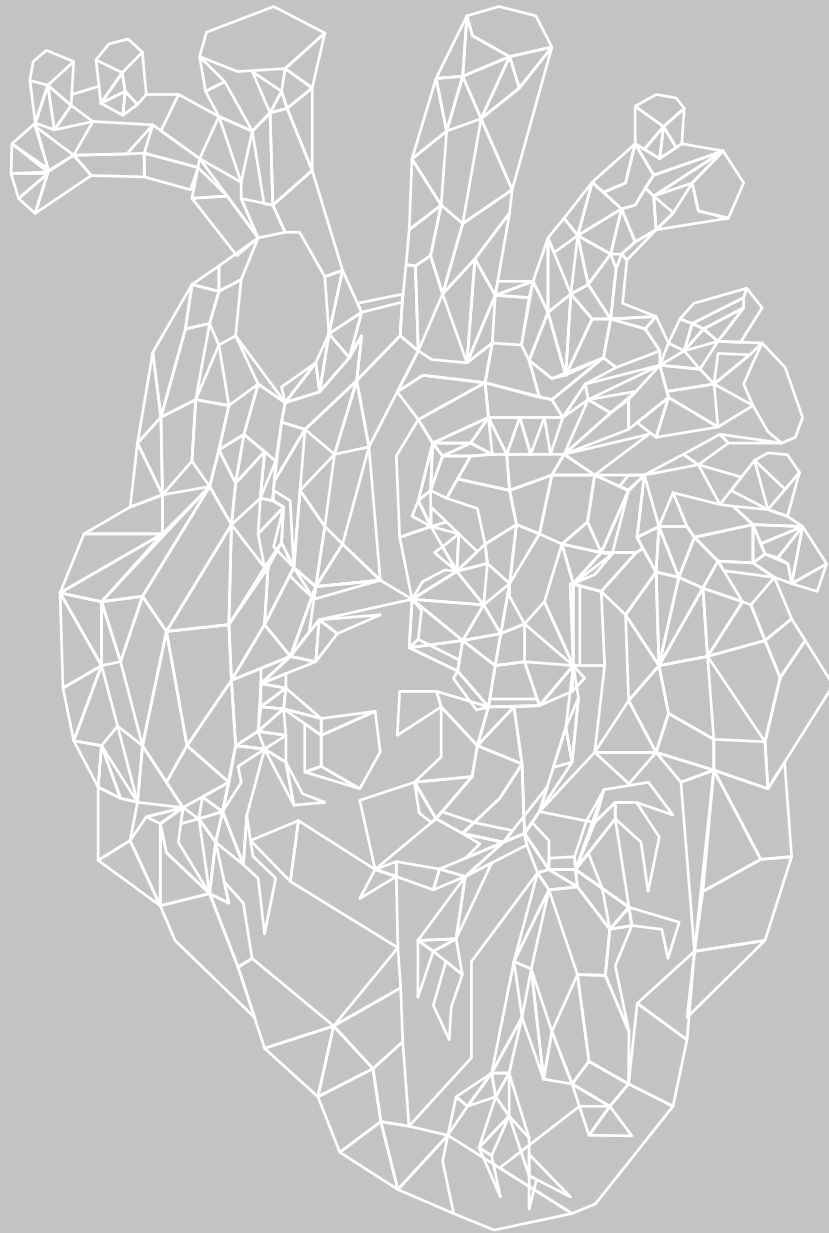
**Supplemental Figure 6. Real-time PCR analysis of *miR-208a* targets in a rat model of Angiotensin II-induced cardiac stress.** Real-time PCR analysis of *miR-208a* targets shown to be upregulated after anti*miR-208a* treatment both after MI surgery and in Dahl rats, determined in rats subjected to Angiotensin II or vehicle (Saline) infusion prior to treatment with anti*miR-208a* or control. **(a)** Data are expressed as mean fold change  $\pm$  SEM for saline anti*miR-208a* (n=5-6) over saline control (n=5-6) and AngII anti*miR-208a* (n=5-6) over AngII control (n=5-6). **(b)** Data are expressed as mean fold change  $\pm$  SEM for saline anti*miR-208a* (n=5-6), AngII control (n=5-6) and AngII anti*miR-208a* (n=5-6) over saline control (n=5-6). \* indicates  $p < 0.05$  for anti*miR-208a* treatment versus control treatment; *f* indicates  $p < 0.05$  for anti*miR-208a* treatment between saline and AngII. Boxed graphs were shown in main figure 2g.



**Supplemental Figure 7. Real-time PCR analysis of *miR-208a* targets in different regions of infarcted rat hearts.** Real-time PCR analysis of *miR-208a* targets shown to be upregulated after anti*miR-208a* treatment both after MI surgery and in Dahl rats, determined in sham-operated hearts or different regions of the MI-operated hearts (Remote, Infarct) after control or anti*miR-208a* treatment. **(a)** Data are expressed as mean fold change  $\pm$  SEM for Sham anti*miR-208a* (n=6-7) over Sham control (n=5-6), MI remote anti*miR-208a* (n=15-17) over MI remote control (n=17-19), and MI infarct anti*miR-208a* (n=15-17) over MI infarct control (n=17-19). **(b)** Data are expressed as mean fold change  $\pm$  SEM for Sham anti*miR-208a* (n=6-7), MI remote control (n=17-19), MI remote anti*miR-208a* (n=15-17), MI infarct control (n=17-19) and MI infarct anti*miR-208a* (n=15-17) over Sham control (n=5-6). \* indicates  $p < 0.05$  for anti*miR-208a* treatment versus control treatment. Boxed graphs were shown in main figure 3c.



**Supplemental Figure 8. Real-time PCR analysis of *miR-208a* targets in different regions of infarcted pig hearts.** Real-time PCR analysis of *miR-208a* targets shown to be upregulated after anti*miR-208a* treatment both after MI surgery and in Dahl rats, determined in different regions (Remote, Infarct) of pig hearts subjected to ischemia-reperfusion injury with subsequent control or anti*miR-208a* treatment. **(a)** Data are expressed as mean fold change  $\pm$  SEM for IR remote anti*miR-208a* (n=3-4) over IR remote control (n=6-7), and IR infarct anti*miR-208a* (n=3-4) over IR infarct control (n=5-6). **(b)** Data are expressed as mean fold change  $\pm$  SEM for IR remote anti*miR-208a* (n=3-4), IR infarct control (n=5-6) and IR infarct anti*miR-208a* (n=3-4) over IR remote control (n=6-7). \* indicates p<0.05 for anti*miR-208a* treatment versus control treatment. Boxed graphs were shown in main figure 3d.



# Chapter 3

## Hydrogel-Based Delivery of antimiR-195 Improves Cardiac Efficacy After Ischemic Injury

Joep E.C. Eding MD<sup>\*§</sup>, Marta Vigil-Garcia MSc<sup>\*§</sup>, Marit Vink MSc<sup>\*</sup>,  
Charlotte J. Demkes PhD<sup>\*†</sup>, Danielle Versteeg BSc<sup>\*†</sup>, Lieneke  
Kooijman BSc<sup>\*</sup>, Maarten H. Bakker PhD<sup>‡</sup>, Maaïke J.G.  
Schotman MSc<sup>‡</sup>, Patricia Y.W. Dankers PhD<sup>‡</sup>,  
Eva van Rooij PhD<sup>\*†</sup>

<sup>§</sup> These authors contributed equally to this work

<sup>\*</sup>Hubrecht Institute, KNAW and University Medical Center Utrecht, Utrecht, the Netherlands

<sup>†</sup> Department of Cardiology, University Medical Center Utrecht, Utrecht, the Netherlands

<sup>‡</sup> Institute for Complex Molecular Systems, Department of Biomedical Engineering,  
Laboratory of Chemical Biology, Eindhoven University of Technology,  
Eindhoven, the Netherlands

## Abstract

**Background.** MicroRNAs (miRs) are potent regulators of biology and disease. The *miR-15* family has been shown to regulate cardiomyocyte proliferation and antimiR-based inhibition induces a cardioprotective effect after myocardial infarction in mice. However, systemic delivery of antimiRs leads to accumulation in kidneys and liver, with relatively poor cardiac exposure. pH-responsive injectable hydrogels serve as a sustained-release drug delivery depot and could potentially be used to improve cardiac efficacy of antimiR therapeutics.

**Objective.** Examine whether hydrogel can improve local delivery of antimiR-195 in ischemic hearts to increase cardiac efficacy and limit off-target effects.

**Methods.** Study the effect of intramyocardial injections of hydrogel-formulated antimiR-195 under both baseline conditions and after ischemic injury.

**Results.** Intracardiac injections of UPy-PEG induced a transient inflammatory response that was no longer present 7 days post-injection. *In vitro* experiments showed that antimiR-195 was released from the gel, and induced microRNA inhibition leading to downstream cardiomyocyte proliferation. *In vivo*, intramyocardial delivery of antimiR-195 in UPy-PEG enhanced cardiac target de-repression compared to PBS-dissolved antimiR-195, despite a low cardiac retention. After ischemic injury, this translated into a greater therapeutic effect by increasing both target de-repression and cardiomyocyte proliferation.

**Conclusions.** UPy-PEG can be used as a cardiac delivery vehicle of antimiRs and intramyocardial injection of UPy-PEG formulated antimiR-195 is sufficient to improve cardiac efficacy of antimiR-195. Follow up experiments in large animals will enable us to assess the true added value of using UPy-PEG to increase cardiac exposure of antimiR therapies.

## Introduction

Ischemic heart disease is one of the leading causes of death worldwide. Given the very limited endogenous proliferative capacity of adult human cardiomyocytes<sup>19</sup>, the cardiomyocytes lost during myocardial infarction will not be regenerated to a meaningful extent. This loss of functional myocardium then activates maladaptive remodeling processes that put the patient at risk of developing heart failure<sup>53</sup>. Replacement of the lost cells by stem cell transplantation has shown promise in preclinical trials<sup>54</sup>. However, as it does not seem to restore cardiac function in clinical trials<sup>55</sup>, the hope is that novel therapeutic strategies promoting the endogenous regenerative capacity of the myocardium will offer a solution.

MicroRNAs (miRs) are short, single-stranded oligonucleotides that suppress protein formation post-transcriptionally by binding to complementary sequences in the mRNA. They have been shown to have an important role in both cardiac pathophysiology, like hypertrophy<sup>31</sup> and fibrosis<sup>23</sup>, as well as non-cardiac diseases like cancer<sup>56</sup>. Several strategies have been developed to either replace or inhibit pathologically regulated miRs<sup>57</sup>, and are currently being tested in clinical studies<sup>58-60</sup>.

The *miR-15* family is a group of 5 miRs (*miR-15a*, *miR-15b*, *miR-16*, *miR-195* and *miR-497*) that share the same seed region, the region of the miR that governs mRNA targeting based on sequence complementarity<sup>61</sup>. The *miR-15* family has been shown to induce a strong inhibition of the cell cycle<sup>62,63</sup>. Inhibition of the *miR-15* family with subcutaneously delivered antimiR has been shown to reduce infarct size in murine myocardial infarction (MI)<sup>24,64</sup>. However, as true for most antimiRs, most of the injected compound ended up in the kidneys and liver<sup>24</sup>, reducing cardiac exposure and increasing the chance of unwanted side effects.

Previous studies have proven the benefit of using hydrogels as an injectable vehicle to improve local delivery and reduce the risk of off-target effects by a local sustained-release drug delivery depot after intramyocardial injection. Burdick and co-workers developed an injectable hyaluronic acid based-hydrogel system<sup>65</sup>, which provided a sustained release of *miR-302* which promoted proliferation of cardiomyocytes. Another example was shown by Christman and co-workers where a hydrogel based on decellularized ECM was used to modulate the release rate of miRs and extracellular vesicles *in vitro*<sup>66</sup>.

Koudstaal et al. pioneered the use of UPy-PEG hydrogel as a catheter-injectable sustained-release drug delivery depot for effective intramyocardial delivery of IGF1/HGF in a porcine model of myocardial infarction<sup>67</sup>. This supramolecular hydrogel is based on the ureido-pyrimidinone moiety, which forms dimers due to the four-four hydrogen bonding moiety. Furthermore, fiber formation is induced by lateral stacking of the urea-groups present in the backbone. While no adverse effects of UPy-PEG injection were observed, the study was not geared towards assessing safety of UPy-PEG for intramyocardial drug delivery in pigs.

Here, we investigate the use of UPy-PEG and a cationic charged UPy-PEG (UPy-Cat) for cardiac delivery of antimiR-195 to enhance cardiac repair after injury. Our data show that, despite low cardiac retention, the use of UPy-PEG for intramyocardial drug delivery is relatively safe and improves antimiR efficacy over delivery in PBS. These findings set the stage for future research in larger animal models and may aid the development of a novel therapeutic strategy to promote the endogenous regenerative capacity of the heart.



## Materials & Methods

Extended materials and methods are available in the online-only Data Supplement\*.

**Mice.** All animal studies were performed in accordance with institutional guidelines and regulations of the Animal Welfare Committee of the Royal Netherlands Academy of Arts and Sciences. All animal experiments were performed on adult C57Bl/6J male mice from Charles River Laboratories (8-9 weeks of age).

**Surgery.** Mice were anesthetized using Ketamine/Xylazine, intubated and ventilated. For permanent LAD ligation MI, a 7-0 silk suture was tied around the LAD. For ischemia-reperfusion injury<sup>68</sup> a similar procedure was followed but the ligature was cut after 60 minutes. Intramyocardial injections were performed using Hamilton syringes with custom 31G 30° beveled needles.

**Echocardiography.** Cardiac function and dimensions were evaluated by 2-dimensional echocardiography using a Vevo® 2100 Ultrasound system (Visual Sonics), under isoflurane anesthesia.

**RNA-Sequencing.** The TRUseq stranded mRNA kit (Illumina) was used to prepare libraries from LV RNA samples, sequenced with 75bp read-length with Illumina NextSeq500 by the Utrecht Sequencing Facility. Reads were mapped to the mouse genome (GRCm38) and data was analyzed with DESeq2.

**AntimiR design.** AntimiR-195 was designed and synthesized by miRagen®. It is an LNA/DNA mixmer: a 16-mer complementary to *miR-195* and partially complementary to the remaining *miR-15* family members (Figure 1A).

**Anti-PEG ELISA.** Quantification of hydrogel retention using Anti-PEG ELISA was done using antibodies obtained from Academia Sinica, according to an optimized version of the manufacturer's protocol.

**Neonatal rat ventricular myocyte (NRVM) isolation.** Neonatal rat ventricular cardiomyocyte (NRVM) cultures were isolated by enzymatic dissociation of neonatal rat hearts, as described previously<sup>69</sup>.

**Statistical analysis.** Values are presented as mean ± SEM. Outliers were identified, and subsequently excluded, using Grubbs' test<sup>70</sup> (GraphPad). Statistical significance was evaluated using one-way ANOVA (GraphPad) or two-way ANOVA (R), followed by post-hoc tests with correction for multiple testing according to the Benjamini-Hochberg procedure. \*, \*\*, \*\*\*, \*\*\*\* indicate  $p < 0.05$ ,  $< 0.01$ ,  $< 0.001$ ,  $< 0.0001$  compared to empty vehicle, respectively. †, ††, †††, †††† indicate  $p < 0.05$ ,  $< 0.01$ ,  $< 0.001$ ,  $< 0.0001$  for UPy-PEG compared to PBS, respectively.

## Results

### The *miR-15* family is induced after ischemic injury and represses pro-proliferative genes

The *miR-15* family consist of 5 members, all containing the same seed region (Figure 1a). To show the dynamics of cardiac expression of the *miR-15* family members in our model of ischemic injury, we subjected mice to permanent LAD ligation (MI) or LAD ligation followed by reperfusion (IR)<sup>68</sup> and quantified miR levels at several timepoints after injury. These data revealed *miR-16* and *miR-195* to be most abundant at baseline (Supplemental Figure 1a), and all *miR-15* family members showing significant and prolonged induction after injury, with the most pronounced increase seen for *miR195* after IR ( $\pm 7$ fold) (Figure 1b, Supplemental Figure 1b-f). *miR-15* family members have been shown to directly regulate several metabolic and cell cycle

genes<sup>71</sup>. In analyzing the expression dynamics of several predicted *miR-15* family targets we observed an initial increase after surgery that peaked around 1-3 days after injury and declined towards baseline at later timepoints (Figure 1c). This suggests that *miR-15* family inhibition after ischemic injury might be able to extend the induction of these proliferation related mRNA target genes leading to enhanced cardiac repair.

To start exploring whether the use of UPy-PEG hydrogel can enhance and prolong *miR-15* family inhibition in the heart, we opted to use anti-miR-195 (an LNA-DNA mixmer<sup>26</sup>) as *miR-195* is highly expressed in the heart and showed the strongest increase in response to IR (Figure 1b). In addition, this anti-miR is also expected to inhibit *miR-16* due to its sequence similarity with *miR-195* (Figure 1a). Therefore, anti-miR-195 will inhibit the two *miR-15* family members that are most highly expressed at baseline and show the highest induction after injury.

### UPy-PEG-hydrogel is an injectable hydrogel that can be modified to tune drug-release properties

The hydrogel we aimed to test is based on the ureido-pyrimidinone (UPy) moiety, which is known to form dimers by four-fold hydrogen bonding. It contains urea moieties protected by an alkyl spacer that induces lateral stacking. Furthermore, it is functionalized with a poly(ethylene glycol) chain (UPy-PEG) and has been shown to have pH-responsiveness<sup>72</sup>. It is a viscous liquid

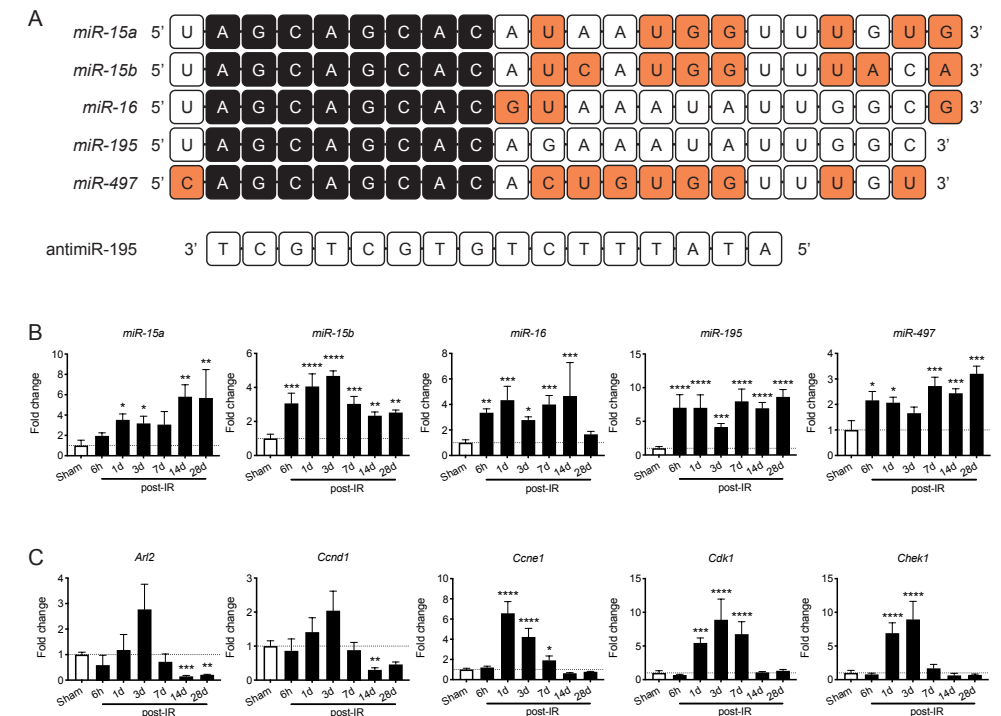


**Figure 1. *miR-15* family is induced in response to IR and represses pro-proliferative genes.** (a) Schematic representation of the sequences of the mature miRs of the *miR-15* family. Black squares represent the seed sequence, orange squares are mismatches to *miR-195*. Below the miRs, the sequence of anti-miR-195 is added. (b) RT-PCR quantification of *miR-15* family members in murine LV tissue at multiple timepoints after IR (n=6). (c) RT-PCR quantification of several predicted *miR-15* family targets in murine LV tissue at multiple timepoints after IR (n=6).

at  $\text{pH} > 8.5$ , which facilitates drug incorporation and (catheter) injection, and gels when  $\text{pH}$  is reduced in contact with the *in vivo* environment (Figure 2a). Introduction of a monofunctional UPy-moiety with a positive charge – UPy with an oligo(ethylene glycol) (OEG) functionalized with an amine (UPy-Amine) – is expected to increase the affinity with the negatively charged anti*miR*. Addition of the monofunctional UPy-Amine resulted in incorporation in the stacks of the network of the UPy-PEG hydrogel, creating a positively charged hydrogel network, cationic UPy-PEG hydrogel (UPy-Cat) (Figure 2b). *In vitro* release experiments showed that anti*miR*-195 release from UPy-Cat occurred over 260 hours, while UPy-PEG released  $>80\%$  of the anti*miR* in approximately 50 hours (Figure 2c). The mechanical properties of UPy-PEG and UPy-Cat hydrogels showed no significant differences, nor did addition of the anti*miR* influence the mechanical properties of either hydrogel. UPy-PEG and UPy-Cat showed a  $G'$  (storage modulus) of approximately 10 kPa, indicating no difference in strength with incorporation of UPy-Amine (Figure 2d), and in line with some of the stronger hydrogels previously tested<sup>73</sup>. Strain sweep experiments showed a linear course of  $G'$  and  $G''$  (loss modulus) until a minimum of 50% deformation, where the crossover point indicated the disruption of both hydrogels (Figure 2e). Additionally, both hydrogels appeared to be in the gelled state over a broad range of frequencies (Figure 2f). Altogether, UPy-PEG and UPy-Cat showed similar mechanical properties and allowed for sustained anti*miR* release.

### Intramyocardial injection of pristine UPy-PEG is safe

To test the *in vivo* safety of both UPy-PEG and UPy-Cat, healthy mice were subjected to intramyocardial injections (2 times 10  $\mu\text{L}$ ) of PBS, UPy-PEG or UPy-Cat in the LAD area. At 3 and 7 days post-injection (dpi), cardiac function and dimensions were measured by echocardiography and tissue was collected for molecular analysis (Figure 3a). Intramyocardial injection of UPy-PEG had no significant effect on fractional shortening or thickness of the anterior or posterior left ventricular wall (LVAW or LVPW, respectively, measured in diastole) compared to intramyocardial injection of PBS (Figure 3b). However, UPy-Cat caused an increase in thickness of both LVAW and LVPW at 3 dpi. As UPy-Cat also caused an increase in cardiac stress- and fibrosis markers natriuretic peptide A (*Nppa*),  $\beta$ -myosin heavy chain (*Myh7*) and collagen type 1 alpha 2 (*Col1a2*, non-significant) (Figure 3c) we decided to continue our further investigations with UPy-PEG.

To get a more detailed view on the cardiac gene expression effects of intramyocardial injection of UPy-PEG, we submitted RNA samples from PBS- and UPy-PEG-injected hearts for RNA-sequencing (Supplemental Figure 2a-b). Gene ontology analysis of differentially expressed genes ( $>1.25$  fold upregulated,  $p < 0.01$ ) suggested the induction of inflammatory genes in response to UPy-PEG (Figure 3d). Realtime PCR analysis indicated the transient nature of this response (Figure 3e). This finding was confirmed in histological sections of murine hearts showing a more prominent infiltration of small cells in UPy-PEG-injected hearts versus those injected with PBS 3 dpi, which largely disappeared in time (Figure 3f). To determine cardiac retention of the UPy-PEG, we performed anti-PEG ELISA on whole-heart lysates which showed that most of the injected hydrogel is removed shortly after injection. Only 6% of the injected UPy-PEG was detected in the heart 6 hours after intramyocardial injection and this declined to approximately 1% at 24 hours after injection (Supplemental Figure 3).

Taken together, these data show that pristine UPy-PEG does not affect cardiac function, although it induces a transient inflammatory response upon intramyocardial injection in the mouse heart despite a low cardiac retention.

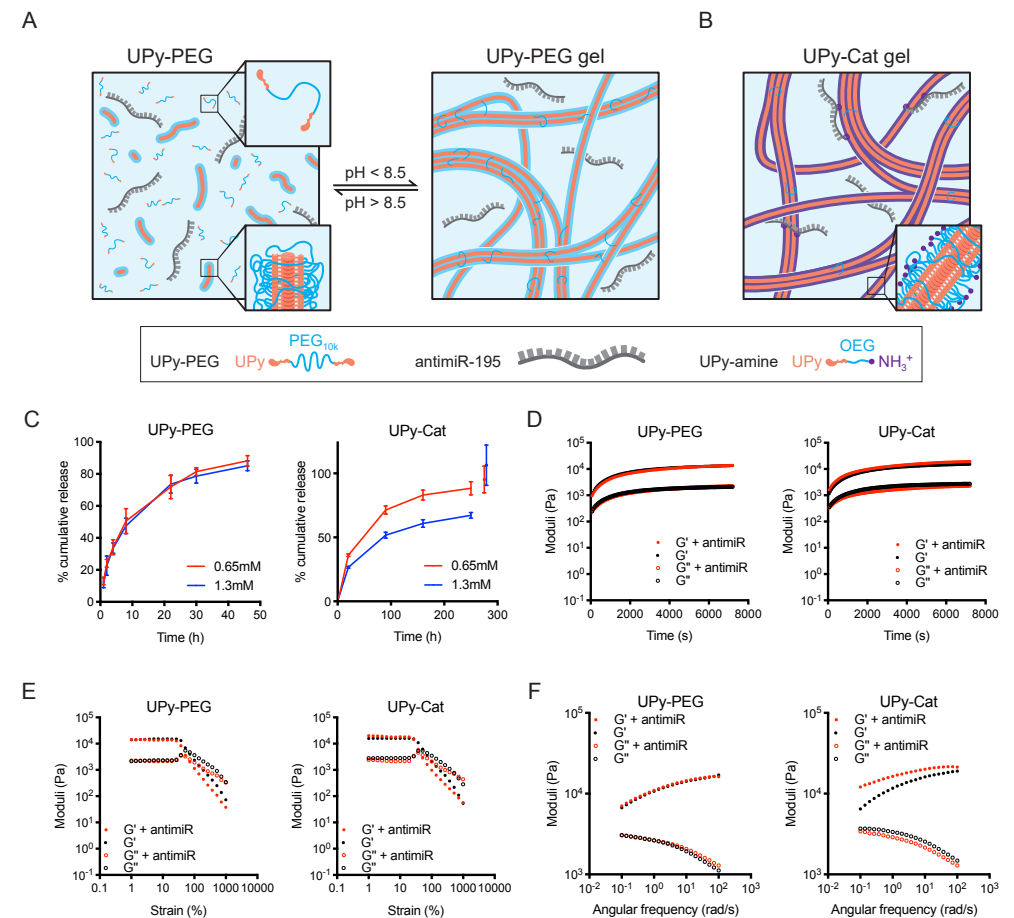


**Figure 2. Schematic representation and material properties of UPy-PEG and cationic UPy-PEG.** (a) Schematic overview of the gelation process of UPy-PEG. At  $\text{pH} > 8.5$  only small fibers are formed with no formation of a transient network, whereas at  $\text{pH} < 8.5$  a hydrogel network is formed. (b) Addition of monofunctional UPy-Amine results in incorporation in the stacks of the network, forming a cationic UPy-PEG network (UPy-Cat). (c) Cumulative release of anti*miR*-195 from UPy-PEG and UPy-Cat over time at 37 °C. (d-f) Storage modulus ( $G'$ ) and loss modulus ( $G''$ ) of UPy-PEG and UPy-Cat at 37 °C as a function of time (d), strain (e), and over angular frequency (f).

### Anti*miR*-195 released from UPy-PEG is functional and increases cardiomyocyte proliferation *in vitro*

To test whether anti*miR*-195 released from UPy-PEG is still functional *in vitro*, anti*miR*-195 was mixed into UPy-PEG after which we collected serial incubations of cell culture medium. Subsequently, neonatal rat ventricular myocytes (NRVM) were cultured with this medium and transcriptomic and proliferation changes were analyzed (Figure 4a). At all timepoints of the incubation, NRVMs cultured with medium incubated on UPy-PEG with anti*miR* showed a robust decrease in both *miR*-16 and *miR*-195 compared to those cultured with medium incubated with pristine UPy-PEG (Figure 4b). Downstream mRNA target Cyclin D1 (*Ccnd1*) showed an increase at all analyzed timepoints that peaked with the lysate coming from the UPy-PEG between D1-3 and D3-5 (Figure 4c). Quantification of cardiomyocyte proliferation by KI67-staining indicated a significant increase in proliferation with the medium that was incubated on UPy-PEG with

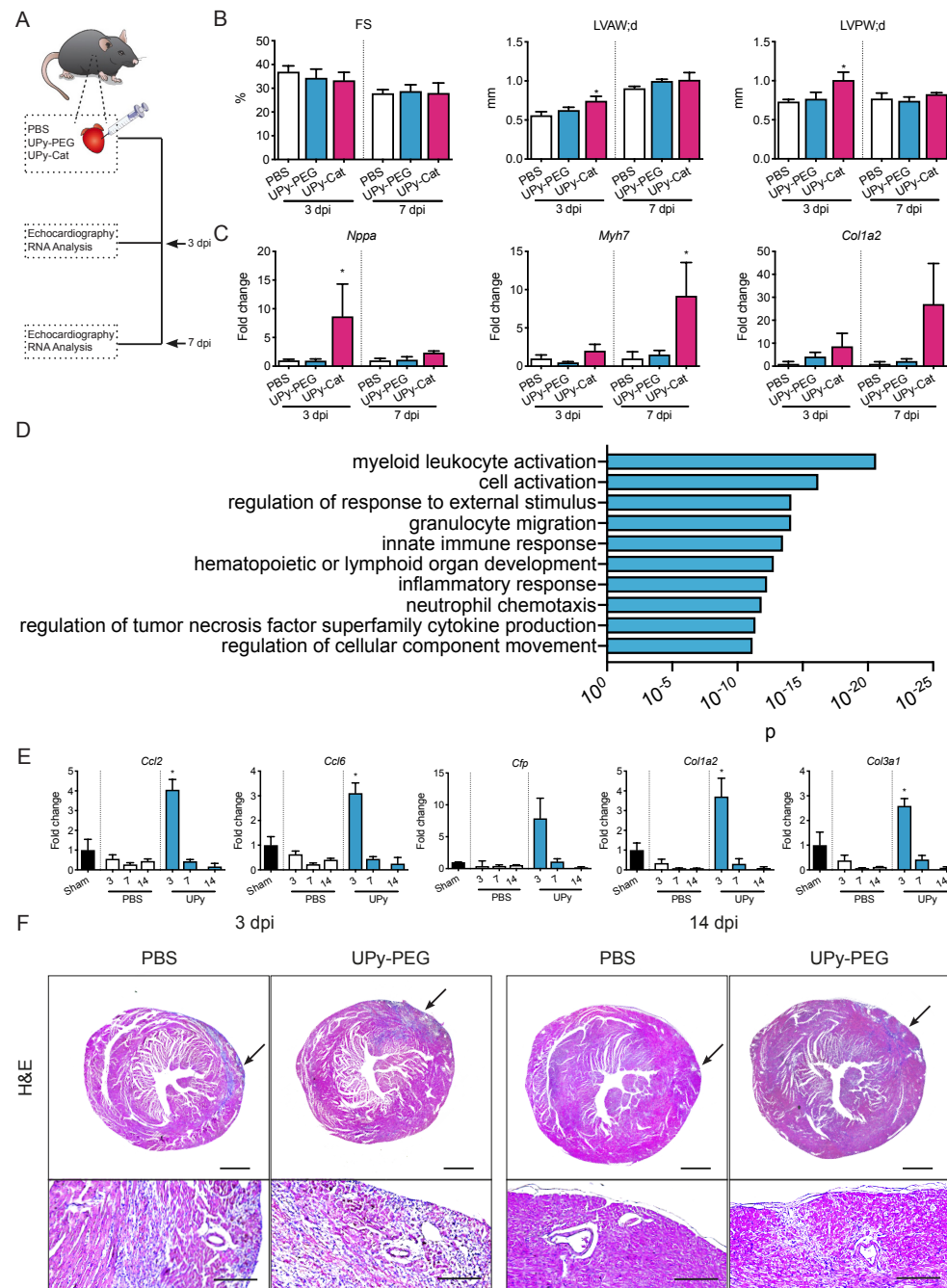


**Figure 3. Injection of pristine UPy-PEG causes a transient inflammatory reaction.** (a) Schematic representation of experiment. (b) Echocardiographic analysis of FS, LVAW;d, LVPW;d (n=4-5). (c) RT-PCR quantification of stress markers *Nppa*, *Myh7* and fibrosis marker *Col1a2* (n=4-5). (d) Gene ontology analysis of differentially expressed genes between mice injected with PBS and those injected with pristine UPy-PEG. (e) Hematoxylin & eosin (H&E) staining of transverse sections of murine hearts at 3 (left) and 14 (right) dpi with PBS or pristine UPy-PEG.

anti-miR between D0-1 (Figure 4d-e). Taken together, these data show that anti-miR-195 released from UPy-PEG is still functional and able to induce proliferation in cardiomyocytes *in vitro*.

### UPy-PEG-based delivery of anti-miR-195 enhances cardiac target derepression

Considering previous studies targeting the miR-15 family in the heart were done via systemic delivery of the anti-miR<sup>24,64</sup>, we first needed to determine the required dose to see transcriptional changes with intramyocardial delivery. To establish a suitable anti-miR dose, healthy mice were subjected to intramyocardial injections of UPy-PEG (2 times 10  $\mu$ L), either pristine or loaded with a low dose (70  $\mu$ g per mouse) or high dose (140  $\mu$ g per mouse) of anti-miR-195. Tissues were collected for molecular analysis at 3 and 7 dpi (Figure 5a). Both doses led to a robust reduction of *miR-16* and *miR-195* in the LV at both timepoints (Figure 5b). This resulted in an increase in mRNA targets ADP-ribosylation factor-like protein 2 (*Arl2*) and *Ccnd1* at 3 dpi, but not 7 dpi (Figure 5c). While miR inhibition and target derepression in the heart seemed to be comparable between the two doses, the higher dose showed stronger *miR-16* and *miR-195* inhibition in kidney and liver RNA (Supplemental Figure 4a,c). Only with the higher anti-miR dose miR inhibition was accompanied by changes in target mRNAs (Supplemental Figure 4b,d). Based on these findings we opted to analyze whether UPy-PEG improved cardiac efficacy of anti-miR-195 over PBS as a delivery vehicle, we subjected healthy mice to intramyocardial injections with PBS or UPy-PEG, either pristine or loaded with anti-miR-195 and collected tissues for molecular analysis at 3 dpi (Figure 5d). With both delivery vehicles, anti-miR-195 caused a strong reduction of *miR-16* and *miR-195* levels (Figure 5e). Pristine UPy-PEG induced a decline of *miR-16* and *miR-195* levels when compared to PBS. This was probably due to the transient stress induced upon intramyocardial injection. However, target transcripts *Arl2* and *Ccnd1* showed a stronger

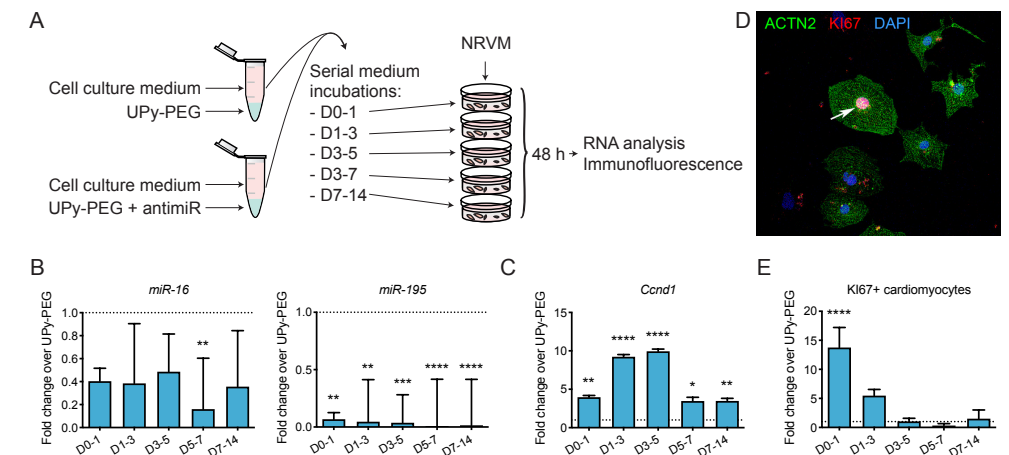


**Figure 4. Anti-miR-195 released from UPy-PEG activates cardiomyocyte proliferation *in vitro*.** (a) Schematic overview of the *in vitro* experiment. Pristine UPy-PEG or UPy-PEG loaded with anti-miR-195 was allowed to gelate in the bottom of a 2 mL Eppendorf tube. Subsequently, multiple incubations with 1.5 mL cell culture medium were performed serially. After each incubation, medium was frozen for storage. Medium was thawed for cell culture experiments, and NRVM were incubated with it for 48 hours. (b,c) RT-PCR quantification of *miR-16* and *miR-195* (b) and *Ccnd1* (c) after treatment with hydrogel-incubated medium (n=3). (d) Representative image of ACTN2 & Ki67 staining on NRVM treated with medium incubated on UPy-PEG with anti-miR. Ki67-positive cardiomyocyte nucleus labeled with white arrow. (e) Quantification of Ki67-positive cardiomyocytes. Values shown are fold change in cells exposed to medium incubated with anti-miR-containing hydrogel over those exposed to medium incubated with pristine hydrogel at that same timepoint.

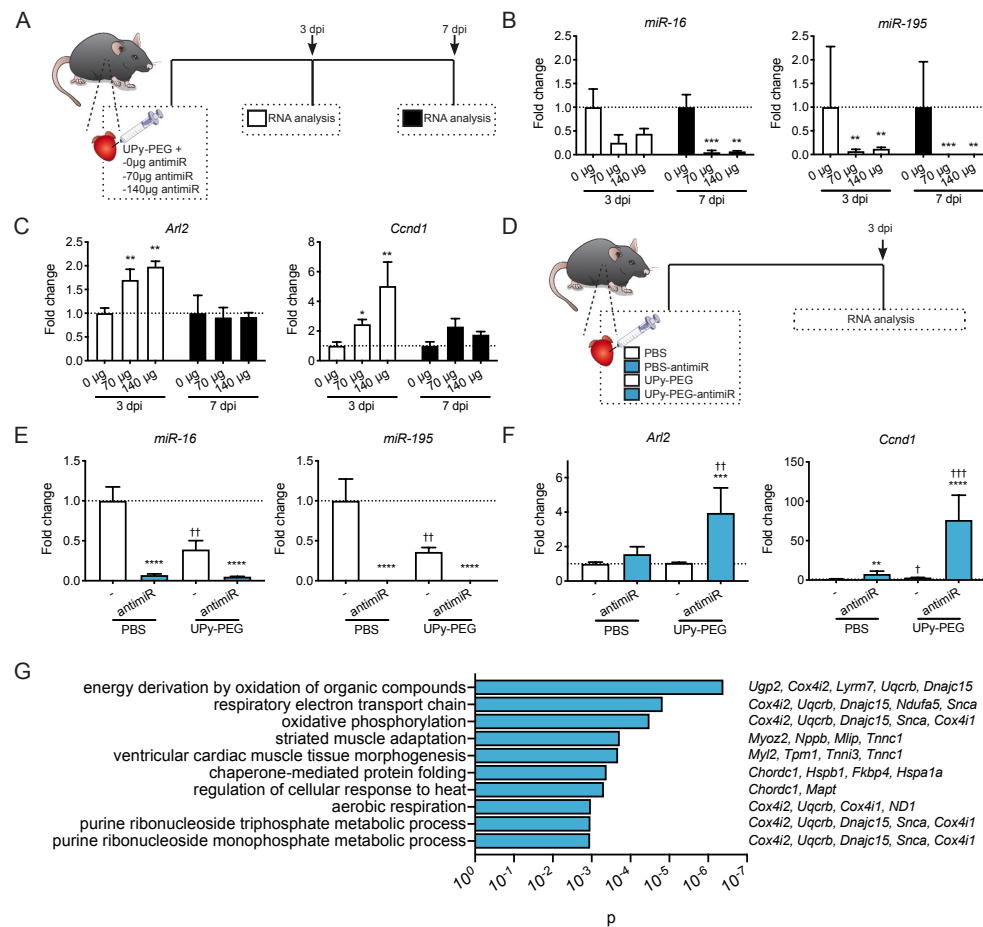


**Figure 5. UPy-PEG-based intramyocardial delivery of anti-miR-195 increases its efficacy over PBS-based intramyocardial delivery.** (a) Schematic representation of experiment. (b) RT-PCR quantification of *miR-16* and *miR-195*. (c) RT-PCR quantification of *Arl2* and *Ccnd1* ( $n=5$ ) (d) Schematic representation of experiment. (e) RT-PCR quantification of *miR-16* and *miR-195* ( $n=5$ ). (f) RT-PCR quantification of *Arl2* and *Ccnd1*. (g) Gene ontology analysis of differentially expressed genes between mice injected with pristine UPy-PEG or UPy-PEG loaded with anti-miR-195 with a dose of 70  $\mu\text{g}$  per mouse.

increase after UPy-PEG-based delivery compared to PBS-based delivery (Figure 5f) showing that hydrogel-based intramyocardial delivery does increase local efficacy. RNA analysis of liver and kidney tissues showed comparable inhibition of *miR-16* and *miR-195* between delivery methods, with no significant effects on *miR-15* family target mRNAs (Supplemental Figure 5a-d).

To investigate the transcriptomic effects of anti-miR-195 delivery, RNA from LV tissue after injection with pristine UPy-PEG versus UPy-PEG with anti-miR-195 was submitted for RNA-sequencing (Supplemental Figure 6a-b). Gene ontology analysis of differentially regulated genes (>1.25 fold increased,  $p < 0.01$ ) revealed mostly genes related to metabolic processes (Figure 5g), which could fit with a previously published effect of the *miR-15* family on mitochondrial integrity through *Arl2*<sup>24</sup>. Taken together, these data show that anti-miR-195 released from UPy-PEG *in vivo* is still functional, that UPy-PEG-based delivery improves the efficacy of anti-miR-195 over PBS-

based delivery in healthy mice, and that with UPy-PEG based intramyocardial delivery there is target mRNA de-repression at a dose far lower than the dose used for systemic injection<sup>75,76</sup>.

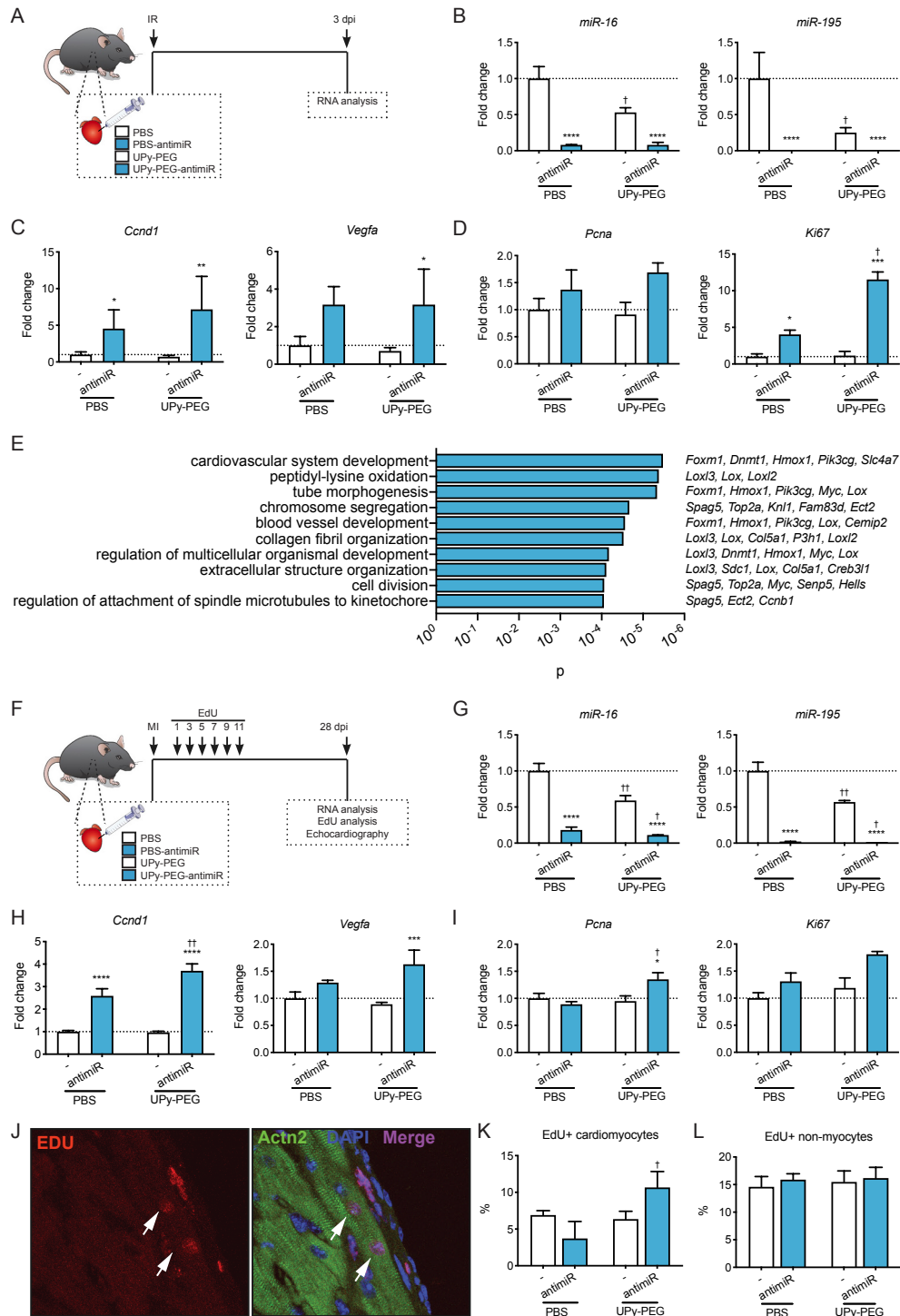
### UPy-PEG-based delivery of anti-miR-195 induces proliferation in cardiomyocytes after ischemic injury

To determine whether the use of UPy-PEG improved cardiac efficacy of anti-miR-195 after IR, mice were subjected to 60 minutes of LAD ligation and, upon reperfusion, received intramyocardial injections (2 times 10  $\mu\text{L}$ ) of PBS or UPy-PEG, either pristine or loaded with anti-miR-195. LV-tissue was collected 3 dpi (Figure 6a). As expected, anti-miR-195 induced a strong reduction of *miR-16* and *miR-195* levels, regardless of the vehicle used for injection (Figure 6b). Accordingly, anti-miR therapy led to upregulation of *Ccnd1* and vascular endothelial growth factor A (*Vegfa*) (Figure 6c). In addition to these *miR-15* family targets, there was a significant increase in *Ki67* between UPy-PEG- and PBS-based delivery of anti-miR-195 (Figure 6d). As expected, we found a decrease of *miR-16* and *miR-195* levels in the kidney and in the liver, with a less profound decrease of *miR-16* in livers of mice injected with anti-miR-195 in UPy-PEG (Supplemental Figure 7a,c). *Ccnd1* was induced in the kidneys after PBS- and hydrogel-anti-miR delivery, but not in the liver (Supplemental Figure 7b,d).

To investigate the broader effect of anti-miR-195 under ischemia-reperfusion stress, RNA from LV-tissue after IR treated with either pristine UPy-PEG or UPy-PEG with anti-miR-195 was submitted for RNA-sequencing (Supplemental Figure 8a-b). Gene ontology analysis of differentially expressed genes (>1.25 fold increased,  $p < 0.01$ ) now resulted in gene classifications linked to tissue morphogenesis and cell division (Figure 6e), suggesting that under stress conditions *miR-15* family repression activates the tissue morphogenesis and cell division.

Previous work from our lab showed that not only the presence or absence of stress, but also the severity of this stress influences anti-miR function<sup>77</sup>. Based on this knowledge we extended our *in vivo* efficacy study and subjected mice to permanent LAD ligation for 28 days. Immediately after LAD ligation, the mice received intramyocardial injections (2 times 10  $\mu\text{L}$ ) with PBS or UPy-PEG, either pristine or loaded with anti-miR-195. To track cell proliferation, mice additionally received subcutaneous EdU-injections every other day for 11 days after surgery. Twenty-eight days after surgery, tissue was collected for histological and molecular analysis (Figure 6f). Four weeks after anti-miR-195 injections, there was still a significant reduction in *miR-16* and *miR-195* levels, with a slightly stronger inhibition after hydrogel-based delivery compared to PBS-based delivery (Figure 6g). UPy-PEG-formulated anti-miR-195 had a stronger derepressive effect on *Ccnd1* and *Vegfa* than PBS-formulated anti-miR-195 and showed a significant induction in *Pcna* (Figure 6h-i). To quantify cardiomyocyte proliferation *in vivo* after MI we counted EdU-positive cells 28 dpi. Hydrogel-based anti-miR-195 delivery caused an increase in EdU-positive cardiomyocytes compared to PBS-formulated anti-miR (Figure 6j-k). Importantly, we saw no difference in EdU-positive non-myocytes (Figure 6l), indicating that anti-miR-195 selectively enhances the proliferation of cardiomyocytes. However, despite the increase in cardiomyocyte proliferation we were unable to detect a beneficial effect of anti-miR-195 on cardiac function by echocardiography (Supplemental Table 1).

RNA analysis of kidney and liver tissue from these mice revealed significant *miR-16* and *miR-195* inhibition 28 days after injection, which appeared stronger with hydrogel-based intramyocardial anti-miR delivery (Supplemental Figure 9a,c). This could suggest a prolonged



washout of anti-miR-195 from the heart after hydrogel-based delivery. However, no effects on target de-repression were observed at this point (Supplemental Figure 9b,d).

Taken together, these data suggest that UPy-PEG-based anti-miR delivery improves local cardiac efficacy and successfully activates cell cycle genes after ischemia to induce cardiomyocyte-specific proliferation.

## Discussion

The current study shows that a pH-responsive hydrogel, UPy-PEG, designed for minimally invasive intramyocardial injection can be used to improve local delivery of an anti-miR. Our data shows that UPy-PEG-based intramyocardial delivery of anti-miR-195 enhances the effect on target derepression and stimulates cardiomyocyte proliferation after MI. While this provides support for follow up investigation, our data also highlight some of the drawbacks and challenges to consider when using this gel.

The hydrogel used here was designed as a versatile sustained release delivery vehicle suitable for catheter-based intramyocardial injections. It has previously been shown to be easily modifiable to facilitate MRI detection<sup>78</sup> or modification of drug retention properties<sup>79</sup>. Additionally, it was used previously in a proof of concept study for the intramyocardial delivery of IGF-1/HGF in a porcine model of ischemic injury<sup>67</sup> which showed the UPy-PEG to enhance delivery of IGF-1/HGF to the injured myocardium. Our study adds a more thorough investigation of the hydrogel's safety and retention in mice and shows that, in addition to the delivery of proteins, the hydrogel can also be used for delivery of oligonucleotides *in vivo*.

However, our experiments investigating the safety of the hydrogel revealed that injection of pristine hydrogel into the healthy mouse heart causes a transient inflammatory reaction and seems to cause more damage than an intramyocardial injection of PBS. Potential triggers causing this response might be inherent to the hydrogel and include the high pH of the gel when injecting and the viscosity and volume of the injections (swelling of the myocardium at the injection site is observed). Alternatively, the mouse model itself may contribute to this effect, as using mice limits us to using conventional needles and a microsurgical intercostal approach as opposed to catheter-based injections. We suspect that mice are not the optimal model to study the safety of intramyocardial injectables due to the unavailability of catheter-based delivery systems and the difficulty of manually injecting in the fast-moving heart of the mouse. Therefore, the injections may cause traumatic injury which is slightly worse in the hydrogel injections because the viscous fluid is harder to inject. We expect to observe less

**Figure 6. UPy-PEG-based intramyocardial delivery of anti-miR-195 induces proliferation in cardiomyocytes after ischemic injury.** (a) Schematic representation of experiment. (b) RT-PCR quantification of *miR-16* and *miR-195* (n=4-5). (c) RT-PCR quantification of *Ccnd1* and *Vegfa* (n=4-5). (d) RT-PCR quantification of *Pcna* and *Ki67* (n=4-5). (e) Gene ontology analysis of differentially expressed genes between mice injected with pristine UPy-PEG or UPy-PEG loaded with anti-miR-195 after IR. (f) Schematic representation of experiment. (g) RT-PCR quantification of *miR-16* and *miR-195* (n=6-9). (h) RT-PCR quantification of *Ccnd1* and *Vegfa* (n=6-9). (i) RT-PCR quantification of *Pcna* and *Ki67* (n=6-9). (j) Representative image of EdU-detection in murine hearts treated with UPy-PEG with anti-miR. White arrows mark EdU-positive cardiomyocytes. (k) Quantification of EdU-positive cardiomyocytes as a percentage of all cardiomyocytes (n=3-6). (l) Quantification of EdU-positive non-myocytes as a percentage of all non-myocytes (n=3-6).

damage if these studies were repeated using a catheter-based delivery system in a large animal model. Furthermore, we are also unsure of the importance of these effects of intramyocardial injections of pristine hydrogel in healthy murine hearts, as the hydrogel is intended to be injected into damaged hearts as a carrier of pro-regenerative drugs. We have not investigated whether injection of the hydrogel still causes additional damage in an area already damaged by ischemia.

An additional issue we encountered when using the gel in mice was the low cardiac retention of the hydrogel at the injection site, with nearly all the UPy-PEG molecules cleared from the heart after 24 hours. Regardless, our results show that anti-miR efficacy is improved with hydrogel-based delivery over PBS-based delivery, with the difference being observable at least 28 days after injection. Presumably, even a short increase in the exposure to anti-miRs allows cardiomyocytes to take up more compound and subsequently, the very stable LNA-DNA mixmer anti-miRs can cause a long-lasting effect. At this point we are not sure whether the short retention of the hydrogel is caused by its failure to gelate fast enough upon injection, the lack of space in the dense cardiac tissue, or whether the hydrogel is pumped out of the heart quickly in the moving and well-perfused myocardium. In the latter case, hydrogel retention may be better with injection in damaged, less contractile, less well-perfused, areas or in larger species that have a lower heart rate. Another option for improving the hydrogel retention may be to add adhesive components.

While previous research has shown high-dose systemic *miR-15* family inhibition after ischemic injury reduces infarct size and improves cardiac function<sup>24</sup>, we could not reproduce those findings with our new delivery method even though we did see an increased efficacy on mRNA targets. Perhaps a further increase in anti-miR dose could improve effect size, but the dose in the current study was picked to have no effect on off-target organs. Alternatively, the timing of the therapy could be further investigated<sup>80</sup>, possibly anti-miR-195 injection is more effective few days or weeks after the ischemic injury. However, this is unattractive in mice because it requires repeated surgery and we think that these investigations would be more suited to a large animal model where catheter delivery of the hydrogel and anti-miR would be possible.

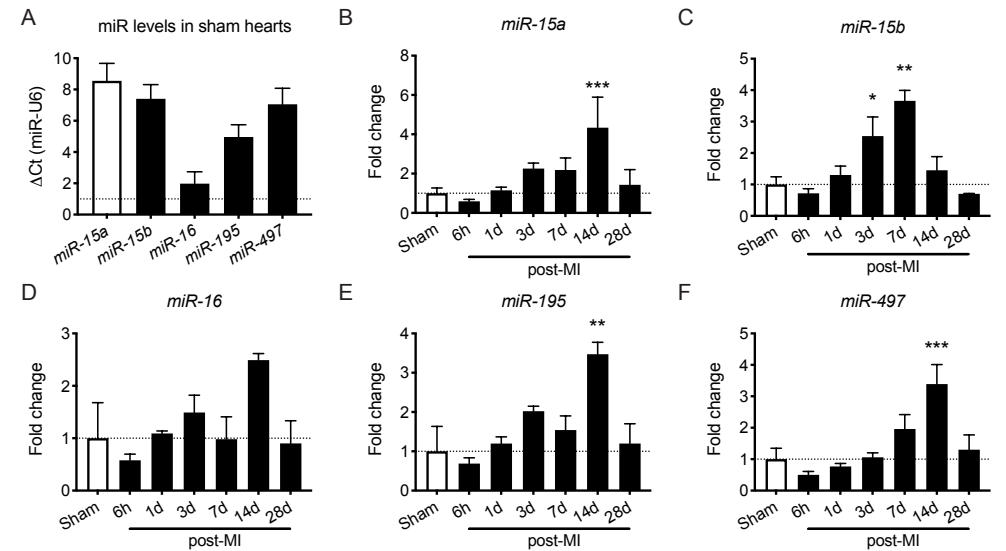
In addition to increasing local efficacy, hydrogel delivery of anti-miR-195 was intended to reduce exposure of the off-target organs, like the kidney and liver. In this study we did not observe a clear difference in *miR-15* family mRNA target derepression in liver and kidney between hydrogel- and PBS-based delivery 3 days after injection. Efforts to improve cardiac retention of the gel will inherently reduce delivery to extra-cardiac tissues and are key.

In summary, we have shown that using a hydrogel as a vehicle for intramyocardial anti-miR-195 delivery in mouse improves efficacy over PBS. We showed increased target derepression and increased cardiomyocyte proliferation. However, this did not lead to a significant improvement in cardiac function. Further research in larger animal models is needed to show whether catheter based intramyocardial injections of UPy-PEG anti-miR-195 will overcome the disadvantages found in the mouse model and show an even greater benefit of using UPy-PEG as cardiac delivery vehicle of anti-miR-195 in the setting of ischemic heart disease.

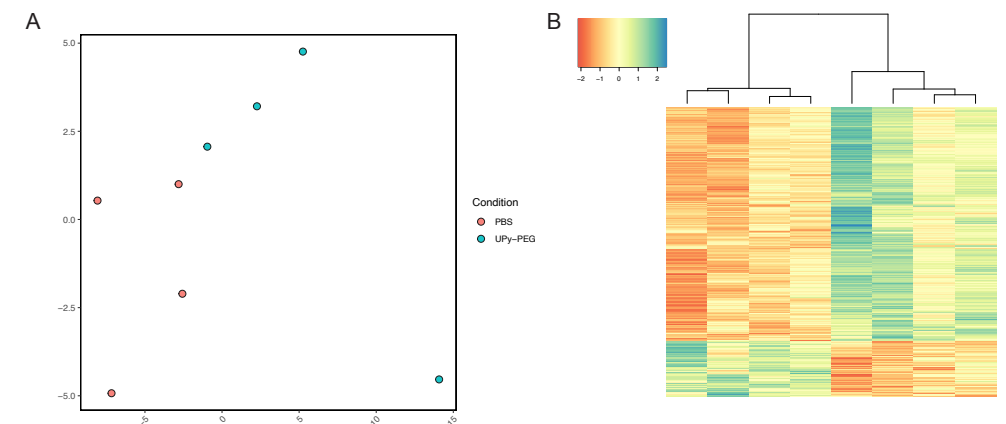
## Sources of funding

We acknowledge the support from the Netherlands Cardiovascular Research Initiative: an initiative with support of the Dutch Heart Foundation, CVON2014-27 REMAIN.

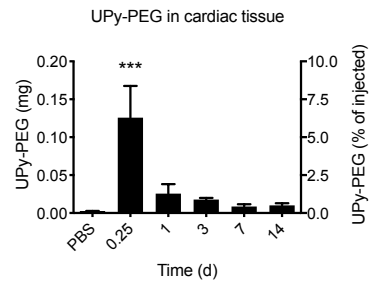
## Supplemental materials



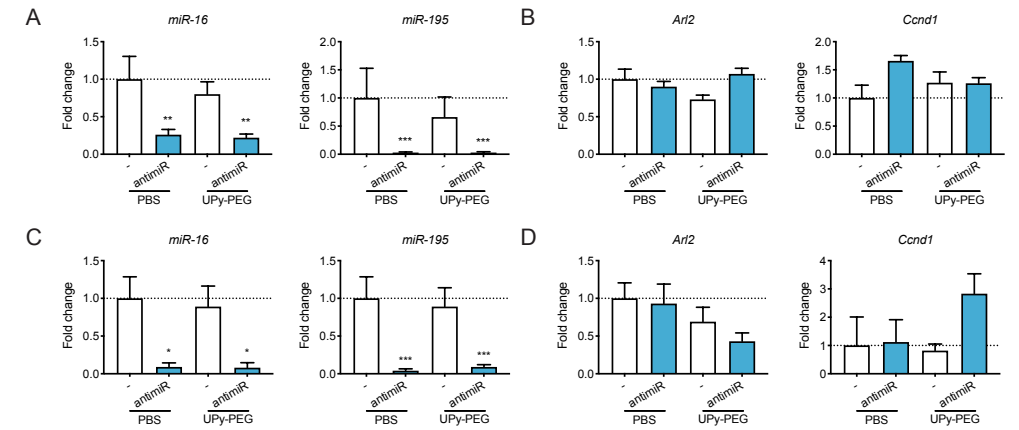
**Supplemental Figure 1. RT-PCR quantification of *miR-15* family members in murine LV tissue.** (a) Comparison of the expression level of the *miR-15* family members in uninjured LV tissue, lower  $\Delta Ct$  is higher expression. (b-f) Changes in expression in each of the *miR-15* family members at multiple timepoints after permanent LAD ligation.



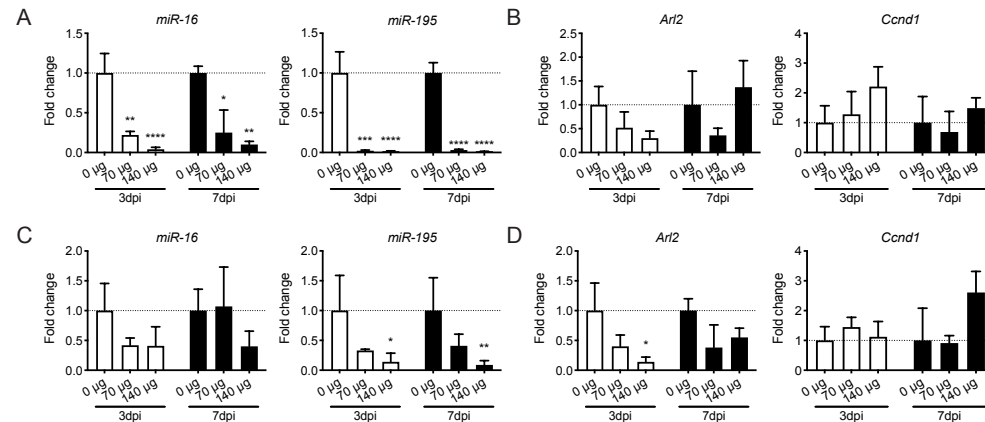
**Supplemental Figure 2. Transcriptomic profiling of the effect of intramyocardial injection of pristine UPy-PEG.** (a) PCA plot showing clustering of samples from mice injected with PBS or UPy-PEG. (b) Heatmap of differentially expressed genes between the two groups.



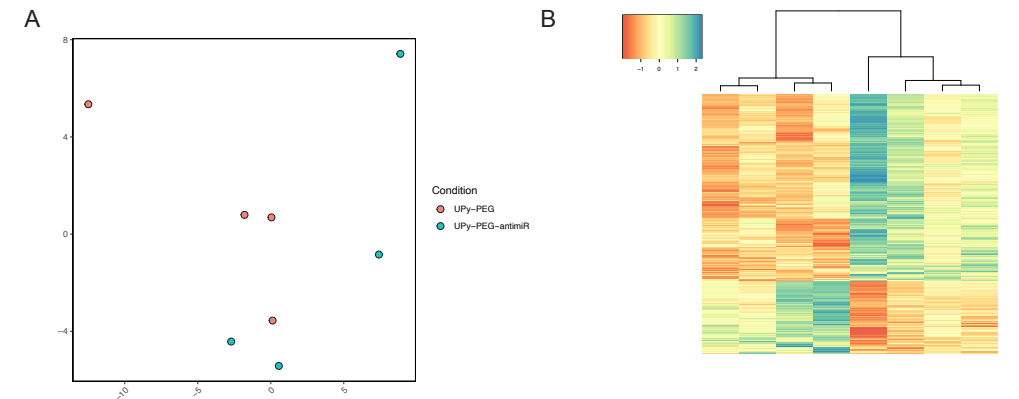
**Supplemental Figure 3. Quantification of UPy-PEG retention in the heart.** Anti-PEG ELISA quantification of the amount of UPy-PEG remaining in the murine heart at different times after intramyocardial injection of 2 times 10  $\mu$ L UPy-PEG.



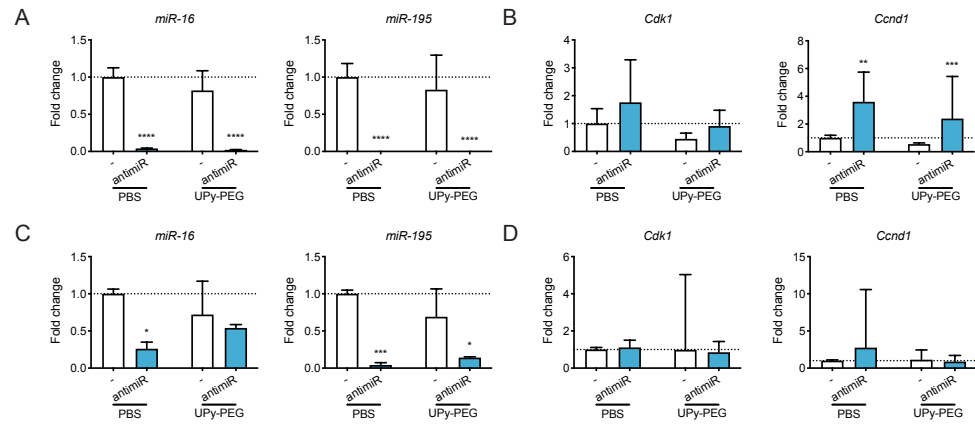
**Supplemental Figure 5. Effect of intramyocardial anti-miR-195 injection in off-target organs with different vehicles.** (a,b) RT-PCR quantification of *miR-16* & *miR-195* (a) and *Arl2* & *Ccnd1* (b) in kidney tissue of mice 3 days after intramyocardial injection with pristine PBS, pristine UPy-PEG or those vehicles loaded with anti-miR-195. (c,d) RT-PCR quantification of *miR-16* & *miR-195* (c) and *Arl2* & *Ccnd1* (d) in liver tissue of mice 3 days after intramyocardial injection with pristine PBS, pristine UPy-PEG or those vehicles loaded with anti-miR-195.



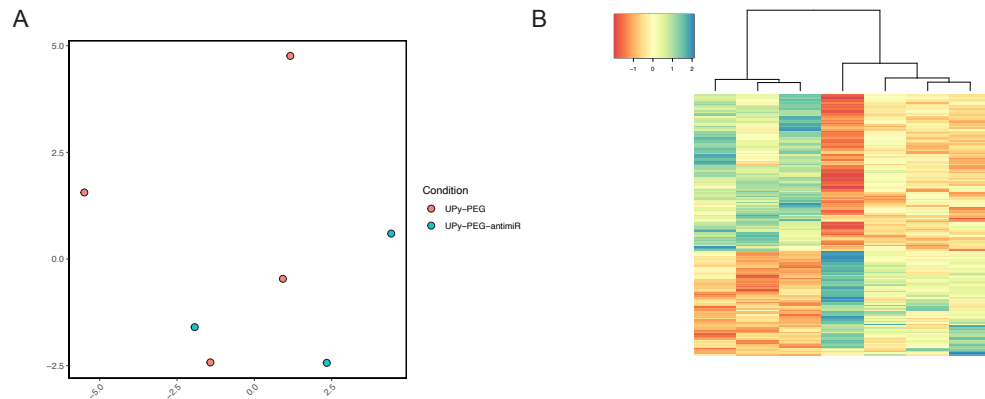
**Supplemental Figure 4. Effect of intramyocardial anti-miR-195 injection in off-target organs at different doses.** (a,b) RT-PCR quantification of *miR-16* & *miR-195* (a) and *Arl2* & *Ccnd1* (b) in kidney tissue of mice 3 or 7 days after intramyocardial injection with UPy-PEG loaded with different concentrations of anti-miR-195. (c,d) RT-PCR quantification of *miR-16* & *miR-195* (c) and *Arl2* & *Ccnd1* (d) in liver tissue of mice 3 or 7 days after intramyocardial injection with UPy-PEG loaded with different concentrations of anti-miR-195.



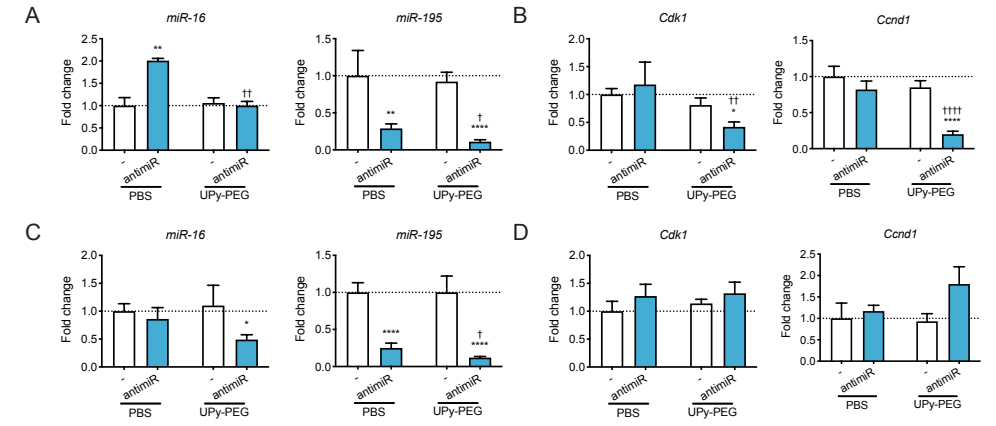
**Supplemental Figure 6. Transcriptomic profiling of the effect of anti-miR-195 after delivery in UPy-PEG.** (a) PCA plot showing clustering of samples from mice injected with pristine UPy-PEG or UPy-PEG loaded with anti-miR. (b) Heatmap of differentially expressed genes between the two groups.



**Supplemental Figure 7. Effect of intramyocardial anti-miR-195 injection in off-target organs with different vehicles after IR.** (a,b) RT-PCR quantification of *miR-16* & *miR-195* (a) and *Cdk1* & *Ccnd1* (b) in kidney tissue of mice 3 days after IR injury and intramyocardial injection with pristine PBS, pristine UPy-PEG or those vehicles loaded with anti-miR-195. (c,d) RT-PCR quantification of *miR-16* & *miR-195* (c) and *Cdk1* & *Ccnd1* (d) in liver tissue of mice 3 days after IR injury and intramyocardial injection with pristine PBS, pristine UPy-PEG or those vehicles loaded with anti-miR-195.



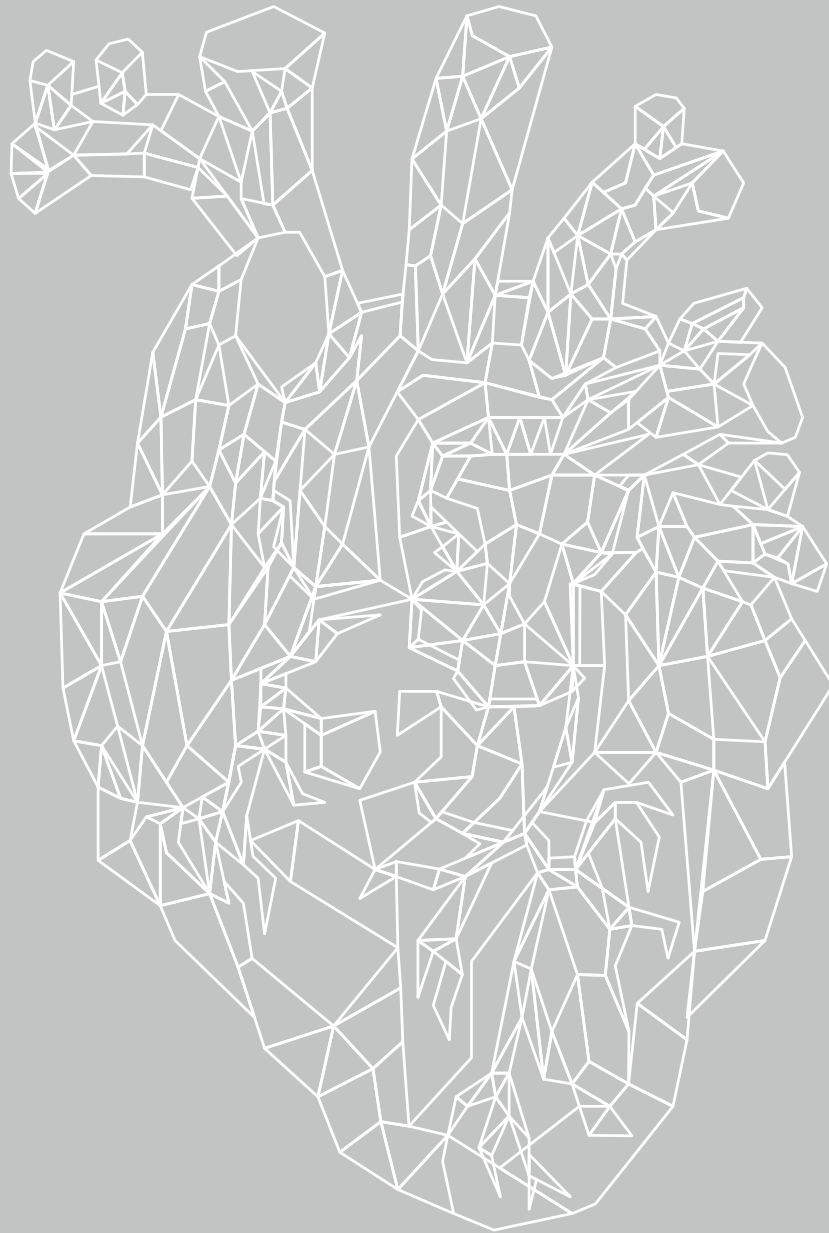
**Supplemental Figure 8. Transcriptomic profiling of the effect of anti-miR-195 after delivery in UPy-PEG after IR.** (a) PCA plot showing clustering of samples from mice injected with pristine UPy-PEG or UPy-PEG loaded with anti-miR-195 after IR-injury. (b) Heatmap of differentially expressed genes between the two groups.



**Supplemental Figure 9. Effect of intramyocardial anti-miR-195 injection in off-target organs with different vehicles after MI.** (a,b) RT-PCR quantification of *miR-16* & *miR-195* (a) and *Cdk1* & *Ccnd1* (b) in kidney tissue of mice 28 days after permanent LAD ligation and intramyocardial injection with pristine PBS, pristine UPy-PEG or those vehicles loaded with anti-miR-195. (c,d) RT-PCR quantification of *miR-16* & *miR-195* (c) and *Cdk1* & *Ccnd1* (d) in liver tissue of mice 28 days after permanent LAD ligation and intramyocardial injection with pristine PBS, pristine UPy-PEG or those vehicles loaded with anti-miR-195.

	Sham PBS (n=10)	MI PBS (n=14)	MI PBS a195 (n=9)	MI UPy-PEG (n=15)	MI UPy-PEG a195 (n=10)
IVS;d (mm)	0,83±0,11	0,91±0,17	0,96±0,15	0,88±0,22	0,96±0,17
LVID;d (mm)	3,60±0,33	4,43±0,61*	4,82±1,19*	4,76±1,16*	4,74±1,30*
LVPW;d (mm)	1,04±0,37	0,95±0,24	0,98±0,14	0,83±0,18	1,14±0,31
IVS;s (mm)	1,12±0,24	1,15±0,25	1,09±0,27	1,03±0,38	1,16±0,31
LVID;s (mm)	2,60±0,65	3,60±0,76*	4,17±1,47*	4,12±1,53*	4,10±1,62
LVPW;s (mm)	1,32±0,52	1,18±0,29	1,22±0,23	1,03±0,30	1,31±0,33
EF (%)	54,42±18,61	38,98±13,84	31,13±18,97*	38,41±18,50	35,61±13,88
FS (%)	28,77±12,10	19,20±7,77	15,19±9,91*	19,21±10,42	17,21±7,19*
LV mass (mg)	98,19±21,33	136,89±36,55*	152,82±42,01*	125,38±28,07	155,26±43,76*
CO (mL/min)	19,11±4,72	16,59±5,07	14,77±2,49	17,28±7,36	17,00±4,80

**Supplemental Table 1. Echocardiography results.** Interventricular septum (IVS); Left ventricular internal diameter (LVID); Left ventricular posterior wall (LVPW) are measured in both diastole (d) and systole (s). Ejection fraction (EF), fractional shortening (FS), left ventricular (LV) mass and cardiac output (CO) were calculated from short axis M-mode measurements by Vevo® LAB 1.7.1 software. a195 refers to anti-miR-195. Data are shown as mean ± SD. \* indicates p < 0.05 compared to empty vehicle.



# Chapter 4

## Single-Cell Transcriptomic Profiling Provides Insights Into Disease-Related Processes in Human Hypertrophic Cardiomyopathy

Joep E.C. Eding MD, MSc<sup>1#</sup>, Anne E. de Leeuw MSc<sup>1#</sup>, Maya Wright Clark MSc<sup>1,2#</sup>, Martijn Wehrens PhD<sup>1</sup>, Cornelis J. Boogerd PhD<sup>1</sup>, Bas Molenaar MSc<sup>1</sup>, Petra H. van der Kraak BSc<sup>3</sup>, Diederik W.D. Kuster PhD<sup>4</sup>, Jolanda van der Velden PhD<sup>4</sup>, Michelle Michels MD, PhD<sup>5</sup>, Aryan Vink MD, PhD<sup>3</sup>, and Eva van Rooij PhD<sup>1,2\*</sup>

<sup>#</sup> These authors contributed equally to this work

<sup>1</sup> Hubrecht Institute, Royal Netherlands Academy of Arts and Sciences (KNAW) and University Medical Center, Utrecht, The Netherlands

<sup>2</sup> Department of Cardiology, University Medical Center Utrecht, The Netherlands

<sup>3</sup> Department of Pathology, University Medical Center Utrecht, The Netherlands

<sup>4</sup> Department of Physiology, Amsterdam UMC, Vrije Universiteit Amsterdam, Amsterdam Cardiovascular Sciences, The Netherlands

<sup>5</sup> Department of Cardiology, Erasmus MC, Rotterdam, The Netherlands

## Abstract

**Background.** Hypertrophic cardiomyopathy (HCM) is a common genetic cardiac disorder that is characterized by the presence of left ventricular hypertrophy, myocyte disarray and fibrosis. Pathologic DNA variants in sarcomeric genes are seen in 50–60% of patients, but the mechanistic origin of the remodeling responses remain unclear. Enhanced molecular insights into these processes could contribute to better understanding the pathogenesis and improve therapeutic strategies for HCM.

**Methods.** To identify gene expression patterns relevant to HCM pathology, we determined intercellular heterogeneity in cardiomyocyte gene expression by performing single-cell RNA sequencing (scRNA-Seq) on myectomy tissue from HCM patients.

**Results.** Septal myectomies provide a unique opportunity to access fresh diseased human heart tissue for scRNA-Seq. We analysed gene expression of individual cardiomyocytes from three HCM patients, who each showed the presence of similar cardiomyocyte subpopulations. Moreover, our data revealed functional links between genes important to HCM. A subpopulation of titin (*TTN*)-enriched cardiomyocytes showed an increased expression of genes involved in muscle contraction and development. A smaller, defined subpopulation of cardiomyocytes expressed high levels of the stress markers Natriuretic Peptide A (*NPPA*) and Natriuretic Peptide B (*NPPB*) and could be linked to muscle development. Further bioinformatic analysis revealed five groups of genes to be tightly correlated in expression (regulons), and allowed us to *de novo* identify transcription factors related to their expression. This expressional correlation could be confirmed in a larger cohort of HCM myectomy samples (n=97). Finally, using forward scatter as a proxy for cell size, we were able to functionally link genes enriched in regulon 2, among which skeletal alpha actin (*ACTA1*), to cell size. The positive link between *ACTA1* and cell size could be confirmed by histology.

**Conclusion.** We have shown that scRNA-Seq on myectomy samples from HCM patients identified new functional links between genes, transcription factors, cell size. These data highlight the presence and influence of cardiomyocyte heterogeneity and provide a wealth of novel insights into molecular events at the base of HCM. Increasing our understanding of disease progression will contribute to the development of improved therapies.

## Introduction

Hypertrophic cardiomyopathy (HCM) is a relatively common genetic cardiac disorder with an incidence of about 1 in 200-500 individuals<sup>81,82</sup>. The phenotype can vary from essentially asymptomatic to end-stage heart failure or cause life-threatening arrhythmias with sudden cardiac death<sup>83</sup>. Typically, patients carry a pathologic DNA variant in genes encoding sarcomere proteins.  $\beta$ -myosin heavy chain (*MYH7*) and myosin binding protein C (*MYBPC3*) are the two most common genes involved. The causal genes in approximately 40% of HCM patients remain to be identified<sup>84</sup>. Clinically, HCM is characterized by unexplained segmental hypertrophy that is usually most pronounced in the basal interventricular septum<sup>85</sup>. Myocyte disarray, a pathological hallmark of HCM, involves 5–40% of the myocardium, and is usually worst in areas of more severe hypertrophy. Other key histological features include interstitial fibrosis and vascular abnormalities<sup>85</sup>.

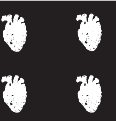
To date the molecular mechanisms that underlie the remodeling processes that occur in HCM remain unclear. While it has been suggested that myocyte disarray and hypertrophy are a direct result from changes in sarcomere function induced by the HCM-related mutations<sup>86</sup>, recent work suggests that the HCM phenotype might also be triggered by a functional imbalance among individual cardiomyocytes. Unequal force generation between adjacent cardiomyocytes can initiate cardiomyocyte and myofibrillar disarray and trigger stretch-induced signaling leading to development of interstitial fibrosis and hypertrophy<sup>87,88</sup>.

Single-cell RNA sequencing (scRNA-Seq) provides a detailed view on gene expression differences between cell types or transcriptome heterogeneity across cells of the same type<sup>89,90</sup>. Recently, we developed an approach that allows us to obtain single cell transcriptomic data from all main cardiac cell types of the adult murine heart under both healthy and diseased conditions<sup>91</sup>. While several studies by now have used scRNA-Seq to study adult cardiac biology in an in-depth manner<sup>68,91-96</sup>, even on adult human cardiomyocytes<sup>94</sup>, so far this has not been done on isolated cells from human HCM myectomy samples.

Here we used scRNA-Seq to study genome-wide transcriptional heterogeneity between individual cardiomyocytes from HCM patients. Single cell analysis on cardiac tissue collected from three patients during septal myectomy indicated the presence of similar subpopulations of cardiomyocytes in each patient. Gene expression analysis allowed us to identify groups of genes that are co-expressed, so-called regulons<sup>97</sup>, and identify the transcription factors that are presumably responsible for their activation. The co-expression of these genes could be validated in bulk-RNA from an independent cohort of myectomy samples. Additionally, index-sorting data enabled us to link gene expression profiles to forward scatter (FSC) as a proxy for cell size, and to link a specific regulon to cardiomyocyte hypertrophy. Finally, we could validate that at least one of the genes from this regulon, skeletal alpha actin (*ACTA1*), was indeed more highly expressed in larger cardiomyocytes. Together these data indicate cardiomyocyte heterogeneity in the human heart and show that scRNA-Seq provides an unprecedented level of insight into cellular and molecular mechanisms that potentially contribute to cardiac remodeling during HCM.

## Materials & Methods

An expanded methods section and any associated references are available in the Online Data Supplement\*. The data, analytic methods, and study materials will be made available by the authors to other researchers for purposes of reproducing the results or replicating the procedure.



**Human heart samples.** Cardiac tissue from the interventricular septum was obtained from myectomy surgery in patients with HCM to relieve left ventricular outflow tract obstruction (n=3 for scRNA-Seq, n=97 for real-time PCR (RT-PCR) analysis and n=1 for scRNA-Seq and index sorting analysis). Approval for the use of human tissue samples was obtained from the local ethics committee (fresh myectomy samples, and bulk myectomy RNA samples) or the local scientific advisory board of the biobank of the University Medical Center Utrecht (explanted heart tissue for histology). Cardiac tissue samples from non-failing donor hearts were used as control (n=9). Four of these were obtained from BioChain (Lots B607033, B711068, B711065 and A504241), the other five were obtained from the Sydney Heart Bank<sup>98</sup>.

**Tissue processing.** Human cardiac tissue samples were digested as described previously<sup>91</sup> and sorted into 384-well plates for scRNA-Seq, or bulk-sorted for RNA quality control (1000 cells/sample) or imaging (5000 cells/well). Additionally, tissue was fixed and embedded for histological analysis.

**Library preparation and sequencing of single cells.** The SORT-seq procedure was applied as described previously<sup>99</sup>. Illumina sequencing libraries were prepared using the TruSeq small RNA primers (Illumina) and sequenced paired-end at 75 bp read length with Illumina NextSeq500.

**Data analysis of scRNA-Seq.** Paired-end reads from Illumina sequencing were mapped with BWA-ALN100 to the human reference genome hg19. For quantification of transcript abundance, the number of transcripts containing unique molecular identifiers (UMIs) per cell-specific barcode were counted for each gene. Next, the RaceID2 algorithm was used to cluster cells based on K-medoids clustering, and provides visualization of single cell gene expression profiles by t-distributed stochastic neighbor embedding (t-SNE)<sup>101, 102</sup>.

**Correlation analyses.** For correlation analyses, the Pearson correlation between the parameter of interest (either expression of a gene of interest or FSC) and every (other) gene was calculated, provided that the gene was expressed in at least 20% of cells.

**Cell size analysis.** Sections were stained using an anti-ACTA1 antibody and WGA and imaged using a confocal microscope. Using ImageJ, cardiomyocytes were manually outlined based on the WGA-signal, then cell area and ACTA1 immunofluorescence were quantified.

## Results

### Single-cell analysis of septal myectomy samples from HCM patients

HCM patients show a heterogeneous remodeling response which is characterized by localized cardiomyocyte hypertrophy, disarray and fibrosis<sup>85</sup>. To explore the molecular mechanisms underlying the cellular heterogeneity observed in HCM, we aimed to examine differential gene expression between individual cardiomyocytes. To this end, we collected cardiac tissue from HCM patients who underwent a septal myectomy for outflow tract obstruction and processed the tissue for scRNA-Seq (Figure 1a). Histological analysis of the myectomy samples confirmed key hallmarks of HCM (Figure 1b). Using our previously optimized method, we enzymatically dispersed cardiac tissue into a single cell suspension and sorted cells into 384-well plates<sup>91</sup>. We gated for larger cells to enrich for cardiomyocytes (Figure 1c). To confirm the viability of the cells after sorting we stained for both DAPI and DRAQ5. Unlike DAPI, DRAQ5 is able to enter live cells and stain the nuclear DNA and therefore enables the segmentation of DAPI-negative events into live cells and cellular debris<sup>103</sup>. Our data showed that 82% of our sorted cells were DAPI negative and DRAQ5 positive (Figure 1d). With each sort, and using the same settings, we additionally collected cells for microscopy and RNA-quality

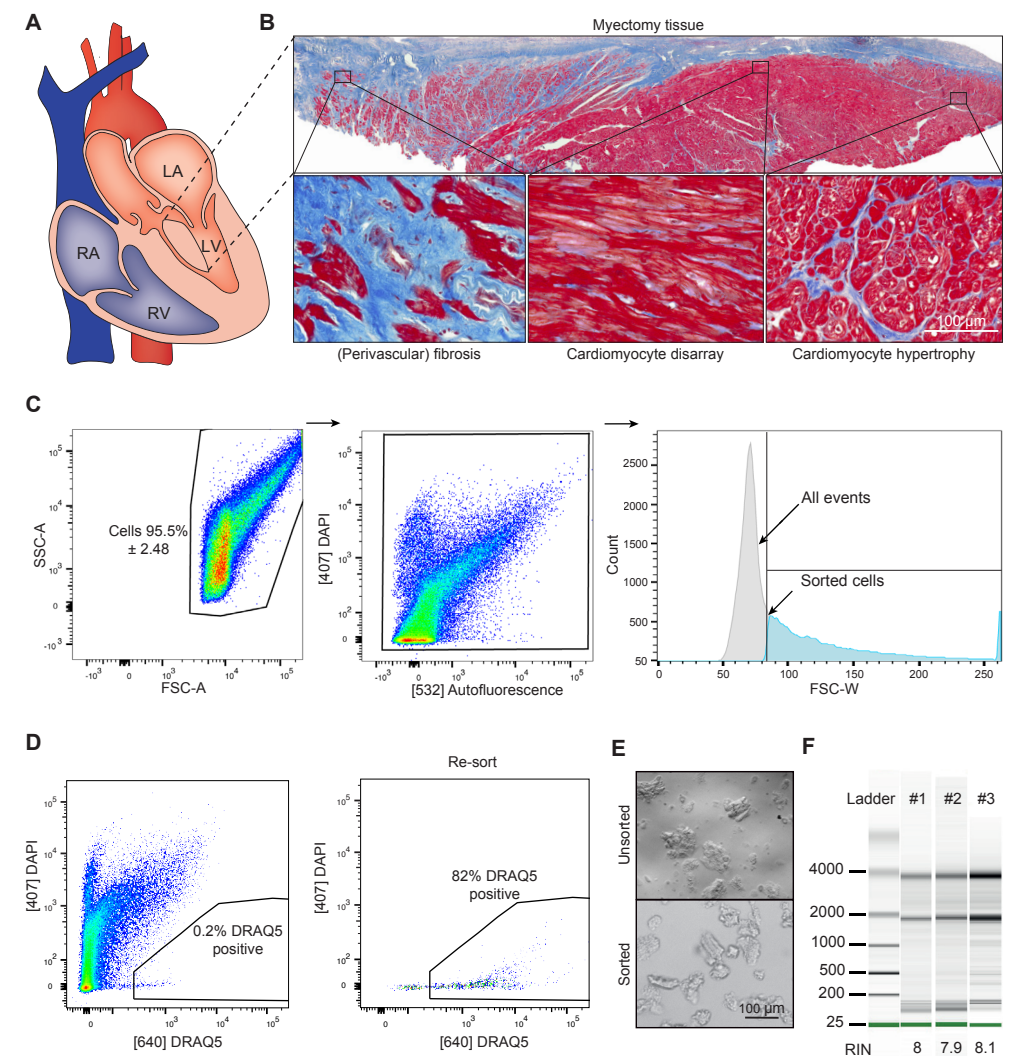


**Figure 1. Single cell analysis of septal myectomy samples from HCM patients.** (a) Schematic representation of the human heart highlighting the septal myectomy sample used for this study. (b) Masson's trichrome staining of myectomy tissue from an HCM patient showing fibrosis, myocardial disarray and cardiomyocyte hypertrophy. (c) Gating strategy used for sorting single cardiomyocytes. (d) Cells collected according to the strategy in (c) were counterstained with DRAQ5 and re-sorted (right panel) to show presence of nucleus in most of the sorted events. Left panel shows the DRAQ5-positive gate to be empty in the first round of sorting, where DAPI-positive events were also still present. (e) Representative images of unsorted (upper image) and sorted cells (lower image). (f) RNA quality control of sorted cells from HCM myectomy tissues. RA indicates right atrium; RV, right ventricle; LA, left atrium; LV, left ventricle; SSC, side scatter; FSC, forward scatter; RIN, RNA integrity number

control. Imaging the cells after sorting visually indicated that we were sorting intact cells (Figure 1e). RNA quality from the dispersed and sorted cells was good, as indicated by RNA Integrity Number<sup>103</sup> (Figure 1f). Together these data showed that our protocol allowed for the collection of good quality RNA from individual, living cells obtained from human septal myectomy samples.

### scRNA-Seq reveals different subpopulations of cardiomyocytes

To obtain single-cell transcriptomes of individual cardiac cells from myectomy samples we used the SORT-Seq protocol as described previously<sup>91,102</sup>. Transcript abundance per gene was quantified according to the method of Grün et al.<sup>89</sup>. After filtering cells for a minimum of 1000 transcripts mapping to the nuclear genome, a total of 1809 cells from three different septal myectomy samples were included for downstream in-silico analysis (Supplemental Figure 1a). Sequencing data was of good quality as only  $49 \pm 16\%$  of transcripts mapped to the mitochondrial genome<sup>104</sup>. Reads mapping to the mitochondrial chromosome were excluded for downstream analysis as they interfere with the clustering. This resulted in an average number of 3496 unique transcripts per cell. Next, the RaceID2 algorithm was applied for identification and clustering of cells (Supplemental Figure 1b)<sup>101, 105</sup>. Cells enriched for *KCNQ1OT1*, a marker of necrotic cells with low-quality RNA<sup>96</sup>, were excluded for subsequent analysis ( $n=174$ , 9.6%) (Supplemental Figure 1c). Clustering of the 1635 remaining cells revealed 5 main clusters ( $n > 10$  cells per cluster) (Figure 2a, Supplemental Figure 1d) to which every patient contributed (Figure 2b, Supplemental Figure 1e). Using the Jaccard similarity, we could confirm that our clusters were sufficiently different to be viewed as separate clusters (Supplemental Figure 1f)<sup>105</sup>. A t-SNE map for *MYH7*, a well-known cardiomyocyte marker, indicated all remaining cells to be cardiomyocytes (Figure 2c).

To get a more detailed view on the cellular identity of the different clusters we looked for the top enriched genes per cluster (Figure 2d, File I in the online-only Data Supplement\*). These data indicated the presence of divergent subpopulations of cardiomyocytes based on differences in gene expression. t-SNE maps for the top enriched genes confirmed the cluster-enriched gene expression (Figure 2e). To explore the functional relevance of the different clusters we performed gene ontology (GO) analysis on the genes that showed at least a 1.2x enrichment per cluster (Figure 2f, Supplemental Figure 2). These data revealed the enriched genes to be involved in processes such as cellular movement (cluster 3), and protein localization and translation (cluster 4) (Figure 2f). In summary, scRNA-Seq on human myectomy samples revealed the presence of functionally different subpopulations of cardiomyocytes in the human HCM heart, which could be relevant for the disease.

### Patient-specific clustering identifies comparable subpopulations of cardiomyocytes

While each patient contributed cells to each of the 5 clusters we identified, these were not equally distributed. To assert whether the clustering was based on biology and not dominated by the data from a single patient, we also performed the clustering analysis for each patient separately. Again, we could identify multiple cardiomyocyte subpopulations in each patient (Figure 3a). For several subpopulations we were able to identify a comparable gene enrichment for all 3 patients, as shown for titin (*TTN*) (Figure 3b).

*TTN* is a large protein that spans from the Z-disc to the M-line around which the sarcomere is organized. The Z-disc assembles and anchors numerous protein complexes of the sarcomere, but also integrates signals that are thought to mediate the stretch response<sup>106</sup>. Because of its importance for sarcomere function, we were intrigued to see that clustering analysis on the pooled samples indicated cluster 3 to be strongly enriched for *TTN* (3.15x compared to all other cells) (Figure 2d). Patient-specific t-SNE maps confirmed the presence of a *TTN*-enriched cluster in each patient (cluster 4, 4, and 8 for patients 1, 2 and 3, respectively) (Figure 3b). Moreover, comparing the enriched genes in these corresponding clusters (1.5x or more), indicated a large overlap in genes ( $n = 29$ ) between the individual patients (Figure 3c, File II in the online-only Data Supplement\*). Histology also con-

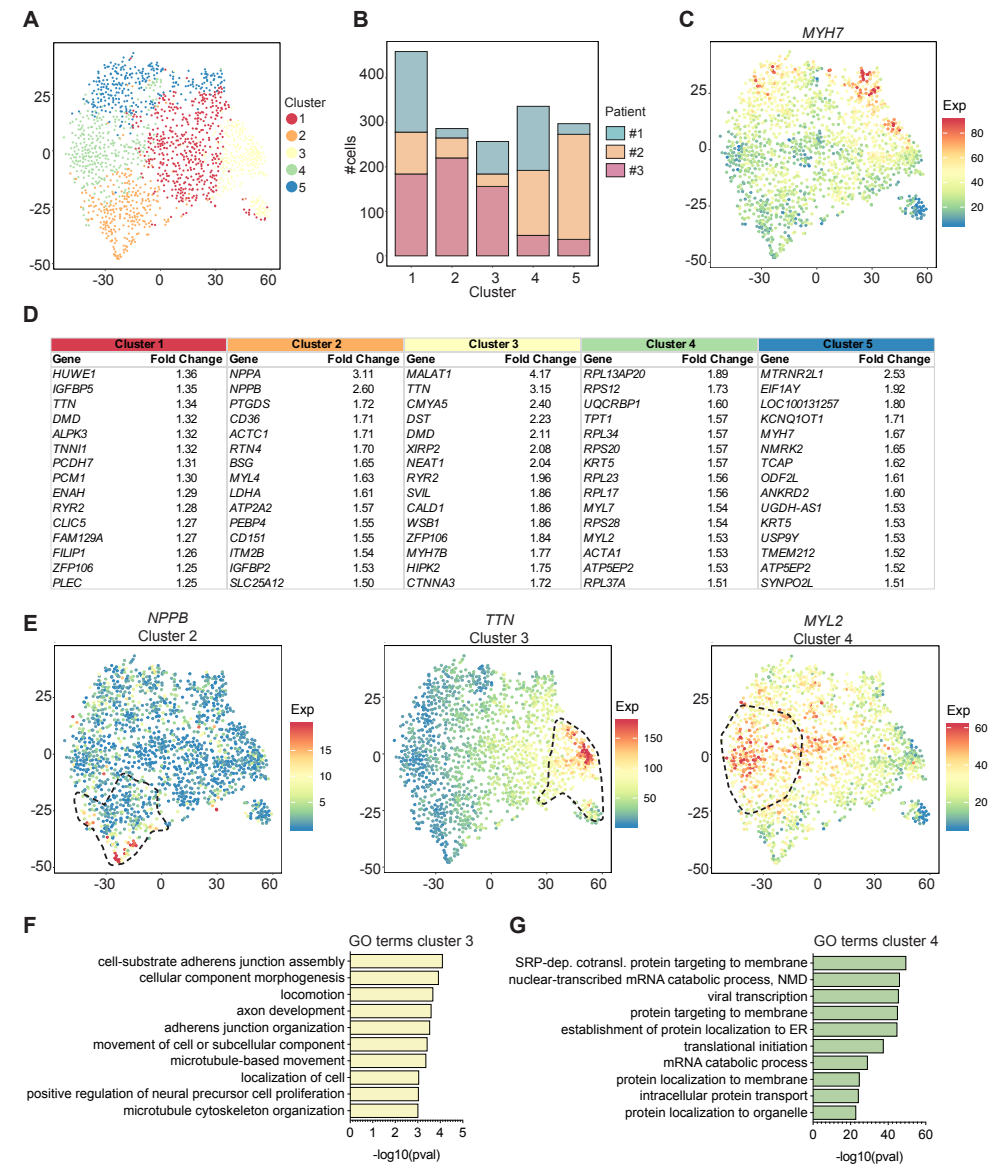


**Figure 2. scRNA-seq revealed different subpopulations of cardiomyocytes.** (a) t-SNE map showing transcriptome similarities between all included cells. The colours represent the clusters identified by RaceID2. (b) Bar graph showing patient contribution to each of the clusters. (c) t-SNE map showing the expression of *MYH7* for each cell. (d) Top 15 most enriched genes in each cluster. Enrichment was calculated for cells in the cluster over all cells outside the cluster. (e) t-SNE maps depicting the expression of *NPPB*, *TTN*, and *MYL2* for all cells. Dashed lines outline the cluster in which each gene was highly enriched. (f, g) Gene ontology analysis for genes showing at least 1.2x enrichment in cluster 3 (f) and in cluster 4 (g). Expression in t-SNE maps is shown as normalized transcript counts on a colour-coded linear scale. t-SNE indicates t-distributed Stochastic Neighbor Embedding; Exp, expression.

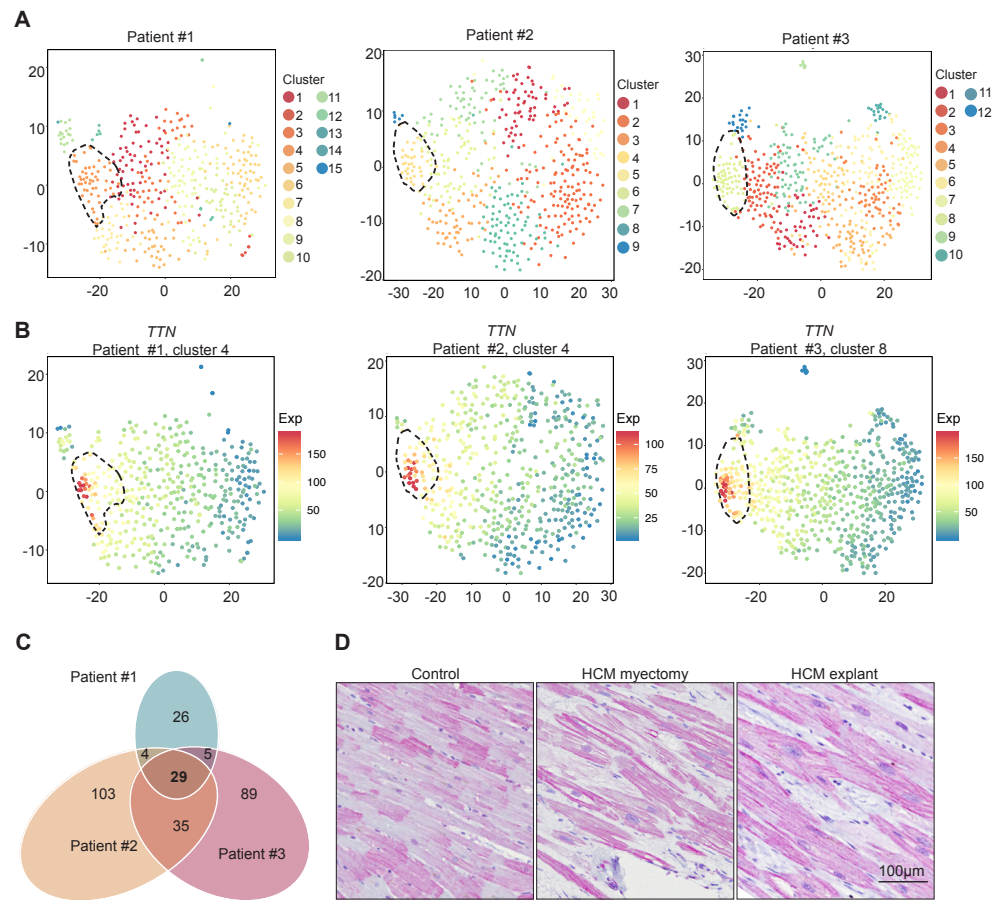


**Figure 3. Patient-specific clustering identified comparable subpopulations of cardiomyocytes.** (a) t-SNE maps for each individual patient depicting transcriptome similarities between all included cells. The colours represent the clusters identified by RaceID2. (b) t-SNE maps showing the distribution in the expression of *TTN* for each individual patient. Dashed lines outline the cluster with the highest *TTN* enrichment for each patient. (c) Venn diagram showing the overlap in gene enrichment between the patient-specific clusters most enriched for *TTN*. Genes more than 1.5x enriched in the *TTN*-enriched clusters were taken along for this analysis. (d) Immunohistochemical staining of septal tissue showing *TTN* expression in an explanted control heart, HCM myectomy tissue and an explanted HCM heart. Expression in t-SNE maps is shown as normalized transcript counts on a colour-coded linear scale. t-SNE indicates t-distributed Stochastic Neighbor Embedding; Exp, expression.

firm heterogeneity in *TTN* at the protein level (Figure 3d). Interestingly, immunohistochemistry also indicated this heterogeneity to be present in control tissue. It is unlikely that the differential staining is caused by differences in titin isoform composition as the antibody should recognize both isoforms. Rather, these findings are in line with previous research showing that *TTN* is one of a set of proteins that have a mosaic expression pattern in the heart<sup>107</sup>.

Taken together, these data confirm that our clustering is not dominated by data obtained from a single patient, nor is it likely to originate from experimental variability. The confirmation of *TTN*-heterogeneity in tissue sections further confirms the validity of our data and suggests that the *TTN*-enriched cell cluster truly is a distinct cardiomyocyte subpopulation.

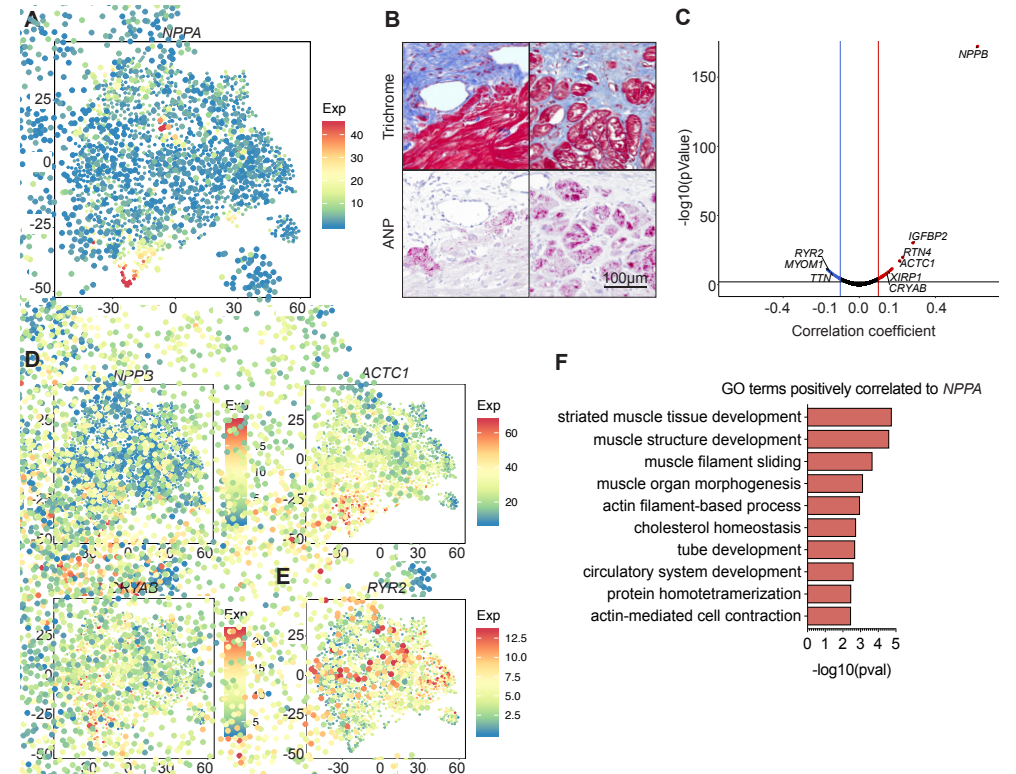


**Figure 4. *NPPA* expression is specific for a subpopulation of cardiomyocytes in HCM patients.** (a) t-SNE map depicting the expression of *NPPA* in all included cells. (b) Representative Masson's trichrome staining (above) and ANP staining (below) on human HCM myectomy tissue showing ANP to be most expressed in cardiomyocytes bordering areas of fibrosis. (c) Volcano plot depicting genes positively (red dots) and negatively (blue dots) correlated to *NPPA* with a p-value < 0.01 and a correlation cut-off set at + or - 0.1. Not all significantly correlated genes are labeled, see Supplemental File III for full list. (d,e) t-SNE maps showing the expression level of the indicated genes which are positively (d) and negatively (e) correlated to *NPPA*. (f) Gene ontology analysis on positively correlated genes with *NPPA*. Expression in t-SNE maps is shown as normalized transcript counts on a colour-coded linear scale; t-SNE indicates t-distributed Stochastic Neighbor Embedding; Exp, expression.

#### *NPPA* expression is specific for a subset of cardiomyocytes in HCM patients

Classically, cardiac expression levels of Natriuretic Peptide A and B (ANP/*NPPA* and BNP/*NPPB*) have served as a hallmark for cardiomyocyte hypertrophy, stress or failure<sup>108</sup>. Our clustering analysis indicated the presence of a subpopulation that is enriched for *NPPA* (cluster 2) (Figure 2d). The heterogeneity in *NPPA* expression was visualized by a t-SNE map indicating the *NPPA* expression per cell (Figure 4a). Immunohistochemistry for ANP on the myectomy samples indicated the ANP-positive cells to predominantly border fibrotic areas in the HCM samples (Figure 4b), while no positive cells could be detected in control hearts (data not shown). Next, we used our scRNA-Seq data to determine which genes show a positive correlation with *NPPA*. Taking a correlation coefficient cut-off of + or - 0.1, we identified 20 positively correlated genes and 13 negatively correlated genes (Figure 4c, File III in the online-only Data Supplement\*). By far the strongest positive correlation was found for *NPPB*, which is in line with expectations and validates the approach as *NPPA* and *NPPB* are expressed in tandem<sup>96</sup>. Strikingly, none of the other correlations (either positive or negative) were particularly strong. t-SNE maps confirmed the specific expression patterns for *NPPB*, cardiac alpha actin (*ACTC1*),

alpha-crystallin B chain (*CRYAB*) and ryanodine receptor 2 (*RYR2*) (Figure 4d and 4e). To explore the cellular function of the *NPPA*-enriched cells we performed GO-analysis on the positively correlated genes and were able to link these genes to development of muscle and the circulatory system (Figure 4f). These data indicate that there is a subpopulation of cardiomyocytes that is enriched for *NPPA* and *NPPB* that are located in stressed, fibrotic regions in HCM hearts. The gene expression profile of these cells could help us identify genes involved in the cardiomyocyte stress response.

### Gene expression heterogeneity reveals patterns of gene coregulation

To better understand gene network underlying HCM, we examined our scRNA-Seq data for correlation patterns in gene expression and identified groups of co-expressed genes (regulons). To identify these regulons, we selected all genes that were expressed in at least 5% of the cells (6079 genes) and generated a correlation matrix. We then selected all genes that had a significant correlation with at least 40 other genes (380 genes). Hierarchical clustering analysis on the correlation matrix for these 380 genes resulted in 5 regulons (Figure 5a and 5b). Among these regulons, regulon #5 contained *TTN* (which we saw strongly enriched in cardiomyocyte cluster #3) as well as a lot of other sarcomere-related genes like cardiomyopathy-associated protein-5 (*CMYA5*) and *RYR2* (Figure 5c, File IV in the online-only Data Supplement\*). Regulon #2 contained a couple of well-known stress markers like myosin regulatory light chain 2, ventricular isoform (*MYL2*) and *ACTA1* (Figure 5c, File IV in the online-only Data Supplement\*).

To identify transcription factors that could potentially be involved in the coregulation of the genes per regulon, we screened the promotor regions of these genes for binding site enrichment. In doing so, we identified several potential transcriptional regulators that could be involved in the expressional correlation (Figure 5c). Both regulon #2 and #5 showed an enrichment for myogenic enhancer factor 2 (MEF2) binding sites, a well-known regulator of muscle genes<sup>109</sup>, which would fit with the GO-term enrichment analysis indicating muscle-related processes (Figure 5c).

Concluding, our data indicate that costameric proteins and those from the myospryn complex are co-expressed and potentially under the control of MEF2. Moreover, these observations illustrate the modularity of gene expression regulation and our ability to extract important regulatory players and interactions based on these features.

### Validation of gene expression correlations in larger cohort of HCM samples

To validate the gene expression correlations found in the identified regulons, we used 97 additional septal myectomy samples from HCM patients (HCM) and included nine left ventricle RNA samples from non-failing donor hearts as controls (CNTRL). Out of the 97 HCM patients, 42 (43%) had a known pathogenic HCM mutation (*MYBPC3*, n=26; *MYH7*, n=7; multiple, n=3; other, n=6) while the causal mutation was unknown for the rest of the HCM patients (Figure 6a, Table I in the online-only Data Supplement\*).

An increase in the ratio of *MYH7* to  $\alpha$ -myosin heavy chain (*MYH6*) has been linked to cardiac disease<sup>110</sup>. To validate the disease phenotype in the different biopsies we first determined the *MYH7*/*MYH6* ratio and expression level of 2 collagen genes. Compared to control hearts the *MYH7*/*MYH6* ratios were clearly increased in the HCM biopsies, as determined by RT-PCR (Figure 6b). Consistently, samples showed an increase in collagen, type II, alpha 1 (*COL2A1*) in the HCM samples compared to control (Figure 6c). RT-PCR confirmed the correlation between genes identified in regulon #2 (Figure 6d) and regulon #5 (Figure 6e). These data independently confirm the validity of the correlations in gene expression that we identified in our scRNA-Seq data.

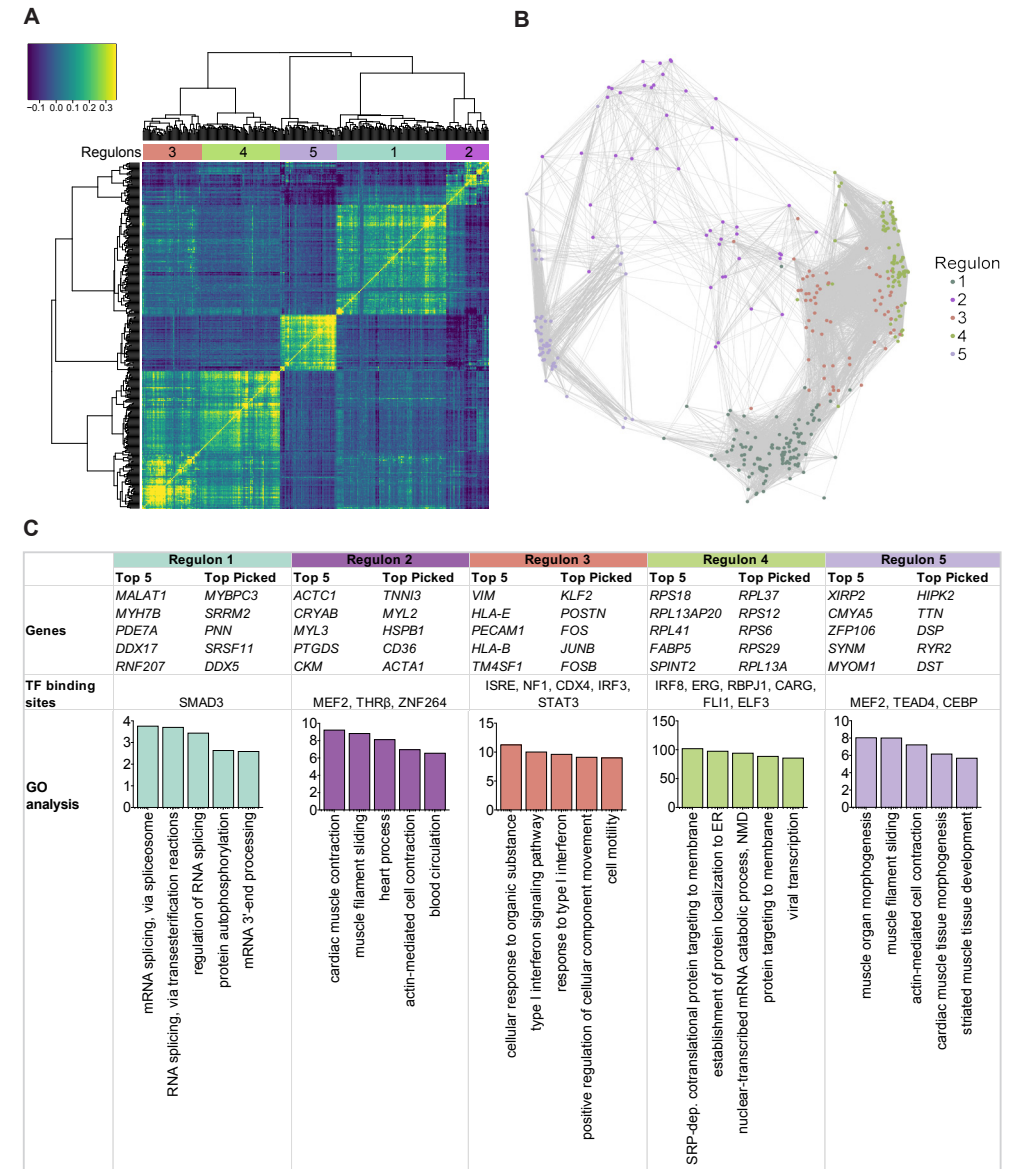


**Figure 5. Gene expression heterogeneity reveals patterns of gene coregulation.** (a) Heatmap of the Pearson correlation matrix of a subset of detected genes that had a significant correlation with at least 40 other genes. Using hierarchical clustering, we identified 5 regulons. (b) Gene interaction network depicting the positive correlations (shown as edges) between genes selected in (a) (shown as nodes). The colours represent the different regulons. (c) Top 5 representative genes (see main text) and genes of interest within each regulons, TF binding sites enriched in the proximal promoters of the genes in each regulon, and gene ontology analysis for each regulon; TF indicates transcription factor.

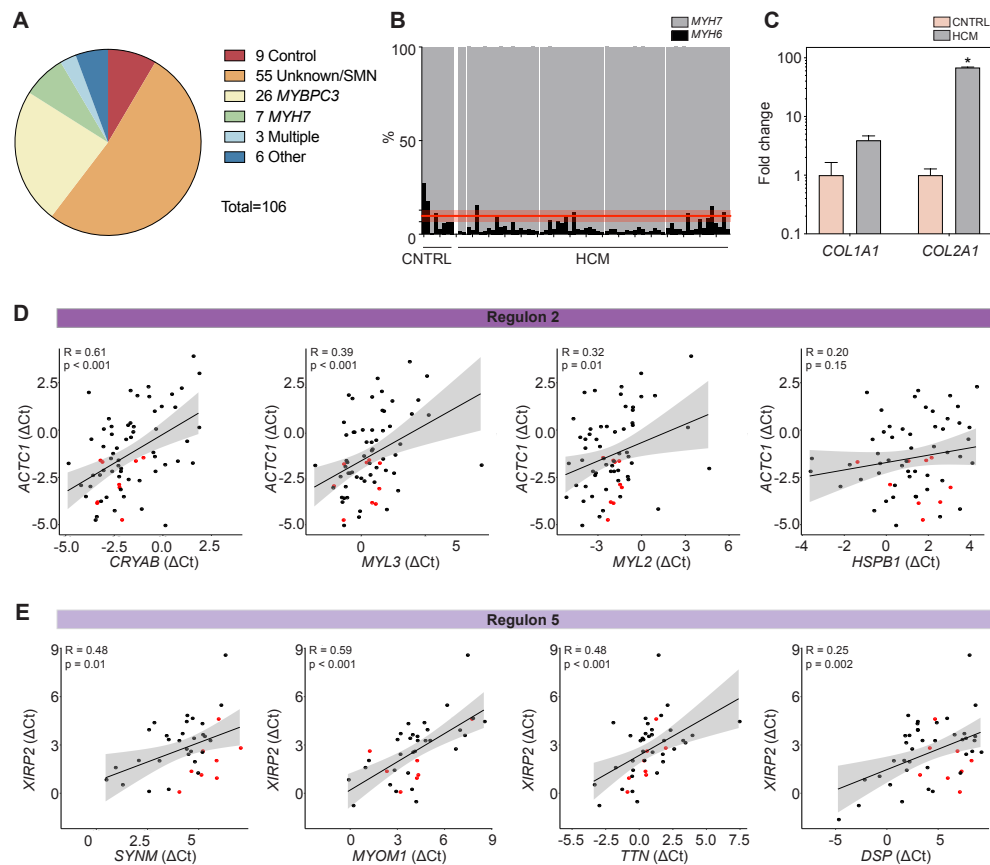


**Figure 6. Gene-gene correlations identified by scRNA-Seq can be validated in independent HCM myectomy bulk RNA samples.** (a) Pie chart showing the distribution of causal HCM mutations in 97 HCM and 9 non-failing donor heart samples. (b) Histogram showing the percentage of *MYH6* and *MYH7* gene expression per HCM sample. Control sample average is shown as a red horizontal line + or - 1 SEM. (c) RT-PCR quantification of *COL1A1* and *COL2A1* expression levels in HCM myectomy samples versus non-failing donor hearts normalized to *GAPDH*. (d) RT-PCR validation of correlation between genes identified together in Regulon 2, and (e) RT-PCR validation of correlation between genes identified together in regulon 5; SMN indicates sarcomere mutation-negative, black dots, HCM samples; red dots, control samples; LV, left ventricle; \*\*\*\*  $P < 0.001$

### Integration of cell size with scRNA-Seq reveals hypertrophy-associated genes

As one of the hallmarks of HCM is cardiomyocyte hypertrophy, it is of great interest to integrate cell size with the transcriptomic data obtained from scRNA-Seq. In a recent paper by Nomura et al.<sup>94</sup>, adult cardiomyocytes were isolated using a Langendorff system, cell area was measured using a microscope and cells were manually picked for sequencing. This is a labor-intensive method and has the risk of causing a selection bias. Previously, index sorting data has been used to integrate morphological parameters obtained from flow cytometry with gene expression data obtained from scRNA-Seq from bone marrow stem cells<sup>111</sup>. To determine the enriched genes in hypertrophic cardiomyocytes, we used FSC-A as a proxy for cell size and linked this to the gene expression profile in the individual cardiomyocytes.

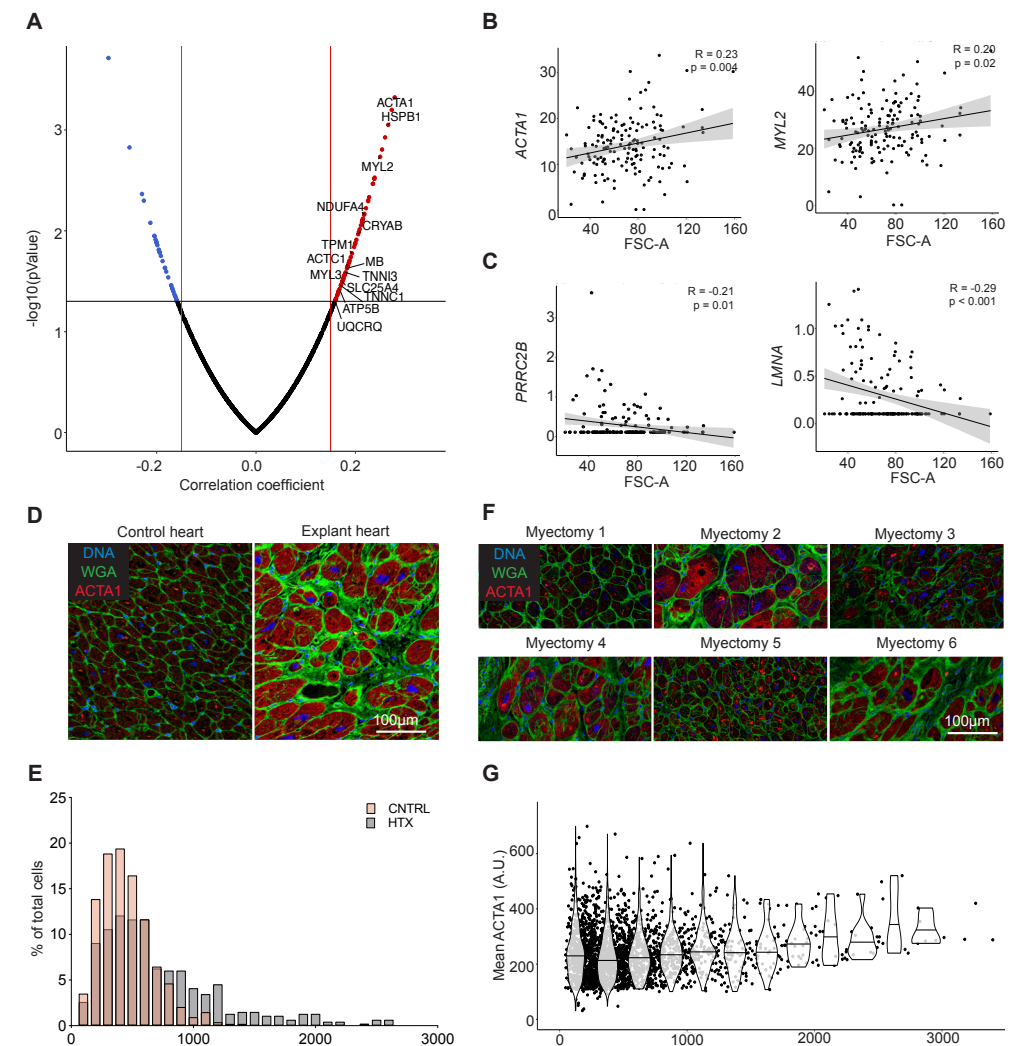


**Figure 7. Index sorting provides a gene expression profile for enlarged cardiomyocytes.** (a) Volcano plot depicting genes positively (red dots) and negatively (blue dots) correlated to FSC-A as a proxy for cell size with a  $p$ -value  $< 0.1$  and a correlation cut-off set at  $-0.2$  and  $0.2$ . (b,c) Scatter plots showing positive (b) and negative (c) correlations between the expression level of indicated genes and FSC-A as a proxy for cell size. Line represents correlation with 95% CI. (d) Representative immunofluorescent images from a control heart and an explanted HCM heart stained for ACTA1 (red) and WGA (green). (e) Histogram showing the different distributions in cardiomyocyte cross-sectional area between a control heart and an explanted HCM heart. (f) Representative images of WGA- (green) and ACTA1- (red) stainings on 6 HCM myectomy samples. (g) Quantification of cardiomyocytes cross-sectional area and mean ACTA1 fluorescence in the samples from (f)

Correlation analysis of cell size versus gene expression revealed genes both positively and negatively correlated with cell size (Figure 7a through 7c, File V in the online-only Data Supplement\*), with *ACTA1*, *MYL2*, myosin regulatory light chain, atrial isoform (*MYL7*) and *MYH7* among the positively correlated genes. While some of these genes have previously been linked to hypertrophy<sup>112</sup>, to our knowledge, we are the first to show the correlation of these genes to cardiomyocyte size on the single-cell level rather than on the organ-wide level. Notably, many of the genes identified in

regulon #2 are also positively correlated to cell size (30%; Figure 5c and 7a (labeled genes), File IV and V in the online-only Data Supplement\*), including the gene most strongly correlated to cell size: *ACTA1*. To further explore this observation we performed immunostaining for *ACTA1* in a human control heart and an end-stage explanted HCM heart. This revealed *ACTA1* to be clearly increased in the HCM heart (Figure 7d) and both mean cardiomyocyte size and the spread of cardiomyocyte size to be larger as well (Figure 7e). In order to further validate the correlation between *ACTA1* and cell size, we performed these same immunostainings in our septal myectomy samples and quantified *ACTA1* immunofluorescence and cell size (Figure 7f). This confirmed the positive correlation between *ACTA1* and cell size (Figure 7g).

In conclusion, we have shown that, with scRNA-Seq, we can identify several cardiomyocyte subpopulations, identify several regulons and the transcription factors potentially responsible for their induction. Additionally, we are able to relate one of these regulons to cardiomyocyte size and confirm these data in additional myectomy samples. These data allow us to identify new targets to investigate in follow-up studies for modulation of the HCM disease process.

## Discussion

Using scRNA-Seq, we are able to show for the first time that myectomy samples from HCM patients consist of subpopulations of cardiomyocytes that are transcriptomically different. Gene correlation analysis revealed transcriptionally related gene clusters, so called regulons, that are likely influencing cellular function. Additionally, based on scatter properties we are able to unveil the gene expression profile linked to larger cardiomyocytes, which could contribute to a better understanding of disease driving mechanisms in HCM.

The heterogeneity we identified is consistent with earlier observations showing phenotypic differences between cardiomyocytes. This is exemplified by heterogeneous calcium sensitivity<sup>87</sup>, differential distribution of sodium channels<sup>113</sup>, differential *TTN* isoform composition across the LV wall<sup>114</sup>, intercellular variation in *MYBPC3* expression<sup>88</sup>, and previous single-cell sequencing papers in the heart showing heterogeneity in adult mouse cardiomyocytes<sup>91,94</sup>. Related to genetic cardiomyopathy, Davis et al. have shown the influence of a sarcomere gene mutation on calcium binding properties to be a key determinant in whether the mutation causes HCM or dilated cardiomyopathy<sup>14</sup>. As patients are generally heterozygous for the pathogenic mutation, intercellular differences in the expression ratio between the healthy and mutant allele may lead to intercellular differences in force generation. This heterogeneity in force generation will then lead to uneven pulling on the myocytes which subsequently triggers local stretch-induced signaling<sup>87</sup>.

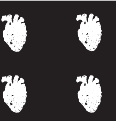
Based on the inter-myocyte transcriptomic heterogeneity, our algorithm clustered the cardiomyocytes into 5 distinct subpopulations. Within those, one cluster was highly enriched for *TTN* as well as for *CMYA5* and Xin actin-binding repeat-containing protein 2 (*XIRP2* or *CMYA3*), which have both been shown to interact with the z-disc<sup>115, 116</sup>. Repeating the clustering for each patient separately yielded similar clusters in each individual patient. The fact that we get similar clustering results in individual patients and that we find co-enrichment for transcripts that have been shown to colocalize at protein level, reinforces that our sequencing data is based on biological regulation rather than random gene expression or random gene detection.

Another cluster was highly enriched for *NPPA* and *NPPB*. A t-SNE map for *NPPA* indicated that only few cells in our dataset express high levels of *NPPA*, while the rest of the cells do not express it, or only at a very low level. The reason we picked up so few cells with high *NPPA* expression may

be due to our single cell isolation protocol. As we show in Figure 4b, ANP-positive cells appear to be in close proximity to highly fibrotic areas, matching previous findings<sup>117</sup>. Their encapsulation by the extracellular matrix (ECM) might make these cells less likely to be successfully liberated from the tissue by our digestion protocol and hence excludes them from our scRNA-Seq analysis.

In addition to clustering cells based on their gene expression, we also clustered genes based on their co-expression across our population of sequenced cells. Among the five regulons we identified this way, two were enriched for MEF2 binding sites. One of these regulons (#5) contained well-known genes of the contractile apparatus, like *TTN*, *RYR2* and dystrophin (*DMD*), but also *CMYA5*. *CMYA5* is a striated muscle specific A kinase anchoring protein (AKAP) that associates with the sarcoplasmic reticulum (SR) and costameres and anchors Protein Kinase A (PKA) to myofilaments<sup>118</sup>. PKA has been shown to phosphorylate a variety of proteins that are important for regulating cardiac contractility and performance in response to  $\beta$ -adrenergic signaling and it needs anchoring by an AKAP to provide it with spatial specificity<sup>119</sup>. Interestingly, *CMYA5* has also been shown to interact with *TTN*, *RYR2* and *DMD*<sup>118, 120, 121</sup>. This implies that genes encoding for the different myospryn complex members are transcriptionally coregulated in human cardiomyocytes and differentially expressed among the different cardiomyocyte clusters. In addition, well over 20% of the genes in regulon #2 were positively correlated to cardiomyocyte size at the single-cell level, and some of these genes have previously been shown to be induced by MEF2 in hypertrophic remodeling<sup>122</sup>. Recently, Nomura et al.<sup>94</sup> isolated single cardiomyocytes from the mouse heart using a Langendorff setup and after scRNA-Seq they identified 'modules' of co-expressed genes. Subsequently, they identified several modules that correlated with cardiomyocyte size in mice one week after transverse aortic constriction (TAC). The genes in our hypertrophy-associated regulon match surprisingly well (62%) with the hypertrophy-associated modules (M1, M2, M5, M11 & M16) in the paper by Nomura et al., especially considering that they are looking at a mouse model of early pressure overload-induced hypertrophy. The fact that our scRNA-Seq method is able to, unbiasedly, re-identify gene-gene or gene-morphology correlations on the single-cell level that match with previously published organ-wide data reinforces that our observations originate from biological regulation, rather than from unconnected random gene expression or experimental variation. Additionally, this highlights the unique benefit of using flow cytometry for scRNA-Seq: the morphological parameters of the sorted cells can be used to link gene expression to cell size.

Comparing our study to other published single-cell studies it is evident that a lot of experimental choices regarding cell collection and obtaining sequencing data can influence the outcome. Firstly, scRNA-Seq of cardiomyocytes is challenging simply due to the size of the cells. In the broader scRNA-Seq field, several strategies are currently used to separate single cells into individual wells or droplets, some of which allow for the high-throughput processing of thousands of transcriptomes in a cost-effective manner. However, all these high-throughput strategies have physical constraints regarding the size of the cells. Commercially available single-cell sorting platforms like Fluidigm C1 and Chromium can currently only sort cells that are up to 25-50  $\mu\text{m}$  in diameter. This is considerably smaller than adult mammalian cardiomyocytes, which can be approximately 125  $\mu\text{m}$  along the longitudinal axis<sup>123</sup>. This challenge has been circumvented by performing single nucleus RNA-sequencing on cardiac tissue, which has the logistical benefit that it can be used on frozen tissue, but the drawbacks are that the RNA-yield per cell is lower and that there will be enrichment for RNAs residing predominantly in the nucleus<sup>124</sup>. In 2018, our group managed to successfully sort adult cardiomyocytes from fresh tissue using flow cytometry<sup>91</sup>. Afterwards, doubts were raised about wheth-



er the cardiomyocytes sorted by gating DAPI-negative events could just be cell fragments without a nucleus<sup>125</sup>. In the current study we show more thoroughly that we are sorting live and intact myocytes by additionally using the membrane-permeable DNA-dye DRAQ5 to show that our DAPI-negative sorted cells are at least 82% DRAQ5-positive, proving they are just unnucleated debris<sup>125</sup>.

A recent paper used large particle FACS (LP-FACS) to isolate cardiomyocytes for scRNA-Seq<sup>104</sup>, showing that by using just the extinction and time of flight flow cytometry parameters, but no DAPI fluorescence, they were able to sort rod-shaped viable myocytes. This supports our observation that, in our protocol, sorting cardiomyocytes based on just the time of flight yields live cardiomyocytes. As a measure for RNA-quality, Kannan et al. analyze the fraction of mitochondrial reads for several published cardiomyocyte scRNA-Seq studies as well as their own data. They show that the approximately 40% mitochondrial transcripts they find fall in the expected range of 30-50% for cardiomyocytes, which matches very well with the 40% mitochondrial transcripts found in a bulk cardiomyocyte sequencing study<sup>104</sup>. In contrast, they show other techniques to result in higher mitochondrial transcript numbers ranging from approximately 70% (Fluidigm C1<sup>127</sup> or handpicking myocytes<sup>94</sup>) to 90% (conventional FACS<sup>91</sup>). However, in our current study, we find a mitochondrial transcript content of 49% in our cardiomyocytes, again reinforcing that our RNA is of suitable quality.

The downside to our flow cytometry approach is that it is relatively expensive per sequenced transcriptome (compared to microfluidics-based approaches) and proven biased towards the larger cells. While it is thought that roughly 30% of cells in the adult heart are cardiomyocytes, in our previous scRNA-Seq study<sup>91</sup>, 75% of the cells that we sequenced were cardiomyocytes and we captured less of the smaller cardiac cell types as a trade-off. Because of these different cellular biases in sorting strategies, the scRNA-Seq technology is currently unable to reliably capture the relative abundance of all adult cardiac cell types in an unbiased fashion. For the current study we utilized this bias towards larger cells to only sort cardiomyocytes. However, we cannot exclude that in our data we are missing a subset of small cardiomyocytes due to the size-gating in our protocol. Additionally, we are missing the full set of small cardiac cells, like fibroblasts, and can therefore not make any statements regarding their contribution to the HCM phenotype or their potential cross-talk with cardiomyocytes.

Of course, some challenges still remain. Here, we used the heterogeneity among cardiomyocytes to identify coregulation among genes and link genes to cardiomyocyte size, but the current study does not help us identify the source of the observed heterogeneity. A likely cause of cardiomyocyte heterogeneity (in mutation-positive HCM) is allelic imbalance, where the ratio between the mutant and healthy allele is not equal between all cardiomyocytes and this results in heterogeneity in force-generation capacity between myocytes<sup>128</sup>. The sequencing method used in this study only captures the 3' end of every transcript and is therefore not suitable for deducing from which allele a read originated. Further studies, focused on capturing allele-discerning SNPs or the mutation itself will be required to shed further light on this matter. Another factor contributing to heterogeneity may be the cellular location in the tissue, environmental factors like wall stress, perfusion and local ECM composition could be easily envisioned to have an effect on the myocyte transcriptome. As we are digesting the tissue, we have no information about the spatial origin of our cells or their relation to one another. Finally, as this study uses fresh tissue obtained from an HCM-specific surgery it is very difficult to obtain suitable control tissue.

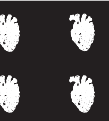
In summary, we used scRNA-Seq of human HCM myectomy samples to analyze transcriptomic heterogeneity between cardiomyocytes. This revealed co-regulation patterns in gene expression and allowed us to link a group of tightly co-expressed genes to cardiomyocyte cell size. We confirmed our findings in a large cohort of independently collected HCM myectomy samples as well as in histological sections of explanted HCM hearts. Further studies will reveal whether any of the genes that we linked to cardiomyocyte cell size can be therapeutic targets. Meanwhile, this study shows the feasibility of our previously published flow cytometry-based single cell sequencing protocol on human cardiac tissue, allowing it to also be applied to obtain more mechanistic insights in other cardiac diseases.

## Acknowledgements

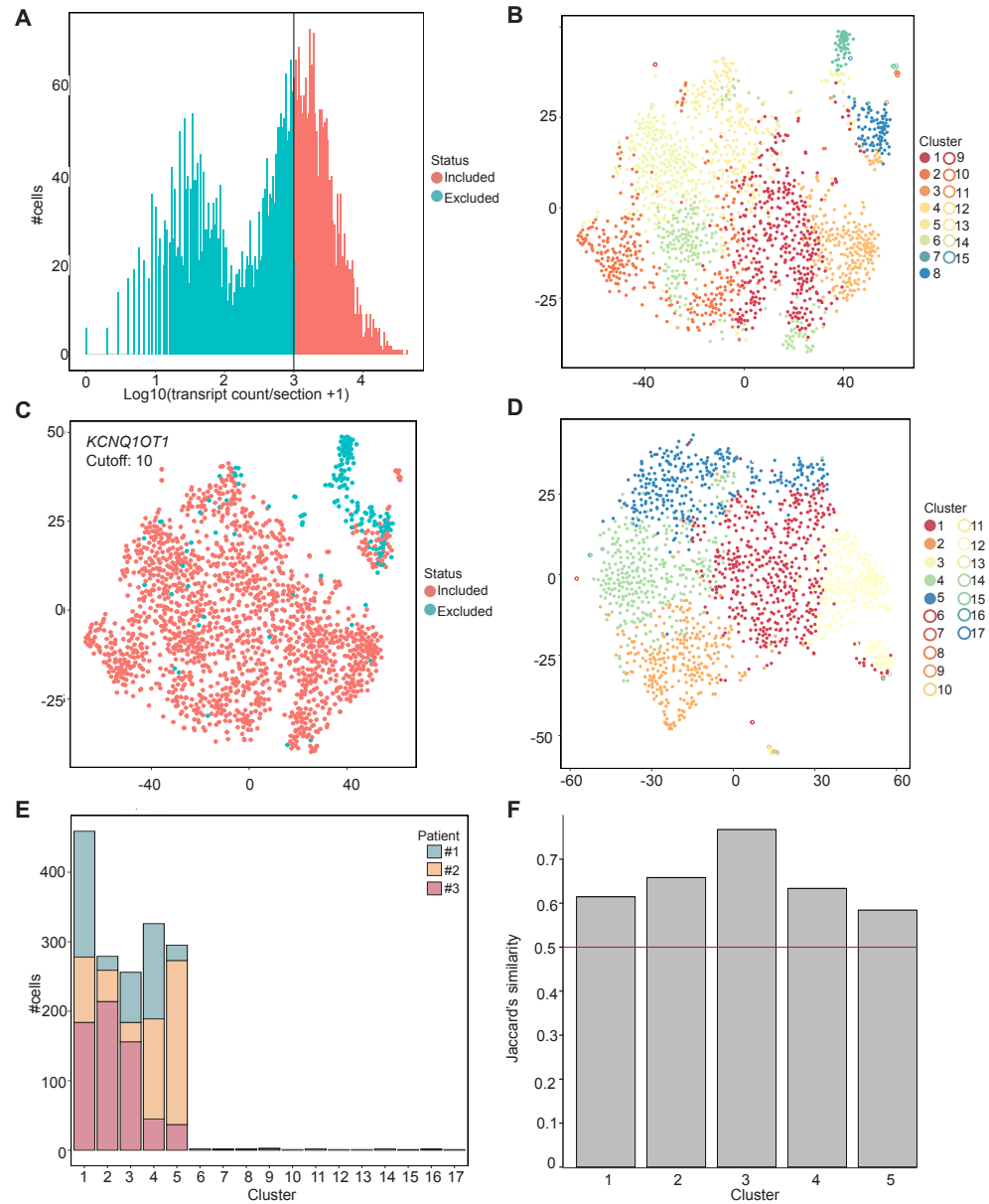
We gratefully acknowledge Roy Huurman, Sylvie Dekker, Martine de Boer, Harm de Wit and Peter van Geel from the Erasmus Medical Center for their help in facilitating sample collection and help with the flow cytometry. We thank Stefan van der Elst from the Hubrecht Institute FACS facility for his help with the viability experiments and presenting our flow cytometry data. We thank Jeroen Korving from the Hubrecht Institute for his help with the myectomy histology. We thank Anko de Graaff and the Hubrecht Imaging Center for supporting the imaging. We thank Cris dos Remedios for the use of donor heart samples from the Sydney Heart Bank.

## Sources of funding

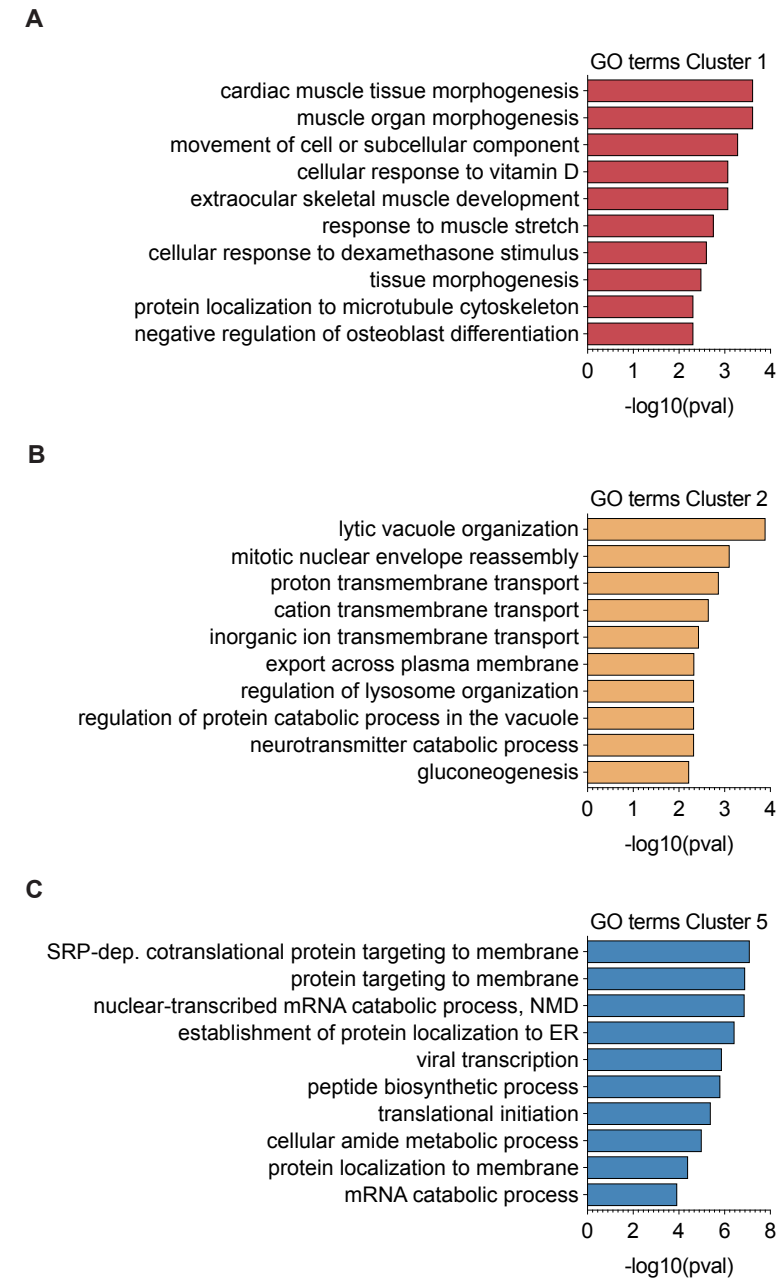
This work was supported by the Leducq Foundation (14CVD04), the European Research Council under the European Union's Seventh Framework Programme (ERC Grant Agreement CoG 615708 MICARUS) and the Dutch CardioVascular Alliance (DCVA), an initiative with support of the Dutch Heart Foundation, DCVA2017-18 ARENA-PRIME and DCVA2014-40 CVON-DOSIS.



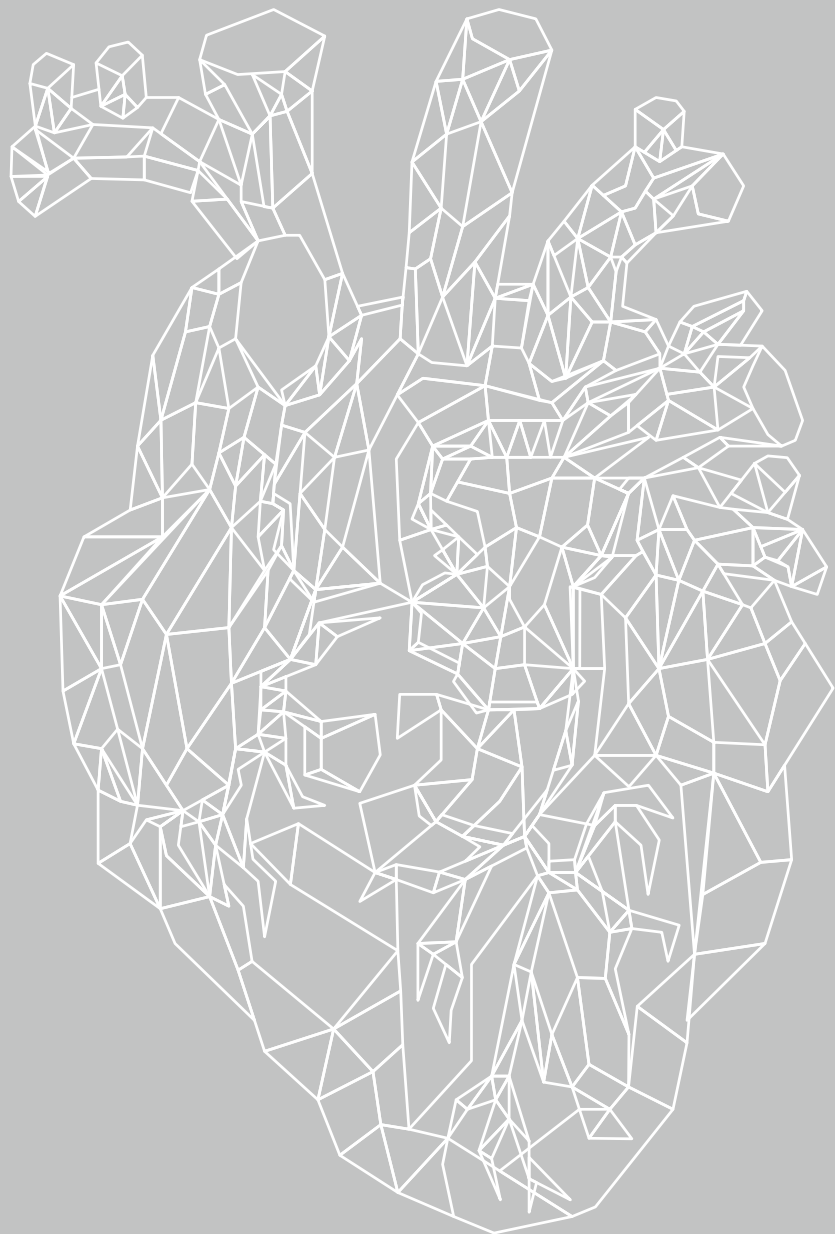
Supplemental Materials



**Supplemental Figure 1.** (a) Histogram showing distribution of number of reads per well. Line represents the 1000 reads/well cut-off for inclusion in the analysis. (b) t-SNE map depicting transcriptome similarity between all included cells. RaceID2 clustering identified 8 primary clusters as well as 7 clusters consisting of cells that are outliers in their respective primary clusters. (c) t-SNE map showing cells coloured according to their expression level of *KCNQ1OT1*. Cells with high expression (over cut-off of 10 reads per cell, after downsampling to 1000 total reads per cell) were excluded from further analysis. (d) t-SNE map depicting transcriptome similarity between remaining cells after exclusion of *KCNQ1OT1*-high cells. RaceID clustering identified 5 primary clusters as well as 12 clusters consisting of cells that are outliers in their respective primary clusters. (e) Bar graph showing patient contribution to each of the clusters. (f) Jaccard's similarity score per cluster. t-SNE indicates t-distributed Stochastic Neighbor Embedding.



**Supplemental Figure 2.** (a-c) Gene ontology analysis on genes showing at least 1.2x enrichment in Cluster 1 (a), Cluster 2 (b) and in Cluster 5 (c).



# Chapter 5

**Discussion**

J.E.C. Eding

## Discussion

Given the enormous healthcare costs and the high morbidity and mortality rates related to cardiovascular disease, there is a need for new and improved cardiac therapies. RNA therapeutics are an example of a novel promising method to increase survival and quality of life of patients suffering from cardiac disease. In this thesis we have studied the workings of cardiac microRNA (miR) therapeutics under different cardiac disease conditions (chapter 2), studied a new cardiac delivery vehicle for RNA therapeutics (chapter 3) and used single-cell RNA-sequencing (scRNA-seq) to identify new possible targets for RNA therapeutics in hypertrophic cardiomyopathy (HCM, chapter 4).

### Designing miR therapeutics requires knowledge of the disease-dependent function of miRs

In early miR studies, miR deletions generally had no overt phenotypic effect in healthy animals. However, these deletions did affect the animals' response to cardiac diseases<sup>31, 129, 130</sup>. Based on this observation, miRs were thought to be involved in the response to stress. Therefore, we expected miR inhibitors (antimiRs) to function differently in health than they do in disease. In **Chapter 2** we proved this hypothesis by showing different target derepression by antimiR-208a in baseline conditions compared to two different types of cardiac disease. In this chapter, we revealed that (anti)miR-208a regulates three sets of target genes: one set that is only regulated in healthy conditions, one specific to the disease condition and one regulated in both health and disease conditions. In line with these findings, others have shown that target regulation may additionally be context-dependent: targets are sometimes targeted *in vitro* but not *in vivo* or vice versa<sup>131</sup>.

Knowing that both context and disease influence the effect of miRs is of crucial importance for the design and interpretation of (pre)clinical trials. Importantly, these results show that *in vitro* testing of miR therapeutics is of limited value as the miR will probably target different mRNAs in an *in vivo* context and that testing the effect of the therapeutics in healthy subjects, whether animals or patients, is of limited value as mRNA targeting is disease-dependent.

In Chapter 2 we did not identify the mechanism by which disease state influences the mRNA targeting of miR-208a. We did show a slightly increased uptake of antimiR-208a in stressed cells compared to non-stressed cells *in vitro*. While an increased uptake is a plausible explanation for an increased level of derepression of miR-208a targets in disease conditions, it does not explain how some targets are disease-specific. The simplest explanation for the differential target regulation in healthy vs diseased conditions lies in disease-specific changes in the transcriptome. For example, if the disease induces the expression of disease-specific genes that are not expressed in healthy conditions, then these genes pose new targets for the miR to regulate that did not exist under baseline conditions. Alternatively, the occurrence of disease could influence the ratio of splice variants of a gene, which may influence the proportion of transcripts of that gene that has a target site for the miR. In addition, alternative polyadenylation, a process in which 3' untranslated regions (UTRs) are shortened in a manner that is highly dependent on cell type and context, may result in the loss of miR binding sites<sup>132</sup>. Finally, the 3D-structure of the 3' UTR of the mRNA determines whether the RNA-induced silencing complex (RISC) will be able to bind the mRNA. If disease conditions influence how the 3' UTR folds, this may also influence miR function<sup>133</sup>.

### Future directions

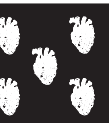
Independent of the mechanism by which disease state affects the miR target landscape, taking into account the effect of disease state is essential to finding successful antimiR therapeutics. The currently popular target prediction algorithms, used to generate lists of mRNAs that are likely targeted by a certain miR (or list of miRs that target a certain mRNA), generally take into account only the presence and evolutionary conservation of a miR's seed sequence in the 3' UTR. These algorithms have false positive rates up to 50%<sup>133</sup>. Improving these algorithms by making them incorporate organ- and disease-specific targeting information will allow researchers to make more informed decisions on the design of their experiments. With the plethora of publicly available RNA sequencing data it might be possible to compile lists of differentially regulated, differentially spliced and/or differentially poly-adenylated genes between healthy and diseased organs and use these to improve target prediction algorithms. Work like this is currently being done, resulting in tools like mirTime<sup>134</sup>, which facilitates the search for miR targets in time-series experiments where both miR- and mRNA sequencing data is available, and TargetExpress<sup>135</sup>, which uses tissue-specific mRNA expression profiles to re-rank the predictions of popular algorithms like TargetScan. These tools will aid in selection of (anti)miRs and possibly result in a higher success rate of trials testing miRNA therapeutics.

### Improving cardiac delivery of RNA therapeutics

In addition to deciding which mRNA to target, another important decision when designing RNA therapeutics is the method of delivery. Subcutaneous injection is a convenient way to systemically deliver RNA therapeutics to practically any organ. However, while systemically delivered RNA therapeutics do target the heart<sup>30</sup>, they preferentially end up in the liver and kidney, resulting in a risk of side-effects in those organs<sup>24</sup>. In order to reduce this risk, several strategies are being developed to better target RNA therapeutics to the heart. These strategies can be divided in strategies in which RNA therapeutics are delivered systemically with a system that results in target organ specificity on the one hand and local delivery to the target organ on the other hand.

### Systemic delivery with targeting

RNA therapeutics can be delivered using viral vectors. Some of these vectors are intrinsically somewhat selective for cardiomyocytes, thereby increasing target organ specificity. Modulation of gene expression with viral vectors can be used to force expression of a silencing RNA (siRNA), a miR, a miR decoy transcript or even to overexpress a protein-coding mRNA. There are several types of viral vectors available that can be used to such an effect, each with their own advantages and disadvantages. An adenoviral vector leads to robust expression in most types of cells. However, this overexpression is short-lived as the targeted cells are only transiently transduced<sup>22</sup>. In contrast, the use of lentiviral vectors results in sustained expression of the delivered gene as the vectors integrate into the host genome. However, as this integration may disrupt host genes, including for example tumor suppressor genes, these vectors can result in detrimental side-effects and are therefore not good candidates for clinical application<sup>22</sup>. Engineered adeno-associated viruses also lead to a strong and persistent expression of the delivered gene, but generally do so without integration into the host genome. Additionally, these vectors have some selectivity for cardiomyocytes. Downsides of these vectors are that (1) controlling the dosage is hard, (2) though less common than with lentivirus, they may still ran-



domly disrupt a gene by genomic integration<sup>136</sup> and (3) up to 70% of healthy individuals have neutralizing antibodies against AAVs<sup>22</sup>.

Another method for targeting RNA therapeutics to the heart is hijacking an endogenous system for intercellular communication: the exosomes. Exosomes transfer mRNAs and miRs from the cell that produced them to other cells. Exosomes are produced by inward budding of the membrane of an endosome, forming a multivesicular body<sup>137</sup>. This multivesicular body can then fuse with the plasma membrane of the cell, releasing the exosomes into the extracellular space. After fusion with other cells, the content of the exosomes has been shown to influence the recipient cell's behavior<sup>22</sup>. This system can be hijacked as a delivery vehicle, as it is possible to load exosomes with proteins or nucleic acids of choice<sup>138</sup>. Systemically delivered exosomes tested to so far primarily target liver, kidney and spleen<sup>138</sup>. However, it has been shown that the cell type from which exosomes are derived determines what the target cells are. This suggests that proteins on the exosome surface are either able to recognize or are recognized by the target cell<sup>138</sup>. Identification of proteins or synthetic peptides that specifically bind to cardiomyocytes might therefore result in the development of exosomes that target the heart specifically<sup>139</sup>.

### Local delivery

Targeting a systemically delivered drug to a specific organ is challenging. While a high concentration of the drug is injected at the injection site, the drug enters the circulation, gets distributed across the whole body and then needs to reach a high concentration specifically at the target site. While viral vectors and endosomes are promising techniques in this direction, viral vectors have significant drawbacks for clinical use and the targeting of endosomes is still in development. The need for a potent targeting system can be circumvented by delivering the therapeutic to the target site directly. A system is available to facilitate targeted injections in the human myocardium. The NOGA MyoStar catheter system uses electromechanical mapping to identify the infarcted area and then allows transendocardial injections in or around this region<sup>140</sup>. However, local injection alone is probably not enough to get robust cardiac targeting. As the heart is a well-perfused organ, injected oligonucleotides will quickly be washed out if they are not delivered with a method that retains them at the injection site. A promising way to locally retain therapeutics is the use of a hydrogel as a vehicle<sup>141</sup>. Hydrogels used for this purpose are typically materials that are in a liquid state during injection, but quickly form a gel once they are injected. The addition of therapeutics into the liquid before injection allows for the use of hydrogels as a drug delivery depot at the injection site that slowly releases the drug to provide maximal local availability. **Chapter 3** of this thesis focused on hydrogel-based intramyocardial delivery of anti-miRs. In this study, we investigated the UPy-PEG hydrogel as a delivery vehicle. This hydrogel is based on the characteristics of the UPy-group to form hydrogen bonds at physiological pH but not a higher pH. Therefore, this hydrogel is in a liquid form at high pH, facilitating the mixing of drugs and injection through a catheter, but forms a gel upon injection. We investigated the safety of this hydrogel and discovered that injection of the gel does not negatively affect cardiac function. When anti-miRs were intramyocardially injected using this hydrogel, they were slightly more efficacious compared to similar injections using PBS as a vehicle. However, this was not enough to obtain a robust regenerative effect after ischemic damage. Possibly, this is due to the fact that the gel is cleared from the heart within 24 hours.

### Future directions

Future research on this gel should focus on increased retention of the gel in the heart. The UPy-PEG system is elegantly extensible by the introduction of monofunctional UPy-molecules: UPy-groups coupled to a group introducing new functionality. For example, the UPy-Cat molecule described in Chapter 3 introduced a positive charge to the hydrogel, resulting in slower anti-miR release. Furthermore, addition of the UPy-Gd molecule, which introduces gadolinium-DOTA to the hydrogel, has been shown to improve MRI detection<sup>78</sup>. Addition of a, yet to be designed, monofunctional UPy-molecule with tissue-adhesive properties could therefore possibly improve tissue retention of the UPy-PEG, thereby increasing targeted delivery of the drugs.

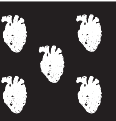
The UPy-PEG system is not the only hydrogel that has been investigated for cardiac delivery of regenerative drugs. Many other materials have also been tested, including hyaluronic acid, alginate, collagen and gelatin<sup>141</sup>. A particularly interesting hydrogel is a hydrogel that is made from the extracellular matrix (ECM) of healthy porcine heart tissue. The healthy porcine heart tissue is decellularized using detergents and the remaining ECM is subsequently dried and milled to a powder. The addition of water reconstitutes the powder into a hydrogel. This hydrogel contains a lot of proteins and proteoglycans native to the heart that turn out to be important environmental clues that instruct cardiac cells on how to reform the myocardium. Injection of this hydrogel without any additional drug was sufficient to improve cardiac function of infarcted rat hearts after myocardial infarction<sup>140</sup>. As this hydrogel has already been shown to remain in the heart for an extended period of time, perhaps it can also be used for cardiac delivery of microRNA therapeutics. Especially as this ECM-derived hydrogel has already been shown to be able to release extracellular vesicles and anti-miRs that are still active in vitro after release<sup>66</sup>.

### Finding new RNA targets in HCM

While several RNA-therapeutics, like anti-miR-15<sup>24</sup>, have been designed to induce regeneration after myocardial infarction in experimental studies, identifying targets in hypertrophic cardiomyopathy is more challenging as the pathogenesis is less well understood. Recently, single-cell sequencing techniques have been developed that allow for transcriptomic profiling at the cellular resolution. This has proven valuable for identifying rare cell types and investigating their transcriptome<sup>142</sup>. In addition, it allows for the investigation of intercellular heterogeneity in cell populations that seem homogenous, like cardiomyocytes. Therefore, its application to HCM may yield more insight into the pathogenesis and help identify targets for RNA therapeutics. In **Chapter 4** of this thesis, we applied a scRNA-seq protocol designed for the murine heart<sup>143</sup> to fresh human HCM myectomy samples. We showed that this protocol yields live and intact cells and used the data to investigate cardiomyocyte heterogeneity in HCM. First, we confirmed the transcriptomic heterogeneity that we expected to find among cardiomyocytes based on earlier reports of contractile heterogeneity between cardiomyocytes in patients with HCM<sup>87</sup>. Combining the single-cell resolution transcriptomic data with cell-size data obtained from the flow cytometer during cell isolation allowed us to identify genes linked to cardiomyocyte size. However, as is to be expected with new techniques, several challenges remain:

### RNA quality

With bulk RNA-seq, tissues can be snap-frozen to stop any biological processes and preserve the RNA which can then later be isolated in bulk from the tissue and used for library prepara-



tion. With scRNA-seq, the tissue is first dissociated into a single-cell suspension. Subsequently, single cells are isolated from this suspension before they can be lysed or frozen. Both dissociation and single cell isolation take time and during this time biological processes may still be active and transcriptome changes may take place, reducing the relevance of the obtained data. These challenges are described in more detail below.

### Single-cell dispersion of tissue

For most solid tissues, like the myocardium, the dispersion of tissue into a single-cell solution generally consists of cutting the tissue into small pieces, then enzymatic digestion of the extracellular matrix followed by mechanical dissociation. It has recently been shown that the enzymatic digestion of skeletal muscle cells causes the expression of stress markers in a subset of skeletal muscle satellite cells, leading to the spurious detection of a new subtype of satellite cells in scRNA-seq<sup>144</sup>. The duration of the enzymatic digestion was an important factor in this phenomenon. Therefore, to keep such detrimental effects to a minimum, it is important to keep the dissociation as short as possible.

Aside from causing stress, cardiomyocytes may also be damaged by the mechanical dissociation step. Healthy adult cardiomyocytes have a rod-shaped appearance, while damaged cardiomyocytes are thought to contract and present a more rounded shape. Rod-shaped cardiomyocytes are most readily obtained from Langendorff-perfusion protocols, where the native vasculature is used to perfuse the tissue with the enzyme solution. While this method yields less damaged myocytes than the traditional tissue chunk-based enzymatic digestion, it also has its drawbacks: (1) it requires access to the native vasculature, which precludes its use in tissue pieces that don't include a large enough branch of the coronary vasculature; (2) the Langendorff method requires specialized materials and expertise with the setup; (3) the digestion protocol takes time during which the transcriptome can change from the *in vivo* situation that is under investigation<sup>145</sup>.

For the study described in chapter 4 of this thesis, Langendorff perfusion was not an option due to the lack of easy access to the native vasculature in myectomy samples. Therefore, we used a chunk-based dissociation protocol of 15 minutes of enzymatic digestion followed by mechanical dissociation in order to minimize the effect of the digestion-time on the transcriptome.

### Single-cell isolation

After the dissociation, single cells need to be isolated for sequencing. Currently popular techniques in non-cardiac fields are based on microfluidics techniques like Drop-seq<sup>146</sup>, where cells and reagents are passed through tiny fluid channels to form small droplets containing a single cell and all required sequencing barcodes. These techniques allow for cost-effective sequencing of large numbers of cells. However, they are not suitable for the sequencing of cardiomyocytes as cardiomyocytes are too big to pass through the microfluidics channels.

Single myocytes can also be isolated using a flow cytometer with a large nozzle that can deposit one myocyte in each well of a 384-well plate that already contains all sequencing reagents, including solution that prevent RNA degradation. This method, SORT-seq<sup>99</sup>, is less cost efficient than the microfluidics methods and has the risk of inducing batch effects between different plates containing cells from a single sample<sup>147</sup>. Handpicking cells and transferring them to a plate for sequencing is also an option<sup>94</sup>, but it is labor intensive, has lower throughput

and comes with the risk of inadvertently introducing a bias based on which cells are picked. Similar to the issue raised with the single-cell dispersion protocol, it is probably best to keep the isolation time to a minimum to prevent stress-induced transcriptomic changes and to prevent researcher-induced bias. For the study described in chapter 4, we felt therefore that using SORT-seq was the best option.

There has been discussion about the effect of flow cytometry on the quality of the isolated cells<sup>125</sup>. Even the largest available nozzle on a flow cytometer is not large enough for cardiomyocytes to pass through in all orientations. Damage caused by passage through the flow cytometer would yield in unviable cells<sup>125</sup>. If so, this would result in rounded instead of rod-shaped cells<sup>125</sup>. Additionally, in the scRNA-seq data, damaged myocytes would be expected to have a disproportionately high mitochondrial read count as cytoplasmic mRNA leaks from the cell while mitochondrial RNA is retained by the mitochondrial membrane<sup>104</sup>. In chapter 4 we have shown the mitochondrial read fraction in our data to correspond with expected mitochondrial read fractions from bulk data, suggesting no extensive damage from our dissociation and isolation procedure.

### Preventing stress-induced transcriptional changes

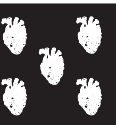
Apart from dissociation- or isolation-induced damage to the cells, a change in the cell's transcriptome can also be caused by the still living cells transcriptionally reacting to a changing environment during the dissociation and isolation phases. This cannot be fully prevented, as some incubation time is essential in any dissociation protocol of live cells. However, transcriptional activity of the cells can be stopped by snap freezing the tissue. While this also precludes the isolation of intact and living single cells, it is still possible to isolate nuclei from this tissue and sequence the nuclear RNA (snRNA-seq)<sup>148</sup>. As an additional benefit, nuclei are compatible with microfluidics approaches, allowing the sequencing of a far greater number of nuclei in a more cost-efficient manner<sup>148</sup>. Downsides of this approach are: (1) the exclusion of cytoplasmic RNA, leading to an overrepresentation of nuclear residing RNAs<sup>148</sup>; (2) the low RNA content of nuclei might make it difficult to detect lowly expressed transcripts<sup>148</sup>; (3) the possibility of sequencing multiple nuclei from a single, multinucleated, myocyte as if they were unrelated cells.

Given these drawbacks, we decided to perform single cell RNA-sequencing on whole cells instead of snRNA-seq.

### Read information

The RNA isolated from single cells needs to be processed into a sequencing library before it can be sequenced. The common commercial sequencing platforms, like Illumina, produce reads of at most 300 base pairs. As this is nowhere near the full length of most transcripts, these library preparation methods all include a step to fragment the RNA (or generated complementary DNA) into smaller pieces. Additionally, to be able to sequence the fragments they need to be tagged with adapters (to attach to the sequencing chip) and barcodes (specific to the cell of origin). Finally, the material needs to be amplified in order for there to be enough of it to be picked up by the sequencer<sup>149</sup>.

The order in which these steps are performed in the protocol greatly influences the final data<sup>149</sup>. The amplification step, for example, creates multiple copies of each cDNA molecule, thus ensuring that at least one of these copies will be detected during sequencing. However, by default it is impossible to distinguish whether two identical reads are two copies of the same



original transcript or whether they are each a copy of a distinct transcript. This can be solved by adding unique molecule identifiers (UMIs) to the adapters, resulting in a more accurate transcript count<sup>149</sup>. However, this only works if adapters are ligated early in the library preparation procedure, before fragmentation and amplification. A downside of ligating the adapters early during the protocol is that this limits the sequencing to the 3' ends of the transcripts and therefore precludes full-length sequencing of transcripts while full-length transcript sequencing provides more information on splice variants and allele-specific expression. However, work is underway to develop a protocol that allows the inclusion of UMIs and also enables full-length transcript sequencing<sup>150</sup>.

#### **Future directions**

In chapter 4 of this thesis, we have shown that performing chunk-based single-cell dissociation of human myectomy tissue followed by single cell isolation using flow cytometry is feasible and allows for the correlation of cell size to gene expression. Our isolation strategy paves the way for future studies which will use new or adapted library preparation protocols to investigate the effect of the healthy-to-mutant transcript ratio on the HCM phenotype.

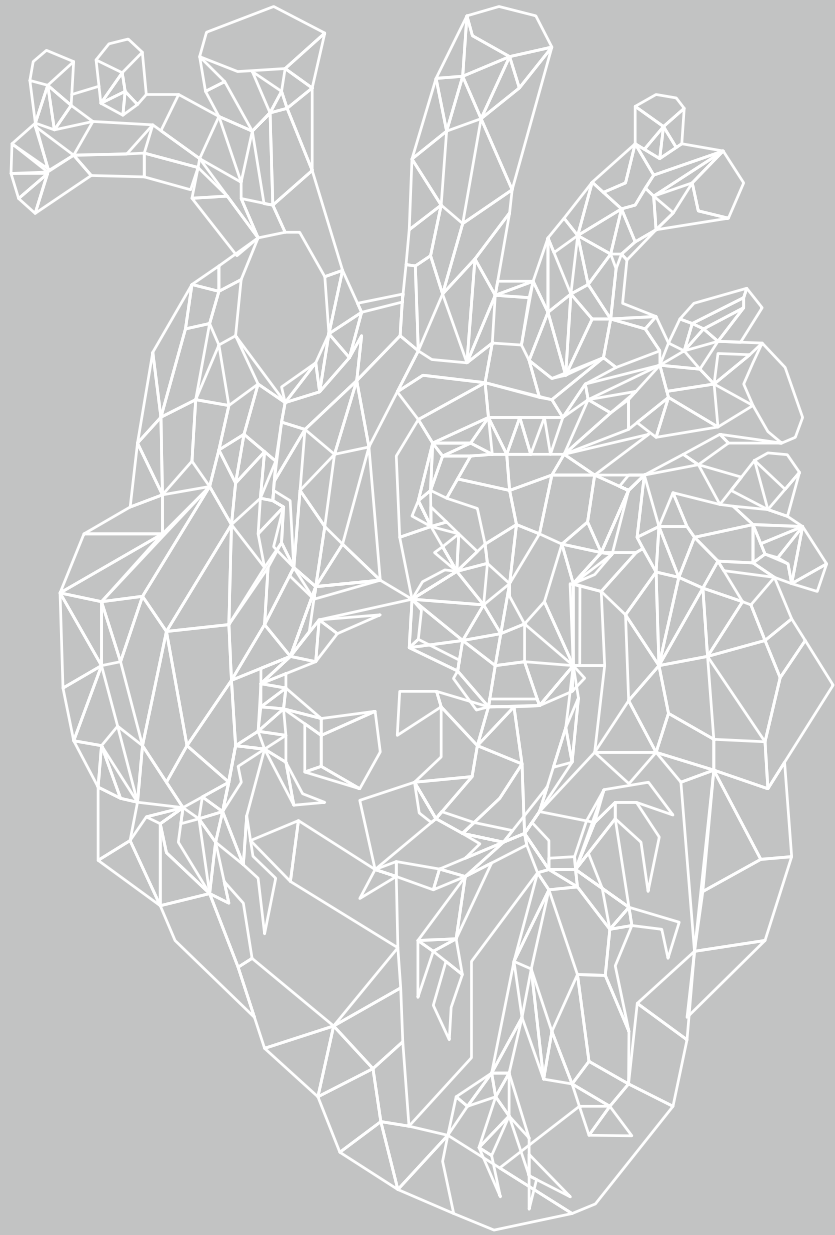
#### **Concluding remarks**

RNA therapeutics are a promising method to treat patients with heart disease. In this thesis we uncovered that microRNA therapeutics have different effects depending on disease conditions. This finding is of utmost importance for the design of future trials, as it shows that diseased cells, tissues and/or animals need to be incorporated in the design early on.

A major challenge of RNA therapeutics is targeting the heart specifically. Efficient targeting decreases side-effects on other organs and increases therapeutic benefits in the heart. We studied a hydrogel-based delivery system for use as a possible targeted delivery system. While our hydrogel is poorly retained in the heart, it did result in a slightly increased cardiac delivery of antimiR-195. Therefore, further studies with other, more promising, hydrogels in combination with RNA therapeutics have great potential.

If the delivery challenges can be solved, RNA therapeutics have the potential to be very powerful drugs by allowing the modulation of the transcriptome without the downsides of traditional gene therapy. To make better informed decisions on the design of new RNA therapeutics, a better understanding of the molecular pathways involved in cardiac disease is essential. To this end, we studied the feasibility of scRNA-seq on fresh human HCM myectomy samples. We show that scRNA-seq is feasible for adult human cardiac tissue and pave the way for future studies to improve our understanding of the pathological mechanism behind the HCM phenotype.

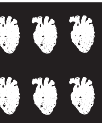




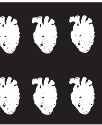
# Appendices

- A. References**
- B. Nederlandse samenvatting**
- C. Acknowledgements**
- D. About the author**

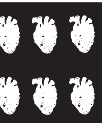
1. Joseph P, Leong D, McKee M, Anand SS, Schwalm J-D, Teo K, Mentz A and Yusuf S. **Reducing the Global Burden of Cardiovascular Disease, Part 1.** *Circulation Research*. 2017;121:677-694.
2. Weber C and Noels H. **Atherosclerosis: current pathogenesis and therapeutic options.** *Nature Medicine*. 2011;17:1410-1422.
3. Gerbin KA and Murry CE. **The winding road to regenerating the human heart.** *Cardiovasc Pathol*. 2015;24:133-140.
4. Porrello ER, Mahmoud AI, Simpson E, Hill JA, Richardson JA, Olson EN and Sadek HA. **Transient regenerative potential of the neonatal mouse heart.** *Science*. 2011;331:1078-80.
5. Haubner BJ, Schneider J, Schweigmann U, Schuetz T, Dichtl W, Velik-Salchner C, Stein J-I and Penninger JM. **Functional Recovery of a Human Neonatal Heart After Severe Myocardial Infarction.** *Circulation Research*. 2016;118:216-221.
6. Bergmann O, Zdunek S, Felker A, Salehpour M, Alkass K, Bernard S, Sjöström SL, Szewczykowska M, Jackowska T, Dos Remedios C, Malm T, Andra M, Jashari R, Nyengaard JR, Possnert G, Jovinge S, Druid H and Frisen J. **Dynamics of Cell Generation and Turnover in the Human Heart.** *Cell*. 2015;161:1566-75.
7. Bergmann O, Bhardwaj RD, Bernard S, Zdunek S, Barnabé-Heider F, Walsh S, Zupicich J, Alkass K, Buchholz BA, Druid H, Jovinge S and Frisén J. **Evidence for cardiomyocyte renewal in humans.** *Science (New York, NY)*. 2009;324:98-102.
8. Ibanez B, James S, Agewall S, Antunes MJ, Bucciarelli-Ducci C, Bueno H, Caforio ALP, Crea F, Goudevenos JA, Halvorsen S, Hindricks G, Kasrati A, Lenzen MJ, Prescott E, Roffi M, Valgimigli M, Varenhorst C, Vranckx P, Widimský P and Group ESC. **2017 ESC Guidelines for the management of acute myocardial infarction in patients presenting with ST-segment elevation: The Task Force for the management of acute myocardial infarction in patients presenting with ST-segment elevation of the European Society of Cardiology (ESC).** *European Heart Journal*. 2017;39:119-177.
9. Elliott P, Andersson B, Arbustini E, Bilinska Z, Cecchi F, Charron P, Dubourg O, Kühn U, Maisch B, McKenna WJ, Monserrat L, Pankuweit S, Rapezzi C, Seferovic P, Tavazzi L and Keren A. **Classification of the cardiomyopathies: a position statement from the european society of cardiology working group on myocardial and pericardial diseases.** *European Heart Journal*. 2007;29:270-276.
10. Brodehl A, Ebbinghaus H, Deutsch MA, Gummert J, Gartner A, Ratnavadivel S and Milting H. **Human Induced Pluripotent Stem-Cell-Derived Cardiomyocytes as Models for Genetic Cardiomyopathies.** *Int J Mol Sci*. 2019;20.
11. Cahill TJ, Ashrafian H and Watkins H. **Genetic Cardiomyopathies Causing Heart Failure.** *Circulation Research*. 2013;113:660-675.
12. Ormerod JOM, Frenneaux MP and Sherrid MV. **Myocardial energy depletion and dynamic systolic dysfunction in hypertrophic cardiomyopathy.** *Nature Reviews Cardiology*. 2016;13:677.
13. Yotti R, Seidman CE and Seidman JG. **Advances in the Genetic Basis and Pathogenesis of Sarcomere Cardiomyopathies.** *Annual Review of Genomics and Human Genetics*. 2019;20:129-153.
14. Davis J, Davis LC, Correll Robert N, Makarewich Catherine A, Schwanekamp Jennifer A, Moussavi-Harami F, Wang D, York Allen J, Wu H, Houser Steven R, Seidman Christine E, Seidman Jonathan G, Regnier M, Metzger Joseph M, Wu Joseph C and Molkentin Jeffery D. **A Tension-Based Model Distinguishes Hypertrophic versus Dilated Cardiomyopathy.** *Cell*. 2016;165:1147-1159.
15. Elliott PM, Anastasakis A, Borger MA, Borggrefe M, Cecchi F, Charron P, Hagege AA, Lafont A, Limongelli G, Mahrholdt H, McKenna WJ, Mogensen J, Nihoyannopoulos P, Nistri S, Pieper PG, Pieske B, Rapezzi C, Rutten FH, Tillmanns C, Watkins H, Contributor A, O'Mahony C, Guidelines ECFP, Zamorano JL, Achenbach S, Baumgartner H, Bax JJ, Bueno H, Dean V, Deaton C, Erol Ç, Fagard R, Ferrari R, Hasdai D, Hoes AW, Kirchhof P, Knuuti J, Kolh P, Lancellotti P, Linhart A, Nihoyannopoulos P, Piepoli MF, Ponikowski P, Sirnes PA, Tamargo JL, Tendera M, Torbicki A, Wijns W, Windecker S, Reviewers D, Hasdai D, Ponikowski P, Achenbach S, Alfonso F, Basso C, Cardim NM, Gimeno JR, Heymans S, Holm PJ, Keren A, Kirchhof P, Kolh P, Lionis C, Muneretto C, Piro S, Salvador MJ, Wolpert C, Zamorano JL, Frick M, Aliyev F, Komissarova S, Mairesse G, Smajić E, Velchev V, Antoniadis L, Linhart A, Bundgaard H, Heliö T, Leenhardt A, Katus HA, Efthymiadis G, Sepp R, Thor Gunnarsson G, Carasso S, Kerimkulova A, Kamzola G, Skouri H, Eldirsi G, Kavoliuniene A, Felice T, Michels M, Hermann Haugaa K, Lenarczyk R, Brito D, Apetrei E, Bokheria L, Lovic D, Hatala R, Garcia Pavia P, Eriksson M, Noble S, Srbinovska E, Özdemir M, Nesukay E and Sekhri N. **2014 ESC Guidelines on diagnosis and management of hypertrophic cardiomyopathy: The Task Force for the Diagnosis and Management of Hypertrophic Cardiomyopathy of the European Society of Cardiology (ESC).** *European Heart Journal*. 2014;35:2733-2779.
16. Banerjee MN, Bolli R and Hare JM. **Clinical Studies of Cell Therapy in Cardiovascular Medicine.** *Circulation Research*. 2018;123:266-287.
17. Menasché P, Vanneaux V, Hagège A, Bel A, Cholley B, Parouchev A, Cacciapuoti I, Al-Daccak R, Benhamouda N, Blons H, Agbulut O, Tosca L, Trouvin J-H, Fabreguettes J-R, Bellamy V, Charron D, Tartour E, Tachdjian G, Desnos M and Larghero J. **Transplantation of Human Embryonic Stem Cell-Derived Cardiovascular Progenitors for Severe Ischemic Left Ventricular Dysfunction.** *Journal of the American College of Cardiology*. 2018;71:429-438.
18. Tang X-L, Li Q, Rokosh G, Sanganalmath SK, Chen N, Ou Q, Stowers H, Hunt G and Bolli R. **Long-Term Outcome of Administration of c-kit<sup>POS</sup> Cardiac Progenitor Cells After Acute Myocardial Infarction.** *Circulation Research*. 2016;118:1091-1105.
19. Lazar E, Sadek HA and Bergmann O. **Cardiomyocyte renewal in the human heart: insights from the fall-out.** *Eur Heart J*. 2017;38:2333-2342.
20. Vagnozzi RJ, Molkentin JD and Houser SR. **New Myocyte Formation in the Adult Heart: Endogenous Sources and Therapeutic Implications.** *Circ Res*. 2018;123:159-176.
21. van Rooij E and Olson EN. **MicroRNA therapeutics for cardiovascular disease: opportunities and obstacles.** *Nature Reviews Drug Discovery*. 2012;11:860-872.
22. Lu D and Thum T. **RNA-based diagnostic and therapeutic strategies for cardiovascular disease.** *Nature Reviews Cardiology*. 2019;16:661-674.
23. van Rooij E, Sutherland LB, Thatcher JE, DiMaio JM, Naseem RH, Marshall WS, Hill JA and Olson EN. **Dysregulation of microRNAs after myocardial infarction reveals a role of miR-29 in cardiac fibrosis.** *Proc Natl Acad Sci U S A*. 2008;105:13027-32.
24. Hullinger TG, Montgomery RL, Seto AG, Dickinson BA, Semus HM, Lynch JM, Dalby CM, Robinson K, Stack C, Latimer PA, Hare JM, Olson EN and van Rooij E. **Inhibition of miR-15 protects against cardiac ischemic injury.** *Circ Res*. 2012;110:71-81.
25. Bartel DP. **MicroRNAs: target recognition and regulatory functions.** *Cell*. 2009;136:215-33.
26. van Rooij E and Olson EN. **MicroRNA therapeutics for cardiovascular disease: opportunities and obstacles.** *Nat Rev Drug Discov*. 2012;11:860-72.



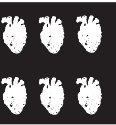
27. Krutzfeldt J, Rajewsky N, Braich R, Rajeev KG, Tuschl T, Manoharan M and Stoffel M. **Silencing of microRNAs in vivo with 'antagomirs'.** Nature. 2005;438:685-9.
28. van Rooij E, Purcell AL and Levin AA. **Developing microRNA therapeutics.** Circ Res. 2012;110:496-507.
29. Janssen HL, Reesink HW, Lawitz EJ, Zeuzem S, Rodriguez-Torres M, Patel K, van der Meer AJ, Patick AK, Chen A, Zhou Y, Persson R, King BD, Kauppinen S, Levin AA and Hodges MR. **Treatment of HCV infection by targeting microRNA.** N Engl J Med. 2013;368:1685-94.
30. Montgomery RL, Hullinger TG, Semus HM, Dickinson BA, Seto AG, Lynch JM, Stack C, Latimer PA, Olson EN and van Rooij E. **Therapeutic inhibition of miR-208a improves cardiac function and survival during heart failure.** Circulation. 2011;124:1537-47.
31. van Rooij E, Sutherland LB, Qi X, Richardson JA, Hill J and Olson EN. **Control of stress-dependent cardiac growth and gene expression by a microRNA.** Science. 2007;316:575-9.
32. Miska EA, Alvarez-Saavedra E, Abbott AL, Lau NC, Hellman AB, McGonagle SM, Bartel DP, Ambros VR and Horvitz HR. **Most Caenorhabditis elegans microRNAs are individually not essential for development or viability.** PLoS genetics. 2007;3:e215.
33. Park CY, Choi YS and McManus MT. **Analysis of microRNA knockouts in mice. Human molecular genetics.** 2010;19:R169-75.
34. Dahl LK, Heine M and Tassinari L. **Role of genetic factors in susceptibility to experimental hypertension due to chronic excess salt ingestion.** Nature. 1962;194:480-2.
35. Kim S, Ohta K, Hamaguchi A, Yukimura T, Miura K and Iwao H. **Angiotensin II induces cardiac phenotypic modulation and remodeling in vivo in rats.** Hypertension. 1995;25:1252-9.
36. Horsthuis T, Houweling AC, Habets PE, de Lange FJ, el Azzouzi H, Clout DE, Moorman AF and Christoffels VM. **Distinct regulation of developmental and heart disease-induced atrial natriuretic factor expression by two separate distal sequences.** Circ Res. 2008;102:849-59.
37. Taegtmeyer H, Sen S and Vela D. **Return to the fetal gene program: a suggested metabolic link to gene expression in the heart.** Ann N Y Acad Sci. 2010;1188:191-8.
38. Frey N and Olson EN. **Cardiac hypertrophy: the good, the bad, and the ugly.** Annu Rev Physiol. 2003;65:45-79.
39. Matkovich SJ, Dorn GW, 2nd, Grossenheider TC and Hecker PA. **Cardiac Disease Status Dictates Functional mRNA Targeting Profiles of Individual MicroRNAs.** Circ Cardiovasc Genet. 2015;8:774-84.
40. Ashraf U, Zhu B, Ye J, Wan S, Nie Y, Chen Z, Cui M, Wang C, Duan X, Zhang H, Chen H and Cao S. **MicroRNA-19b-3p Modulates Japanese Encephalitis Virus-Mediated Inflammation via Targeting RNF11.** J Virol. 2016;90:4780-95.
41. Hu H, Jiang W, Xi X, Zou C and Ye Z. **MicroRNA-21 attenuates renal ischemia reperfusion injury via targeting caspase signaling in mice.** Am J Nephrol. 2014;40:215-23.
42. Wang H, Bei Y, Huang P, Zhou Q, Shi J, Sun Q, Zhong J, Li X, Kong X and Xiao J. **Inhibition of miR-155 Protects Against LPS-induced Cardiac Dysfunction and Apoptosis in Mice.** Mol Ther Nucleic Acids. 2016;5:e374.
43. Chang J, Nicolas E, Marks D, Sander C, Lerro A, Buendia MA, Xu C, Mason WS, Moloshok T, Bort R, Zaret KS and Taylor JM. **miR-122, a mammalian liver-specific microRNA, is processed from hcr mRNA and may downregulate the high affinity cationic amino acid transporter CAT-1.** RNA biology. 2004;1:106-13.
44. Erhard F, Haas J, Lieber D, Malterer G, Jaskiewicz L, Zavolan M, Dolken L and Zimmer R. **Widespread context dependency of microRNA-mediated regulation.** Genome Res. 2014;24:906-19.
45. Leung AK and Sharp PA. **MicroRNA functions in stress responses.** Molecular cell. 2010;40:205-15.
46. Eichhorn SW, Guo H, McGeary SE, Rodriguez-Mias RA, Shin C, Baek D, Hsu SH, Ghoshal K, Villen J and Bartel DP. **mRNA destabilization is the dominant effect of mammalian microRNAs by the time substantial repression ensues.** Mol Cell. 2014;56:104-15.
47. Guo H, Ingolia NT, Weissman JS and Bartel DP. **Mammalian microRNAs predominantly act to decrease target mRNA levels.** Nature. 2010;466:835-40.
48. Hendrickson DG, Hogan DJ, McCullough HL, Myers JW, Herschlag D, Ferrell JE and Brown PO. **Concordant regulation of translation and mRNA abundance for hundreds of targets of a human microRNA.** PLoS biology. 2009;7:e1000238.
49. Baek D, Villen J, Shin C, Camargo FD, Gygi SP and Bartel DP. **The impact of microRNAs on protein output.** Nature. 2008;455:64-71.
50. Selbach M, Schwanhauser B, Thierfelder N, Fang Z, Khanin R and Rajewsky N. **Widespread changes in protein synthesis induced by microRNAs.** Nature. 2008;455:58-63.
51. McCall FC, Telukuntla KS, Karantalis V, Suncion VY, Heldman AW, Mushtaq M, Williams AR and Hare JM. **Myocardial infarction and intramyocardial injection models in swine.** Nat Protoc. 2012;7:1479-96.
52. Schuleri KH, Boyle AJ, Centola M, Amado LC, Evers R, Zimmet JM, Evers KS, Ostbye KM, Scorpio DG, Hare JM and Lardo AC. **The adult Gottingen minipig as a model for chronic heart failure after myocardial infarction: focus on cardiovascular imaging and regenerative therapies.** Comp Med. 2008;58:568-79.
53. Hunter JJ and Chien KR. **Signaling Pathways for Cardiac Hypertrophy and Failure.** New England Journal of Medicine. 1999;341:1276-1283.
54. Jansen of Lorkeers SJ, Eding JEC, van der Spoel TIG, Vesterinen HM, Sena ES, Duckers HJ, Doevendans PA, Macleod MR and Chamuleau SAJ. **Similar effect of autologous and allogeneic cell therapy for ischaemic heart disease: systematic review and meta-analysis of large animal studies.** European Journal of Clinical Investigation. 2014;44:5-6.
55. Fisher SA, Zhang H, Doree C, Mathur A and Martin-Rendon E. **Stem cell treatment for acute myocardial infarction.** Cochrane Database of Systematic Reviews. 2015.
56. Wang Y and Lee CG. **MicroRNA and cancer--focus on apoptosis.** J Cell Mol Med. 2009;13:12-23.
57. van Rooij E and Kauppinen S. **Development of microRNA therapeutics is coming of age.** EMBO Mol Med. 2014;6:851-64.
58. Rupaimoole R and Slack FJ. **MicroRNA therapeutics: towards a new era for the management of cancer and other diseases.** Nat Rev Drug Discov. 2017;16:203-222.
59. Hanna J, Hossain GS and Kocerha J. **The Potential for microRNA Therapeutics and Clinical Research.** Front Genet. 2019;10:478.
60. Bonneau E, Neveu B, Kostantin E, Tsongalis GJ and De Guire V. **How close are miRNAs from clinical practice? A perspective on the diagnostic and therapeutic market.** Ejjfcc. 2019;30:114-127.
61. Small EM, Frost RJ and Olson EN. **MicroRNAs add a new dimension to cardiovascular disease.** Circulation. 2010;121:1022-32.
62. Ofir M, Hacohen D and Ginsberg D. **MiR-15 and miR-16 are direct transcriptional targets of E2F1 that limit E2F-induced proliferation by targeting cyclin E.** Mol Cancer Res. 2011;9:440-7.



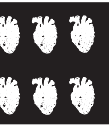
63. Porrello ER, Johnson BA, Aurora AB, Simpson E, Nam YJ, Matkovich SJ, Dorn GW, 2nd, van Rooij E and Olson EN. **MiR-15 family regulates postnatal mitotic arrest of cardiomyocytes.** *Circ Res.* 2011;109:670-9.
64. Porrello ER, Mahmoud AI, Simpson E, Johnson BA, Grinsfelder D, Canseco D, Mammen PP, Rothmel BA, Olson EN and Sadek HA. **Regulation of neonatal and adult mammalian heart regeneration by the miR-15 family.** *Proc Natl Acad Sci U S A.* 2013;110:187-92.
65. Wang LL, Liu Y, Chung JJ, Wang T, Gaffey AC, Lu M, Cavanaugh CA, Zhou S, Kanade R, Atluri P, Morrisey EE and Burdick JA. **Local and sustained miRNA delivery from an injectable hydrogel promotes cardiomyocyte proliferation and functional regeneration after ischemic injury.** *Nat Biomed Eng.* 2017;1:983-992.
66. Hernandez MJ, Gaetani R, Pieters VM, Ng NW, Chang AE, Martin TR, van Ingen E, Mol EA, Sluijter JPG and Christman KL. **Decellularized Extracellular Matrix Hydrogels as a Delivery Platform for MicroRNA and Extracellular Vesicle Therapeutics.** *Adv Ther (Weinh).* 2018;1.
67. Koudstaal S, Bastings MMC, Feyen DAM, Waring CD, van Slochteren FJ, Dankers PYW, Torella D, Sluijter JPG, Nadal-Ginard B, Doevendans PA, Ellison GM and Chamuleau SAJ. **Sustained Delivery of Insulin-Like Growth Factor-1/Hepatocyte Growth Factor Stimulates Endogenous Cardiac Repair in the Chronic Infarcted Pig Heart.** *Journal of Cardiovascular Translational Research.* 2014;7:232-241.
68. Sereti KI, Nguyen NB, Kamran P, Zhao P, Ranjbarvaziri S, Park S, Sabri S, Engel JL, Sung K, Kulkarni RP, Ding Y, Hsiai TK, Plath K, Ernst J, Sahoo D, Mikkola HKA, Iruela-Arispe ML and Ardehali R. **Analysis of cardiomyocyte clonal expansion during mouse heart development and injury.** *Nat Commun.* 2018;9:754.
69. van Rooij E, Fielitz J, Sutherland LB, Thijssen VL, Crijns HJ, Dimaio MJ, Shelton J, De Windt LJ, Hill JA and Olson EN. **Myocyte enhancer factor 2 and class II histone deacetylases control a gender-specific pathway of cardioprotection mediated by the estrogen receptor.** *Circ Res.* 2010;106:155-65.
70. E. Grubbs F. **Procedure for Detecting Outlying Observations in Samples.** *Technometrics.* 1974;11:53.
71. Finnerty JR, Wang W-X, Hébert SS, Wilfred BR, Mao G and Nelson PT. **The miR-15/107 group of microRNA genes: evolutionary biology, cellular functions, and roles in human diseases.** *J Mol Biol.* 2010;402:491-509.
72. Bastings MM, Koudstaal S, Kieltyka RE, Nakano Y, Pape AC, Feyen DA, van Slochteren FJ, Doevendans PA, Sluijter JP, Meijer EW, Chamuleau SA and Dankers PY. **A fast pH-switchable and self-healing supramolecular hydrogel carrier for guided, local catheter injection in the infarcted myocardium.** *Adv Healthc Mater.* 2014;3:70-8.
73. Matsumura Y, Zhu Y, Jiang H, D'Amore A, Luketich SK, Charwat V, Yoshizumi T, Sato H, Yang B, Uchibori T, Healy KE and Wagner WR. **Intramyocardial injection of a fully synthetic hydrogel attenuates left ventricular remodeling post myocardial infarction.** *Biomaterials.* 2019;217:119289.
74. Nishi H, Ono K, Iwanaga Y, Horie T, Nagao K, Takemura G, Kinoshita M, Kuwabara Y, Mori RT, Hasegawa K, Kita T and Kimura T. **MicroRNA-15b modulates cellular ATP levels and degenerates mitochondria via Arl2 in neonatal rat cardiac myocytes.** *J Biol Chem.* 2010;285:4920-30.
75. Williams AL, Walton CB, MacCannell KA, Avelar A and Shohet RV. **HIF-1 regulation of miR-29c impairs SERCA2 expression and cardiac contractility.** *Am J Physiol Heart Circ Physiol.* 2019;316:H554-h565.
76. Rogg EM, Abplanalp WT, Bischof C, John D, Schulz MH, Krishnan J, Fischer A, Poluzzi C, Schaefer L, Bonauer A, Zeiher AM and Dimmeler S. **Analysis of Cell Type-Specific Effects of MicroRNA-92a Provides Novel Insights Into Target Regulation and Mechanism of Action.** *Circulation.* 2018;138:2545-2558.
77. Eding JEC, Demkes CJ, Lynch JM, Seto AG, Montgomery RL, Semus HM, Jackson AL, Isabelle M, Chimenti S and van Rooij E. **The Efficacy of Cardiac Anti-miR-208a Therapy Is Stress Dependent.** *Mol Ther.* 2017;25:694-704.
78. Bakker MH, Tseng CCS, Keizer HM, Seevinck PR, Janssen HM, Van Slochteren FJ, Chamuleau SAJ and Dankers PYW. **MRI Visualization of Injectable Ureidopyrimidinone Hydrogelators by Supramolecular Contrast Agent Labeling.** *Adv Healthc Mater.* 2018;7:e1701139.
79. Bakker MH, van Rooij E and Dankers PYW. **Controlled Release of RNAi Molecules by Tunable Supramolecular Hydrogel Carriers.** *Chemistry – An Asian Journal.* 2018;13:3501-3508.
80. Nguyen MM, Gianneschi NC and Christman KL. **Developing injectable nanomaterials to repair the heart.** *Curr Opin Biotechnol.* 2015;34:225-31.
81. Maron BJ, Ommen SR, Semsarian C, Spirito P, Olivetto I and Maron MS. **Hypertrophic cardiomyopathy: present and future, with translation into contemporary cardiovascular medicine.** *J Am Coll Cardiol.* 2014;64:83-99.
82. Semsarian C, Ingles J, Maron MS and Maron BJ. **New perspectives on the prevalence of hypertrophic cardiomyopathy.** *J Am Coll Cardiol.* 2015;65:1249-1254.
83. Maron BJ and Maron MS. **Hypertrophic cardiomyopathy.** *Lancet.* 2013;381:242-55.
84. Marian AJ. **Hypertrophic cardiomyopathy: from genetics to treatment.** *Eur J Clin Invest.* 2010;40:360-9.
85. Marian AJ and Braunwald E. **Hypertrophic Cardiomyopathy: Genetics, Pathogenesis, Clinical Manifestations, Diagnosis, and Therapy.** *Circ Res.* 2017;121:749-770.
86. Di Domenico M, Casadonte R, Ricci P, Santini M, Frati G, Rizzo A, Carratelli CR, Lamberti M, Parrotta E, Quaresima B, Faniello CM, Costanzo F and Cuda G. **Cardiac and skeletal muscle expression of mutant beta-myosin heavy chains, degree of functional impairment and phenotypic heterogeneity in hypertrophic cardiomyopathy.** *J Cell Physiol.* 2012;227:3471-6.
87. Montag J, Kowalski K, Makul M, Ernstberger P, Radocaj A, Beck J, Becker E, Tripathi S, Keyser B, Muhlfield C, Wissel K, Pich A, van der Velden J, Dos Remedios CG, Perrot A, Francino A, Navarro-Lopez F, Brenner B and Kraft T. **Burst-Like Transcription of Mutant and Wildtype MYH7-Alleles as Possible Origin of Cell-to-Cell Contractile Imbalance in Hypertrophic Cardiomyopathy.** *Front Physiol.* 2018;9:359.
88. Parbhudayal RY, Garra AR, Gotte MJW, Michels M, Pei J, Harakalova M, Asselbergs FW, van Rossum AC, van der Velden J and Kuster DWD. **Variable cardiac myosin binding protein-C expression in the myofilaments due to MYBPC3 mutations in hypertrophic cardiomyopathy.** *J Mol Cell Cardiol.* 2018;123:59-63.
89. Grun D, Kester L and van Oudenaarden A. **Validation of noise models for single-cell transcriptomics.** *Nat Methods.* 2014;11:637-40.
90. Kolodziejczyk AA, Kim JK, Svensson V, Marioni JC and Teichmann SA. **The technology and biology of single-cell RNA sequencing.** *Mol Cell.* 2015;58:610-20.
91. Gladka MM, Molenaar B, de Ruiter H, van der Elst S, Tsui H, Versteeg D, Lacraz GPA, Huibers MMH,



- van Oudenaarden A and van Rooij E. **Single-Cell Sequencing of the Healthy and Diseased Heart Reveals Cytoskeleton-Associated Protein 4 as a New Modulator of Fibroblasts Activation.** *Circulation*. 2018;138:166-180.
92. Farbehi N, Patrick R, Dorison A, Xaymardan M, Janbandhu V, Wystub-Lis K, Ho JW, Nordon RE and Harvey RP. **Single-cell expression profiling reveals dynamic flux of cardiac stromal, vascular and immune cells in health and injury.** *Elife*. 2019;8.
93. Hu P, Liu J, Zhao J, Wilkins BJ, Lupino K, Wu H and Pei L. **Single-nucleus transcriptomic survey of cell diversity and functional maturation in postnatal mammalian hearts.** *Genes Dev*. 2018;32:1344-1357.
94. Nomura S, Satoh M, Fujita T, Higo T, Sumida T, Ko T, Yamaguchi T, Tobita T, Naito AT, Ito M, Fujita K, Harada M, Toko H, Kobayashi Y, Ito K, Takimoto E, Akazawa H, Morita H, Aburatani H and Komuro I. **Cardiomyocyte gene programs encoding morphological and functional signatures in cardiac hypertrophy and failure.** *Nat Commun*. 2018;9:4435.
95. Skelly DA, Squiers GT, McLellan MA, Bolisetty MT, Robson P, Rosenthal NA and Pinto AR. **Single-Cell Transcriptional Profiling Reveals Cellular Diversity and Intercommunication in the Mouse Heart.** *Cell Rep*. 2018;22:600-610.
96. Kretzschmar K, Post Y, Bannier-Helaouet M, Mattiotti A, Drost J, Basak O, Li VSW, van den Born M, Gunst QD, Versteeg D, Kooijman L, van der Elst S, van Es JH, van Rooij E, van den Hoff MJB and Clevers H. **Profiling proliferative cells and their progeny in damaged murine hearts.** *Proc Natl Acad Sci U S A*. 2018;115:E12245-E12254.
97. Stewart-Ornstein J, Weissman Jonathan S and El-Samad H. **Cellular Noise Regulons Underlie Fluctuations in *Saccharomyces cerevisiae*.** *Molecular Cell*. 2012;45:483-493.
98. dos Remedios CG, Lal SP, Li A, McNamara J, Keogh A, Macdonald PS, Cooke R, Ehler E, Knöll R, Marston SB, Stelzer J, Granzier H, Bezzina C, van Dijk S, De Man F, Stienen GJM, Odeberg J, Pontén F, Linke W and van der Velden J. **The Sydney Heart Bank: improving translational research while eliminating or reducing the use of animal models of human heart disease.** *Biophysical Reviews*. 2017;9:431-441.
99. Muraro MJ, Dharmadhikari G, Grun D, Groen N, Dielen T, Jansen E, van Gorp L, Engelse MA, Carlotti F, de Koning EJ and van Oudenaarden A. **A Single-Cell Transcriptome Atlas of the Human Pancreas.** *Cell Syst*. 2016;3:385-394 e3.
100. Li H and Durbin R. **Fast and accurate short read alignment with Burrows-Wheeler transform.** *Bioinformatics*. 2009;25:1754-60.
101. Grun D, Muraro MJ, Boisset JC, Wiebrands K, Lyubimova A, Dharmadhikari G, van den Born M, van Es J, Jansen E, Clevers H, de Koning EJ and van Oudenaarden A. **De Novo Prediction of Stem Cell Identity using Single-Cell Transcriptome Data.** *Cell Stem Cell*. 2016;19:266-77.
102. Grun D and van Oudenaarden A. **Design and Analysis of Single-Cell Sequencing Experiments.** *Cell*. 2015;163:799-810.
103. Smith PJ, Wiltshire M and Errington RJ. **DRAQ5 labeling of nuclear DNA in live and fixed cells.** *Curr Protoc Cytom*. 2004;Chapter 7:Unit 7 25.
104. Kannan S, Miyamoto M, Lin BL, Zhu R, Murphy S, Kass DA, Andersen P and Kwon C. **Large Particle Fluorescence-Activated Cell Sorting Enables High-Quality Single-Cell RNA Sequencing and Functional Analysis of Adult Cardiomyocytes.** *Circulation Research*. 2019;125:567-569.
105. Grun D, Lyubimova A, Kester L, Wiebrands K, Basak O, Sasaki N, Clevers H and van Oudenaarden A. **Single-cell messenger RNA sequencing reveals rare intestinal cell types.** *Nature*. 2015;525:251-5.
106. Gautel M and Djinovic-Carugo K. **The sarcomeric cytoskeleton: from molecules to motion.** *J Exp Biol*. 2016;219:135-45.
107. Wang TY, Lee D, Fox-Talbot K, Arking DE, Chakravarti A and Halushka MK. **Cardiomyocytes have mosaic patterns of protein expression.** *Cardiovascular Pathology*. 2018;34:50-57.
108. Man J, Barnett P and Christoffels VM. **Structure and function of the Nppa-Nppb cluster locus during heart development and disease.** *Cell Mol Life Sci*. 2018;75:1435-1444.
109. Black BL and Olson EN. **Transcriptional control of muscle development by myocyte enhancer factor-2 (MEF2) proteins.** *Annu Rev Cell Dev Biol*. 1998;14:167-96.
110. Miyata S, Minobe W, Bristow MR and Leinwand LA. **Myosin Heavy Chain Isoform Expression in the Failing and Nonfailing Human Heart.** *Circulation Research*. 2000;86:386-390.
111. Wilson Nicola K, Kent David G, Buettner F, Shehata M, Macaulay Iain C, Calero-Nieto Fernando J, Sánchez Castillo M, Oedekoven Caroline A, Diamanti E, Schulte R, Ponting Chris P, Voet T, Caldas C, Stingl J, Green Anthony R, Theis Fabian J and Göttgens B. **Combined Single-Cell Functional and Gene Expression Analysis Resolves Heterogeneity within Stem Cell Populations.** *Cell Stem Cell*. 2015;16:712-724.
112. Lim DS, Roberts R and Marian AJ. **Expression profiling of cardiac genes in human hypertrophic cardiomyopathy: insight into the pathogenesis of phenotypes.** *Journal of the American College of Cardiology*. 2001;38:1175-1180.
113. Remme CA, Verkerk AO, Hoogaars WM, Aanhaanen WT, Scicluna BP, Annink C, van den Hoff MJ, Wilde AA, van Veen TA, Veldkamp MW, de Bakker JM, Christoffels VM and Bezzina CR. **The cardiac sodium channel displays differential distribution in the conduction system and transmural heterogeneity in the murine ventricular myocardium.** *Basic Res Cardiol*. 2009;104:511-22.
114. van der Velden J, Merkus D, de Beer V, Hamdani N, Linke WA, Boontje NM, Stienen GJ and Duncker DJ. **Transmural heterogeneity of myofilament function and sarcomeric protein phosphorylation in remodeled myocardium of pigs with a recent myocardial infarction.** *Front Physiol*. 2011;2:83.
115. Huang HT, Brand OM, Mathew M, Ignatiou C, Ewen EP, McCalmon SA and Naya FJ. **Myomaxin is a novel transcriptional target of MEF2A that encodes a Xin-related alpha-actinin-interacting protein.** *J Biol Chem*. 2006;281:39370-9.
116. Durham JT, Brand OM, Arnold M, Reynolds JG, Muthukumar L, Weiler H, Richardson JA and Naya FJ. **Myospryn is a direct transcriptional target for MEF2A that encodes a striated muscle, alpha-actinin-interacting, costamere-localized protein.** *J Biol Chem*. 2006;281:6841-9.
117. Lacraz GPA, Junker JP, Gladka MM, Molenaar B, Scholman KT, Vigil-Garcia M, Versteeg D, de Ruiter H, Vermunt MW, Creighton MP, Huibers MMH, de Jonge N, van Oudenaarden A and van Rooij E. **Tomoseq Identifies SOX9 as a Key Regulator of Cardiac Fibrosis During Ischemic Injury.** *Circulation*. 2017;136:1396-1409.
118. Tsoupri E and Capetanaki Y. **Myospryn: a multifunctional desmin-associated protein.** *Histochem Cell Biol*. 2013;140:55-63.
119. Dodge-Kafka KL and Kapiloff MS. **The mAKAP signaling complex: integration of cAMP, calcium, and MAP kinase signaling pathways.** *Eur J Cell Biol*. 2006;85:593-602.
120. Benson MA, Tinsley CL, Waite AJ, Carlisle FA, Sweet SMM, Ehler E, George CH, Lai FA, Martin-Rendon E and Blake DJ. **Ryanodine receptors are part of the myospryn complex in cardiac muscle.** *Sci*



- Rep. 2017;7:6312.
121. Sarparanta J, Blandin G, Charton K, Vihola A, Marchand S, Milic A, Hackman P, Ehler E, Richard I and Udd B. **Interactions with M-band titin and calpain 3 link myospryn (CMYA5) to tibial and limb-girdle muscular dystrophies.** J Biol Chem. 2010;285:30304-15.
  122. Dirkx E, da Costa Martins PA and De Windt LJ. **Regulation of fetal gene expression in heart failure.** Biochim Biophys Acta. 2013;1832:2414-24.
  123. Sorenson ALT, D.; Sonnenblick, E.H., Robinson, T.F.; Capasso J.M. **Size and shape of enzymatically isolated ventricular myocytes from rats and cardiomyopathic hamsters.** Cardiovasc Res. 1985;19:793-799.
  124. Selewa A, Dohn R, Eckart H, Lozano S, Xie B, Gauchat E, Elorbany R, Rhodes K, Burnett J, Gilad Y, Pott S and Basu A. **Systematic Comparison of High-throughput Single-Cell and Single-Nucleus Transcriptomes during Cardiomyocyte Differentiation.** bioRxiv. 2019:585901.
  125. Ackers-Johnson M, Tan WLW and Foo RS. **Following hearts, one cell at a time: recent applications of single-cell RNA sequencing to the understanding of heart disease.** Nat Commun. 2018;9:4434.
  126. Chevalier M, Vermij SH, Wyler K, Gillet L, Keller I and Abriel H. **Transcriptomic analyses of murine ventricular cardiomyocytes.** Sci Data. 2018;5:180170.
  127. DeLaughter DM, Bick AG, Wakimoto H, McKean D, Gorham JM, Kathiriya IS, Hinson JT, Homsy J, Gray J, Pu W, Bruneau BG, Seidman JG and Seidman CE. **Single-Cell Resolution of Temporal Gene Expression during Heart Development.** Dev Cell. 2016;39:480-490.
  128. Kraft T and Montag J. **Altered force generation and cell-to-cell contractile imbalance in hypertrophic cardiomyopathy.** Pflügers Archiv - European Journal of Physiology. 2019;471:719-733.
  129. Williams AH, Valdez G, Moresi V, Qi X, McAnally J, Elliott JL, Bassel-Duby R, Sanes JR and Olson EN. **MicroRNA-206 Delays ALS Progression and Promotes Regeneration of Neuromuscular Synapses in Mice.** Science. 2009;326:1549.
  130. Park CY, Choi YS and McManus MT. **Analysis of microRNA knockouts in mice.** Hum Mol Genet. 2010;19:R169-R175.
  131. Besnier M, Shantikumar S, Anwar M, Dixit P, Chamorro-Jorganes A, Sweaad W, Sala-Newby G, Madeddu P, Thomas AC, Howard L, Mushtaq S, Petretto E, Caporali A and Emanuelli C. **miR-15a/-16 Inhibit Angiogenesis by Targeting the Tie2 Coding Sequence: Therapeutic Potential of a miR-15a/16 Decoy System in Limb Ischemia.** Molecular Therapy - Nucleic Acids. 2019;17:49-62.
  132. Sandberg R, Neilson JR, Sarma A, Sharp PA and Burge CB. **Proliferating Cells Express mRNAs with Shortened 3' Untranslated Regions and Fewer MicroRNA Target Sites.** Science. 2008;320:1643-1647.
  133. Cloonan N. **Re-thinking miRNA-mRNA interactions: Intertwining issues confound target discovery.** BioEssays. 2015;37:379-388.
  134. Kang H, Ahn H, Jo K, Oh M and Kim S. **mirTime: Identifying Condition-Specific Targets of MicroRNA in Time-series Transcript Data using Gaussian Process Model and Spherical Vector Clustering.** Bioinformatics. 2019.
  135. Ovando-Vázquez C, Lepe-Soltero D and Abreu-Goodger C. **Improving microRNA target prediction with gene expression profiles.** BMC Genomics. 2016;17:364.
  136. Deyle DR and Russell DW. **Adeno-associated virus vector integration.** Curr Opin Mol Ther. 2009;11:442-7.
  137. Denzer K, Kleijmeer MJ, Heijnen HF, Stoorvogel W and Geuze HJ. **Exosome: from internal vesicle of the multivesicular body to intercellular signaling device.** J Cell Sci. 2000;113 Pt 19:3365-74.
  138. Liu C and Su C. **Design strategies and application progress of therapeutic exosomes.** Theranostics. 2019;9:1015-1028.
  139. Mentkowski KI and Lang JK. **Exosomes Engineered to Express a Cardiomyocyte Binding Peptide Demonstrate Improved Cardiac Retention in Vivo.** Scientific Reports. 2019;9:10041.
  140. Singelyn JM, Sundaramurthy P, Johnson TD, Schup-Magoffin PJ, Hu DP, Faulk DM, Wang J, Mayle KM, Bartels K, Salvatore M, Kinsey AM, Demaria AN, Dib N and Christman KL. **Catheter-deliverable hydrogel derived from decellularized ventricular extracellular matrix increases endogenous cardiomyocytes and preserves cardiac function post-myocardial infarction.** J Am Coll Cardiol. 2012;59:751-63.
  141. Pena B, Laughter M, Jett S, Rowland TJ, Taylor MRG, Mestroni L and Park D. **Injectable Hydrogels for Cardiac Tissue Engineering.** Macromol Biosci. 2018;18:e1800079.
  142. Grün D, Lyubimova A, Kester L, Wiebrands K, Basak O, Sasaki N, Clevers H and van Oudenaarden A. **Single-cell messenger RNA sequencing reveals rare intestinal cell types.** Nature. 2015;525:251.
  143. Gladka MM, Molenaar B, de Ruiter H, van der Elst S, Tsui H, Versteeg D, Lacraz GPA, Huibers MMH, van Oudenaarden A and van Rooij E. **Single-Cell Sequencing of the Healthy and Diseased Heart Reveals Ckap4 as a New Modulator of Fibroblasts Activation.** Circulation. 2018.
  144. van den Brink SC, Sage F, Vértesy Á, Spanjaard B, Peterson-Maduro J, Baron CS, Robin C and van Oudenaarden A. **Single-cell sequencing reveals dissociation-induced gene expression in tissue subpopulations.** Nature Methods. 2017;14:935-936.
  145. Farago N, Kocsis GF, Feher LZ, Csont T, Hackler L, Jr., Varga-Orvos Z, Csonka C, Kelemen JZ, Ferdinandy P and Puskas LG. **Gene and protein expression changes in response to normoxic perfusion in mouse hearts.** J Pharmacol Toxicol Methods. 2008;57:145-54.
  146. Macosko EZ, Basu A, Satija R, Nemesh J, Shekhar K, Goldman M, Tirosh I, Bialas AR, Kamitaki N, Martersteck EM, Trombetta JJ, Weitz DA, Sanes JR, Shalek AK, Regev A and McCarroll SA. **Highly Parallel Genome-wide Expression Profiling of Individual Cells Using Nanoliter Droplets.** Cell. 2015;161:1202-1214.
  147. Luecken MD and Theis FJ. **Current best practices in single-cell RNA-seq analysis: a tutorial.** Mol Syst Biol. 2019;15:e8746.
  148. Krishnaswami SR, Grindberg RV, Novotny M, Venepally P, Lacar B, Bhutani K, Linker SB, Pham S, Erwin JA, Miller JA, Hodge R, McCarthy JK, Kelder M, McCorrison J, Aevermann BD, Fuertes FD, Scheuermann RH, Lee J, Lein ES, Schork N, McConnell MJ, Gage FH and Lasken RS. **Using single nuclei for RNA-seq to capture the transcriptome of postmortem neurons.** Nat Protoc. 2016;11:499-524.
  149. Ziegenhain C, Vieth B, Parekh S, Reinius B, Guillaumet-Adkins A, Smets M, Leonhardt H, Heyn H, Hellmann I and Enard W. **Comparative Analysis of Single-Cell RNA Sequencing Methods.** Molecular Cell. 2017;65:631-643.e4.
  150. Hagemann-Jensen M, Ziegenhain C, Chen P, Ramsköld D, Hendriks G-J, Larsson AJM, Faridani OR and Sandberg R. **Single-cell RNA counting at allele- and isoform-resolution using Smart-seq3.** bioRxiv. 2019:817924.



## Nederlandse samenvatting

Hart- en vaatziekten zijn wereldwijd de grootste oorzaak van sterfte en ziektelast. Het hart kan op verschillende manieren ziek worden. De meest voorkomende daarvan is het hartinfarct. Door vernauwing, en uiteindelijk afsluiting, van de vaten die de hartspier van zuurstof voorzien kan een stuk van de hartspier afsterven. Hierdoor gaat een deel van de pompkracht verloren. Het resterende deel van het spierweefsel zal proberen hiervoor te compenseren, maar uiteindelijk zal het hart als geheel steeds slechter gaan pompen, met hartfalen als gevolg. Met medicatie wordt geprobeerd om deze achteruitgang van de hartfunctie zoveel mogelijk te voorkomen, maar het herstellen van de opgelopen schade is nog niet mogelijk. Hartfalen kan eveneens ontstaan door een erfelijke aanleg voor hartziekten. Deze erfelijke aanleg ontstaat door fouten in het DNA die ertoe leiden dat de hartcellen zich anders gedragen dan normaal, met een afwijkende hartfunctie tot gevolg.

### Van erfelijk materiaal naar celfunctie

#### Van gen naar eiwit

Het erfelijk materiaal van de mens is vastgelegd in het DNA. Een kopie van het gehele DNA is vastgelegd in de kern van elke cel. Delen van het DNA, de genen, beschrijven blauwdrukken voor het maken van specifieke eiwitten. Om een nieuw eiwit te maken wordt eerst een kopie, messenger RNA, van het relevante stuk DNA gemaakt. RNA kan de celkern verlaten om in de rest van de cel als bouwtekening voor dat eiwit te dienen. Deze eiwitten zijn de bouwstenen van de cel en de moleculen die zorg dragen voor de uitvoer van celfuncties. Een verandering in welke eiwitten er gemaakt worden kan dus effect hebben op het gedrag van de cel, bijvoorbeeld op celdeling. Omdat eiwitten zo belangrijk zijn voor het functioneren van de cel, wordt het proces van eiwitproductie op meerdere niveaus gereguleerd.

#### De rol van microRNAs

Naast de stukken DNA die een bouwtekening van een eiwit bevatten, zijn er ook stukken DNA waar RNA-kopieën van gemaakt worden die geen bouwtekening voor een eiwit bevatten. Deze groep RNA-moleculen heten non-coding RNAs. Onderdeel hiervan is een groep met hele kleine RNA-moleculen die microRNAs (verder miRs) heten. De functie van miRs is het reguleren van de eiwitproductie. Ze doen dit doordat ze opgenomen kunnen worden in een complex van enkele eiwitten (RNA-Induced Silencing Complex, RISC). In dit complex fungeert de miR als herkeningsmechanisme om gewone RNA-moleculen te binden. Elke miR heeft een aantal specifieke RNA-moleculen die het kan binden. Wanneer een RNA-molecuul gebonden wordt door een miR (en RISC), dan kan er geen eiwit meer gemaakt worden van dit RNA-molecuul. Op deze manier beïnvloeden miRs de eiwitproductie in een cel.

#### Therapeutische beïnvloeding van eiwitproductie

In eerder onderzoek zijn manieren gevonden om, via het systeem van de miRs, de eiwitproductie in een cel te beïnvloeden en zo het gedrag van de cel te veranderen. Het is mogelijk om met kunst-miRs de productie van bepaalde eiwitten te remmen. Andersom is het mogelijk om met antimiriRs de werking van de miRs te blokkeren, hierdoor wordt de remming van de eiwitproductie van bepaalde RNAs opgeheven en wordt er juist meer van dat eiwit gemaakt.

## RNA-doelwitten bij hartziekten

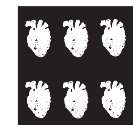
Om een effectieve therapie te kunnen ontwikkelen die werkt door het beïnvloeden van de eiwitproductie is het nodig om heel goed te weten hoe deze middelen zich gedragen in een ziek hart. Daarnaast moeten deze middelen van buiten het lichaam komen en is het zaak om ze zo goed mogelijk om hun plek in het hart te krijgen. Tenslotte is het belangrijk om te weten van welke eiwitten de productie beïnvloed moet worden.

In **hoofdstuk 2** hebben we onderzocht hoe de functie van een antimiriR tegen *miR-208* verschilt tussen een gezond hart en harten met verschillende soorten hartziekten. We tonen hier aan dat het type hartziekte in belangrijke mate bepaalt op welke RNAs *miR-208* zich richt.

In **hoofdstuk 3** hebben we onderzoek gedaan naar de rechtstreekse injectie van antimiriRs in het hart. We onderzochten of injectie met een hydrogel ervoor zou zorgen dat de antimiriR beter op zijn plek zou blijven (retentie) dan injectie in water. De hydrogel gaf een kleine verbetering van de retentie van de antimiriR, maar niet voldoende om harten te repareren die door een hartinfarct beschadigd waren.

In **hoofdstuk 4** hebben we onderzoek gedaan naar nieuwe RNAs die kunnen worden beïnvloed ter behandeling van hypertrofe cardiomyopathie (HCM). HCM is een erfelijke hartziekte waarbij de hartspiercellen te groot worden en de hartspier als geheel daardoor te dik wordt. We hebben hartspierweefsel van patiënten met HCM gesplitst tot losse cellen. Vervolgens hebben we bepaald welke eiwitten er geproduceerd werden in elk van die cellen. Die informatie hebben we gekoppeld aan de grootte van de spiercellen.

In de discussie (**hoofdstuk 5**) worden de bevindingen uit de voorgaande hoofdstukken nog eens samengevat, besproken in het licht van de actuele literatuur en worden de mogelijkheden voor vervolgonderzoek besproken.



## Acknowledgements

It's done. From November 2014 until November 2019 I've worked on the research described in this thesis. During these five years I've had the pleasure of working with a lot of amazing people. Thanks to these people the past 5 years have been an awesome journey.

Ten eerste, **Eva**. Het is nu ongeveer 7 jaar geleden dat we elkaar leerden kennen. Ik als masterstudent, die niet wist wie Hans Clevers was, op zoek naar een stage in het lab. Jij nog niet zo heel lang terug uit de VS en net een nieuw lab startende in het Hubrecht. Die stage kreeg een vervolg en dat vervolg werd weer opgevolgd door een promotietraject. Dankjewel voor de lange tijd die ik onder jouw hoede in het Hubrecht door heb mogen brengen, ik heb veel geleerd van alle onze discussies en ben erg dankbaar voor de vrijheid die ik kreeg om me te ontwikkelen en de rest van mijn carrière op de rails te zetten, inclusief 6 maanden onderbreking van mijn onderzoek om in de kliniek te werken. Het was geweldig om het lab zo te zien groeien in de afgelopen jaren en ik wens je veel succes met alle interessante nieuwe projecten!

Aan de leden van mijn lees- en promotiecommissie: bedankt voor het lezen en beoordelen van mijn proefschrift en de gelegenheid om daarover met jullie van gedachten te wisselen.

Mijn directe collega's: **Charlotte**, jij was er vanaf het begin al bij en van een hoop van het lab-opzetwerk dat jij gedaan hebt, heb ik in de jaren daarna kunnen profiteren. Maar nog belangrijker was jouw altijd opgewekte houding (*circadian rhythm*-experimenten of niet) die zo goed was voor de sfeer in het lab. Wat een plezier was het om jarenlang jou als kantoormaatje te hebben. Dank ook voor je hulp met hoofdstuk 2 en 3 van dit boek. Ik vond het erg leuk om in 2018 jouw paranimf te zijn en ben blij dat jij dat nu voor mij ook bent! **Jenny**, thank you for the many early morning chats. Whether they were about buying houses, Game of Thrones, science, career or life in general, they brightened my mornings without exception. Thank you for keeping our office 'hydrated'. And thank you for the caloric support, continuing even during my half year at the UMC. I'm very happy you'll also be supporting this final stretch of my PhD as my paranymph! **Monika**, thank you for teaching me how to pipet as well as many other lab skills! **Hesther**, waar zou het lab zijn zonder jou als labmoeder die ons allemaal in het gareel houdt en de organisatie bewaakt? **Bas**, jij hebt voor het lab een enorme berg werk verzet m.b.t. de analyse van (single-cell) RNA-sequencing data. Zonder jouw werk als basis hadden de analyses in hoofdstuk 4 mij een stuk meer tijd en moeite gekost. **Marta**, thank you continuing the hydrogel project during my intermezzo working in the hospital and for helping shape chapter 3 into what it is now. **Marit**, het is indrukwekkend hoe snel jij zelfstandig aan de slag kon tijdens je masterstage in ons lab en dat het je gelukt is om het brakke ELISA-protocol dat we kregen toch aan de praat te krijgen! **Danielle, Lieneke**, geen van de dierproeven in hoofdstuk 3 waren mogelijk geweest zonder jullie hulp bij het opzetten en uitvoeren van de operaties en het zorgen voor de muizen. **Anne, Maya, Martijn**, thank you for your collaboration on the single-cell sequencing project. Anne, het is dankzij jouw oog voor detail dat de figuren van hoofdstuk 4 de mooiste uit dit boekje zijn geworden. Maya, thank you for keeping all logistics running smoothly and keeping our external collaborators in the loop. Martijn, jij raakte pas wat later bij dit project betrokken, maar we hebben erg veel gehad aan jouw frisse blik en nieuwe ideeën. **Jantine, Ilaria**, thank you for your support of the iPSC cultures and differentiations. It's strange to think how much time I spent culturing and differentiating cardiomyocytes without any of it ending up in my thesis, but it would have been harder without your help. **Arwa, Kees, Jenny, Maya, Sebastiaan** Brain

**Brian**, thanks for the fun/interesting discussions, (mostly) friday afternoon drinks and for making our office the coolest. **Andrea, Eirini, Iliana, Louk, Su Ji**, and past lab members **Ronald, Koen, Ana Rita, Farhad, Mariska, Marjolein, Greg, AK, Andreas**, I enjoyed having each of you as colleagues and am grateful for the nice lab atmosphere you all created.

**Annabel, Bas, Daniel, Euclides, Kim, Sander, Wouter**, thank you for an amazing year of organizing *borrels* and other activities as *PV 2015*. **Bas**, dank voor de vele ochtenden op de squashbaan waarbij we elkaar ofwel alle hoeken van de zaal lieten zien of echt geen bal raak sloegen.

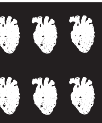
Het Hubrecht Instituut biedt een aantal uitstekende faciliteiten om ons als onderzoekers het leven makkelijker te maken. Waar zaken vanzelf lijken te gaan, is dit te danken aan het talent van de mensen die deze faciliteiten bemannen: **Stefan**, dank voor je hulp en inzichten bij het opzetten en analyseren van onze FACS-experimenten; **Jeroen**, dank voor al je hulp met de histologie, na het zelf geprobeerd te hebben weet ik des te beter wat een precies werk het is; **Judith** en **Mauro**, dank voor jullie hulp en advies bij het opzetten en analyseren van onze single-cell-experimenten; **Anko**, dank voor de hulp met de microscopen; **proefdierversorgers, civiele dienst, mediakeuken**, zonder jullie zou niemand ooit nog wat gedaan krijgen.

**Sanne**, jij begeleidde mijn eerste wetenschappelijke stage waarbij we samen een meta-analyse schreven. Dank voor je enthousiaste begeleiding en alles wat ik van je leerde tijdens deze periode. Het was een geweldig begin van mijn onderzoekscarrière en opende mijn ogen voor de meer experimentele kant van de cardiologie. **Steven**, ook jij bedankt voor de begeleiding tijdens deze stage en vooral voor het advies om eens bij Eva te gaan praten, dat bleek een gouden zet! **Maarten-Jan**, ik leerde jou als tutor kennen op mijn eerste dag als student (toen ik je nog met *meneer* aansprak). Ik ben je erg dankbaar voor je betrokkenheid bij mijn voortgang tijdens mijn studie en daarna, voor de geweldige speech tijdens mijn afstuderen en alle hulp en advies tijdens mijn periode als ANIOS.

Lieve **Harrie, Lia, Annelie, Avi, Ilse**, jullie zijn de beste schoonfamilie die ik me kan wensen. Dank voor de introductie aan het skiën en het doen herleven van mijn lol in Sinterklaasvieringen.

Lieve **papa, mama, Tom**, dankjulliewel voor de interesse in mijn PhD en voor het feit dat jullie altijd klaarstonden voor Eline en mij. Het is geweldig dat we jullie altijd, voor alles, kunnen bellen. Dank ook voor de frequente hulp en advies tijdens onze verhuizing.

En tenslotte **Eline**. Lieve Eline, wat was het fijn om thuis de frustraties en overwinningen die inherent zijn aan het onderzoek met je te kunnen delen. Jij hielp me de frustraties te relativiseren en kon ook de kleine overwinningen op waarde schatten. Alle tekst in dit boek is op enig moment in de afgelopen 5 jaar door jou van commentaar voorzien en daar beter van geworden. Een half jaar geleden schreef jij in je dankwoord "Groenlo, here we come!". Nu zijn we er en het had niet beter uit kunnen pakken. Ik heb ontzettend veel zin in onze toekomst samen!



## List of publications

Jansen of Lorkeers SJ, **Eding JEC**, Vesterinen HM, van der Spoel TIG, Sena ES, Duckers HJ, Doevendans PAFM, Macleod MR, Chamuleau SAJ. **Similar Effect of Autologous and Allogeneic Cell Therapy for Ischemic Heart Disease: Systematic Review and Meta-Analysis of Large Animal Studies.** *Circulation Research*. 2015;116:80-86

Adolphs APJ, Boersma NA, Diemel BDM, **Eding JEC**, Flokstra E, Wegner I, Grolman W, Braunius W. **A Systematic Review of Computed Tomography Detection of Cartilage Invasion in Laryngeal Carcinoma.** *The Laryngoscope*. 2015;125:1650-1655

**Eding JEC**, Demkes CJ, Lynch JM, Seto AG, Montgomery RL, Semus HM, Jackson AL, Isabelle M, Chimenti S, van Rooij E. **The Efficacy of Cardiac Anti-miR-208a Therapy Is Stress Dependent.** *Molecular Therapy*. 2017;25:694-704

Zwetsloot PP, Kouwenberg LHJA, Sena ES, **Eding JEC**, den Ruijter HM, Sluijter JPG, Pasterkamp G, Doevendans PAFM, Hofer IE, Chamuleau SAJ, van Hout GPJ, Jansen of Lorkeers SJ. **Optimization of Large Animal MI Models; A Systematic Analysis of Control Groups From Preclinical Studies.** *Scientific Reports*. 2017;7:14218

**Eding JEC**, van Rooij E. **Keeping the Heart Fitm2 during Chemotherapy.** *Molecular Therapy*. 2018;27:10-12 (Editorial)

## Manuscripts in preparation

**Eding JEC**, Vigil-Garcia M, Vink M, Demkes CJ, Versteeg D, Kooijman L, Bakker MH, Schotman MJG, Dankers PYW, van Rooij E. **Hydrogel-Based Delivery of AntimiR-195 Improves Cardiac Efficacy After Ischemic Injury.** *In preparation*

**Eding JEC**, de Leeuw AE, Wright Clark M, Wehrens M, Boogerd CJ, Molenaar B, van der Kraak PH, Kuster DWD, van der Velden J, Michels M, Vink A, van Rooij E. **Single-cell transcriptomic profiling provides insights into disease-related processes in human hypertrophic cardiomyopathy.** *In preparation*

## Curriculum Vitae

Joep Egbert Coenraad Eding was born on December 28<sup>th</sup> 1989 in Wageningen, the Netherlands. In 2008 he received his high school diploma at the Pantarijn in Wageningen and then moved to Utrecht to study Medicine. During most of his Bachelor's and Master's studies he worked as a web developer at Fotoalbum BV. In the course of obtaining his Master's degree, Joep completed several research internships. The first of these was at the UMC Utrecht Department of Cardiology, where he participated in the meta-analysis of stem cell therapy for ischemic heart disease. This internship resulted in a first scientific publication and awakened an interest in the molecular aspects of cardiology. This led to an extracurricular internship in the lab of prof. dr. Eva van Rooij at the Hubrecht Institute where Joep was introduced to microRNA research. In November 2014, after completing his Master's degree, Joep returned to the lab of prof. van Rooij as a PhD candidate. In February 2018, he interrupted his research for half a year of clinical work at the UMC Utrecht Department of Cardiology, returning to the lab afterwards. This thesis presents the results of Joep's research. Since completing his thesis, Joep started work as a software developer at Nedap Healthcare.

